Newborn EEG Seizure Detection Using Adaptive Time-Frequency Signal Processing

Luke Rankine

Bachelor of Engineering (Aerospace Avionics)
First Class Honours

Thesis submitted as a requirement for the degree of

Doctor of Philosophy

Signal Processing Research
School of Engineering Systems
Faculty of Built Environment and Engineering

Queensland University of Technology

2006

KEYWORDS

adaptive, atomic decomposition, automatic detection, electroencephalogram, fractal dimension, matching pursuit, neonate, newborn, nonlinear, nonstationary, optimal window scale, quadratic time–frequency distribution, seizure, simulation, spike, structural complexity, time–frequency signal analysis, time–frequency signal synthesis

Abstract

Dysfunction in the central nervous system of the neonate is often first identified through seizures. The difficulty in detecting clinical seizures, which involves the observation of physical manifestations characteristic to newborn seizure, has placed greater emphasis on the detection of newborn electroencephalographic (EEG) seizure.

The high incidence of newborn seizure has resulted in considerable mortality and morbidity rates in the neonate. Accurate and rapid diagnosis of neonatal seizure is essential for proper treatment and therapy. This has impelled researchers to investigate possible methods for the automatic detection of newborn EEG seizure. This thesis is focused on the development of algorithms for the automatic detection of newborn EEG seizure using adaptive time–frequency signal processing.

The assessment of newborn EEG seizure detection algorithms requires large datasets of nonseizure and seizure EEG which are not always readily available and often hard to acquire. This has led to the proposition of realistic models of newborn EEG which can be used to create large datasets for the evaluation and comparison of newborn EEG seizure detection algorithms. In this thesis, we develop two simulation methods which produce synthetic newborn EEG background and seizure. The simulation methods use nonlinear and time-frequency signal processing techniques to allow for the demonstrated nonlinear and nonstationary characteristics of the newborn EEG.

Atomic decomposition techniques incorporating redundant time-frequency dictionaries are exciting new signal processing methods which deliver adaptive signal representations or approximations. In this thesis we have investigated two prominent atomic decomposition techniques, matching pursuit and basis pursuit, for their possible use in an automatic seizure detection algorithm. In our investigation, it was shown that matching pursuit generally provided the sparsest (i.e. most compact) approximation for various real and synthetic signals over a wide range of signal approximation levels. For this reason, we chose MP as our preferred atomic decomposition technique for this thesis.

A new measure, referred to as structural complexity, which quantifies the level or

degree of correlation between signal structures and the decomposition dictionary was proposed. Using the change in structural complexity, a generic method of detecting changes in signal structure was proposed. This detection methodology was then applied to the newborn EEG for the detection of state transition (i.e. nonseizure to seizure state) in the EEG signal. To optimize the seizure detection process, we developed a time–frequency dictionary that is coherent with the newborn EEG seizure state based on the time–frequency analysis of the newborn EEG seizure. It was shown that using the new coherent time–frequency dictionary and the change in structural complexity, we can detect the transition from nonseizure to seizure states in synthetic and real newborn EEG.

Repetitive spiking in the EEG is a classic feature of newborn EEG seizure. Therefore, the automatic detection of spikes can be fundamental in the detection of newborn EEG seizure. The capacity of two adaptive time-frequency signal processing techniques to detect spikes was investigated. It was shown that a relationship between the EEG epoch length and the number of repetitive spikes governs the ability of both matching pursuit and adaptive spectrogram in detecting repetitive spikes. However, it was demonstrated that the law was less restrictive for the adaptive spectrogram and it was shown to outperform matching pursuit in detecting repetitive spikes.

The method of adapting the window length associated with the adaptive spectrogram used in this thesis was the *maximum correlation criterion*. It was observed that for the time instants where signal spikes occurred, the optimal window lengths selected by the maximum correlation criterion were small. Therefore, spike detection directly from the adaptive window optimization method was demonstrated and also shown to outperform matching pursuit.

An automatic newborn EEG seizure detection algorithm was proposed based on the detection of repetitive spikes using the adaptive window optimization method. The algorithm shows excellent performance with real EEG data. A comparison of the proposed algorithm with four well documented newborn EEG seizure detection algorithms is provided. The results of the comparison show that the proposed algorithm has significantly better performance than the existing algorithms (i.e. Our proposed algorithm achieved a good detection rate (GDR) of 94% and false detection rate (FDR) of 2.3% compared with the leading algorithm which only produced a GDR of 62% and FDR of 16%).

In summary, the novel contribution of this thesis to the fields of time-frequency signal processing and biomedical engineering is the successful development and application of sophisticated algorithms based on adaptive time-frequency signal processing techniques to the solution of automatic newborn EEG seizure detection.

Contents

List of Figures

List of Tables

Acronyms and Abbreviations

ARMA	Autoregressive Moving Average
ASPEC	Adaptive Spectrogram
BP	Basis Pursuit
BT	Bandwidth–Duration
CA	Conceptional Age
CNS	Central Nervous System
CP	Cosine Packet
CW	Choi–Williams
CWD	Choi–Williams Distribution
ECG	Electrocardiogram
ECoG	Electrocorticogram
EEG	Electroencephalogram
EMG	Electromyogram
EOG	Electrooculogram
FD	Fractal Dimension
FDR	False Detection Rate
FFT	Fast Fourier Transform
FM	Frequency Modulated
FN	False Negative
FP	False Positive
FT	Fourier Transform
GDR	Good Detection Rate
HSSI	Histogram of Successive Spike Intervals
IAF	Instantaneous Autocorrelation Function
IF	Instantaneous Frequency
LFM	Linear Frequency Modulated

MB	Modified B
MDL	Minimum Description Length
MP	Matching Pursuit
MSTFT	Modified Short–Time Fourier Transform
NICU	Neonatal Intensive Care Unit
NEO	Nonlinear Energy Operator
OMP	Orthogonal Matching Pursuit
OWS	Optimal Window Scale
pdf	Probability Density Function
QTFD	Quadratic Time–Frequency Distribution
RID	Reduced Interference Distribution
SBR	Seizure to Background Ratio
SC	Structural Complexity
SNEO	Smoothed Nonlinear Energy Operator
SNR	Signal to Noise Ratio
SPWVD	Smoothed Pseudo Wigner–Ville Distribution
SSA	Singular Spectrum Analysis
STFT	Short–Time Fourier Transform
SVD	Singular Value Decomposition
TF	Time–Frequency
TFR	Time–Frequency Representation
TFSA	Time–Frequency Signal Analysis
TFSP	Time–Frequency Signal Processing
TFSS	Time–Frequency Signal Synthesis
TP	True Positive
WP	Wavelet Packet
WT	Wavelet Transform
WVD	Wigner–Ville Distribution

Authorship

The work contained in this thesis has not been previously submitted for a degree or diploma at this or any other higher educational institute. To the best of my knowledge and belief, the thesis contains no material previously published or written by another person except where due reference is made.

Signed: .....

Date: .....

Acknowledgments

I would like to begin my acknowledgments by thanking my principle supervisor, Prof. Boualem Boashash, for introducing me to the subject of time–frequency signal processing, guiding my research to the interesting topic of biomedical signal processing and providing a wonderful working environment. I would also like to express my deepest gratitude to my associate supervisor, Dr. Mostefa Mesbah, for his time spent reviewing this thesis, and other technical documents, as well as his time and guidance during the countless number of impromptu meetings over the duration of my PhD.

Many thanks go out to the former and current administrative staff and students of the signal processing laboratory, formerly the signal processing research centre (SPRC). In no particular order, Ali, Calvin, Dan, Hamid, John, Malar, Nathan, Peggy, Shobhna and Victor have all contributed in some way, shape or form over the duration of this PhD, which has helped me in arriving at this point.

I am thankful to Prof. Paul Colditz from the Perinatal Research Centre (PRC), who provided the real newborn EEG data used in this research project. Acknowledgments also go to Dr. Chris Burke and Ms. Jane Richmond, from the Neurosciences Department of the Royal Childrens Hospital in Brisbane, for their medical expertise and precious time in reviewing and labeling the newborn EEG data.

I would like to express my appreciation to my lovely girlfriend, Rheannon, for partnering me through the final stages of this PhD and helping with the editing of this document.

Finally a very *special* thank you goes to my parents and sister for everything they have done for me. I am indebted to my mum and Chuck for all their support, encouragement and assistance over my entire tertiary education, which I deeply appreciate.

Preface

It has been a winding path to this thesis' end, and one which has explored some of the diverse areas in which signal processing is applicable. I was introduced to the fundamentals of signal processing and its possible applications in the aerospace industry throughout my undergraduate degree. I further developed my signal processing skills during my honours year, taking on a project with Prof. Boashash in mobile communications. This project was my conception to the field of time–frequency signal processing and its powerful ability in representing nonstationary signals often encountered in real applications. On finishing my undergraduate degree, I continued working as a research assistant in the signal processing research centre, analysing the newborn EEG signal using time–frequency signal analysis techniques. This work inspired my continued research in this area and helped define the topic of this thesis.

A significant aspect of the newborn EEG signal, in particular the newborn seizure EEG, is its nonstationarity. This implies that time–frequency techniques are highly suitable for the analysis and processing of the newborn EEG. However, there are a multitude of techniques for providing joint time–frequency representation. Therefore, how is a specific technique decided upon? The answer is "Assessment of available techniques."

Throughout this thesis, I have enjoyed investigating many time–frequency signal processing techniques. It has also been quite interesting to see how fundamental time–frequency techniques can be presented in a number of ways, depending on the authors ideas on these topics. Understanding the links between various time–frequency techniques and the benefits of particular techniques over others in certain applications has helped immensely in the completion of this thesis.

A number of detection algorithms, with application to newborn EEG seizure, are developed in this thesis. Mostly, they are derived using multiple time–frequency techniques to benefit from their particular advantages.

It is my hope that the results of this research will be a benchmark for others to compare newly proposed newborn EEG seizure detection algorithms against and motivate further research in this area. Hopefully, it will also emphasize the advantages of

broadening one's signal processing skills.

Luke Rankine
Brisbane, Australia
April 2005

Chapter 1

Introduction

Biomedical signals are key tools used by physicians for monitoring the health of patients. They originate from various biological systems which include; the digestive, musculoskeletal, respiratory, circulatory and nervous systems [2]. These signals are recorded in various forms, such as pressure, temperature or electric potential [3]. There are numerous reasons for recording biomedical signals such as diagnosis, monitoring of health, research, therapy and prognosis [2]. All of which aim to improve the overall level of health care for the community.

Bioelectrical signals, which are specific types of biomedical signals, are obtained by electrodes that record the variations in *electrical* potential generated by a physiological system. Bioelectric potentials result from large groups of neural or muscular cells producing an electric field which propagates through various tissues in the body [3].

Electroencephalogram (EEG), electrooculogram (EOG), electrocardiogram (ECG) and electromyogram (EMG) are a few bioelectric signals which are used regularly in the clinic. The EEG is used to monitor neural activity, EOG to record eye movement, ECG to assess heart functioning and EMG to measure muscular activity. There are copious amounts of information regarding the health of a biological system attainable from bioelectric signals. However, information relating to particular pathologies is not always clear from the raw bioelectric recording. This is where the field of biomedical signal processing can assist.

Biomedical signal processing involves the manipulation, or transformation, of biomedical signals to enhance the relevant information in the recorded signals for accurate diagnosis and prognosis. Another facet of biomedical signal processing, particularly due to the emergence of digital signal processing and powerful digital computers, is the ability for automatic detection and classification of pathological events. This is currently a major area of research as it has the potential to provide many health and economic

benefits to the community.

1.1 Motivation of Research

Seizures are the result of excessive, synchronized electrical discharges from a collection of neurons. They are caused by a number of brain abnormalities and are expressed through physical manifestations and particular EEG characteristics.

In the newborn, seizures are the most frequent and sometimes only clinical sign of central nervous system (CNS) pathologies [4]. Seizure events in the newborn are of great concern for physicians because of the possible cause of the brain disorder as well as the effects they may have on the developing brain. Some major causes of neonatal seizures include; energy failure (e.g. hypoxic–ischaemic encephalopathy), metabolic disturbances (e.g. hypoglycemia, hypocalcaemia), cerebrovascular lesions (e.g. intracranial hemorrhage), and infections (e.g. bacterial meningitis, herpes, syphilis and rubella) [5].

The highest incidence of seizure occurs during the neonatal period. This is due to the immature brain having particular features that make it more susceptible to seizure generation. These factors include enhanced cellular excitation, enhanced synaptic excitation and enhanced propagation of an epileptic discharge [4]. The incidence rate of seizure in newborns is in the range of 0.15% to 0.55% [4]. It was found that the incidence of seizure is correlated with the birth weight of the neonate. The incidence rate for very low birth weight neonates (i.e. less than 1,500g) was found to be 10 times greater than the average incidence rate [6, 7]. High risk newborns (i.e. those with energy failure, metabolic disturbances, cerebrovascular lesions or infections) have an incidence rate of 25%.

There are two signs of newborn seizure; clinical and electrical. Clinical seizures are recognized by certain physical manifestations while electrical seizures are identified by particular abnormal patterns (i.e. ictal patterns) that are observed in the EEG. These seizure signs may occur simultaneously or separately. EEG seizure without clinical manifestations is called *subclinical*.

Clinical seizures are characterized by sucking, chewing, tongue protrusions, twitching, drooling, ocular fixation, foaming at the mouth, rowing or swimming movements of arms and pedaling or bicycling movements of the legs [4, 8]. However, some of these characteristics are also normal behaviour in newborns. Therefore, recognition of these characteristics as seizure attributes often depends on both the skill of the observer, which may be parents, family or medical staff, and length of time that the newborn is being observed. Physical manifestations of newborn seizure are also often very subtle, of short duration and infrequent, making detection of newborn seizure extremely difficult.

The recognition of electrical seizure activity is also more difficult in the newborn than in older children and adults where the electrographic seizure is easily recognizable against the low amplitude background. Neonatal seizures may be covert and their electrographic manifestations erratic and fragmented. Its patterns are also highly variable, with complex and varied frequency content and morphology [8]. Neonatal seizures are progressive in nature with the buildup of rhythmic activity at various frequencies. Another factor that makes detection of EEG seizure difficult in the newborn is the fact that normal babies have a large variety of peculiar electrographic manifestations which can mimic real seizures [9]. Therefore, much care is needing in discerning seizure from nonseizure activity. Because of these difficulties, overdiagnosis of seizure has been a recent occurrence [9].

Identification of seizures is extremely important for evaluating the long term outcome of sick neonates. Since the advent of the neonatal intensive care unit (NICU), mortality and morbidity rates have declined. However, newborn seizures are still significantly related to mortality. Mortality rates associated with newborns suffering seizure range between 21% and 55% [10, 11, 12]. The morbidity statistics of newborns who have experienced seizure events are also poor. Rates of severe handicaps such as spasticity, mental retardation, cerebral palsy, language delay and sensory deficits are between 38% and 56% of those who survive [10, 13].

There are a number of benefits in using the EEG to identify seizure activity in the newborn. Often neonates, especially premature neonates, are paralyzed for artificial respiration. In this case, clinical manifestations are subdued, leaving the EEG as the only method of assessing the CNS [9]. The EEG also can provide unique information for diagnosis and therapy of seizures [8].

The complexity of EEG recordings usually requires a neurologist to identify seizure events. However, due to the often infrequent nature of neonatal EEG seizure, lengthy recording sessions are required to capture EEG seizure events. The review process is an arduous and time consuming task. Therefore, an accurate automatic seizure detection method is highly desirable as it removes the need for a neurologist to review an entire EEG recording.

Continual excessive discharge of neurons that occurs during seizure may cause permanent brain damage [14]. Therefore, the early detection of newborn seizure is vital in minimizing the brain injury [1]. In full term neonates with hypoxic-ischaemic encephalopathy, for example, it may be possible to reduce delayed neural death or programmed cell death [15]. The duration of the window for therapeutic intervention is considered to be 2–6 hours after birth asphyxia. The treatment, however, may have serious side effects which means early and accurate detection of seizures is important.

Therefore, online automatic detection of neonatal seizures may play a pivotal role in preventing or reducing brain damage.

1.2 Existing Newborn EEG Seizure Detection Techniques

A number of methods for seizure detection have previously been proposed using a variety of signal processing techniques. These techniques can be divided into two broad classes, namely; stationary and nonstationary. However, it has been shown that the newborn EEG signal is highly variable and nonstationary. Therefore, the assumption of stationarity implied by using stationary signal processing techniques is inaccurate and leads to suboptimal detection algorithms [16].

In this section, we provide a review of the most widely cited automatic EEG seizure detection algorithms for the newborn. The techniques reviewed are classified into either stationary or nonstationary techniques.

1.2.1 Stationary Techniques

The term stationary was originally defined in statistics to describe a particular type of random process [17]. Generally speaking, a random process is said to be stationary if all of its statistical properties do not change with time [18]. All other random processes are referred to as non-stationary. However, for a deterministic signal, which is characterized by the ability to predict future values from past values, the term stationary refers to those signals whose power spectra are independent of time.

The autocorrelation function is a time domain analysis tool. It is a useful method of assessing the similarity of a signal with itself over varying time shifts and hence, periodicity in the signal. The autocorrelation function of a deterministic signal, $x(t)$, is given by

$$R_{xx}(\tau) = \int_{-\infty}^{\infty} x(t)x(t+\tau)dt \tag{1.1}$$

It can be seen that the autocorrelation function is a function of the variable τ only, which represents a time shift of the signal x. This indicates that the autocorrelation function cannot accurately represent the time–varying information contained in nonstationary signals.

A seizure detection algorithm, developed by Liu et al. [19], incorporated the autocorrelation function to assess the periodicity of the signal as the algorithm assumes that the EEG seizure is a periodic signal. The details of the algorithm are as follows.

In this method, each EEG channel was segmented into epochs of 30 seconds. The

epochs were further subdivided into 5 windows, as shown in Figure 1.1, and 5 autocorrelation functions were obtained. For periodic behaviour, peaks of the autocorrelation function are separated by the same time difference. Therefore the ratio of the time differences between peaks of the autocorrelation function were used as the distinguishing feature for this algorithm.

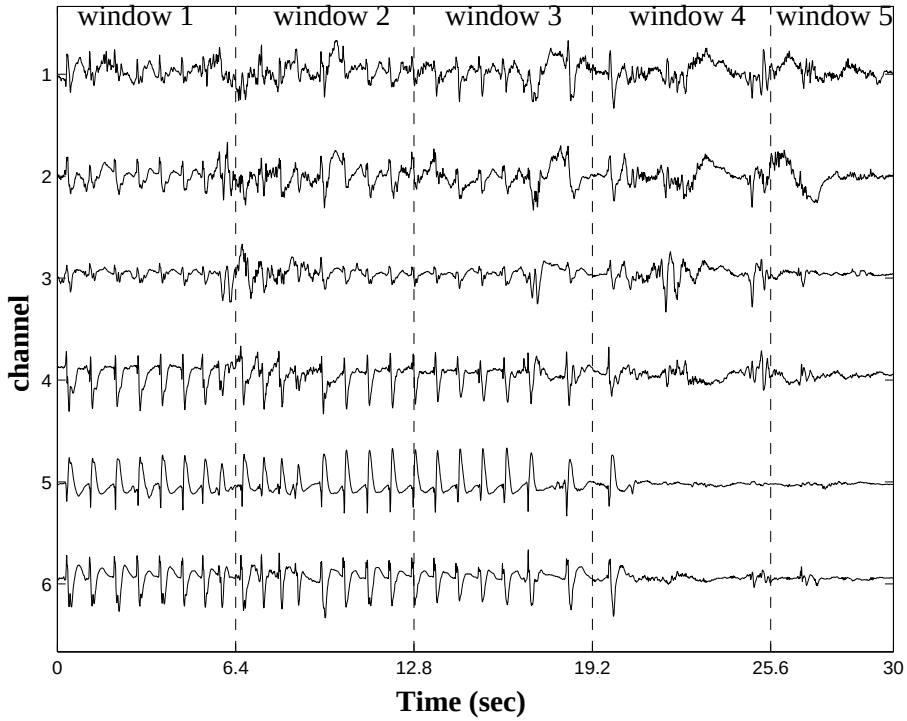

Figure 1.1: Liu's method of windowing epochs for autocorrelations to be calculated.

Liu assumed that the newborn EEG is stationary over a 6 second epoch. However, it has been shown that the EEG can have major variations in frequency content for periods less than 6 seconds [20]. Therefore, the assumption of local stationarity and a periodic seizure signal are not always satisfied. This means that accurate detection of seizure cannot always be achieved.

Spectral estimation is one of the key analysis tools used in all facets of applied signal processing. The frequency content is commonly used as a feature of EEG to help in classification, diagnosis and interpretation. The Fourier transform (FT) is a linear integral transform that provides a frequency domain representation. The FT of a signal $x(t)$ is given as

$$\mathcal{F}\{x(t)\} = X(f) = \int_{-\infty}^{\infty} x(t)e^{-j2\pi ft}dt \tag{1.2}$$

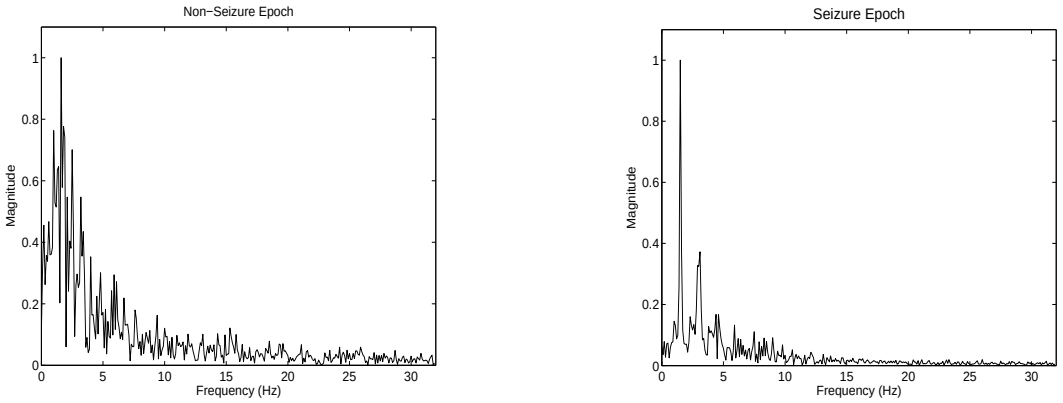

Figure 1.2: Two epochs, one nonseizure and one seizure, are shown here to have significant differences in the frequency domain.

where $\mathcal{F}\{\cdot\}$ is called the FT *operator* and $e^{j2\pi ft}$ is the FT *kernel*. To obtain a power spectrum, $S(f)$, we take the square magnitude of (1.2). An alternative method of obtaining the power spectrum is through the Wiener-Khintchine theorem [18, 21]. This theorem states that the power spectrum of a stationary signal can be attained through the FT of its autocorrelation function (1.1).

In [22], a method for automatic seizure detection using the power spectrum was presented. Spectral analysis was used to find rhythmic discharges at various frequencies. In this method the FT was applied to a sliding window of 10 seconds. Features such as dominant frequency, width of dominant frequency and power ratio between dominant frequency bands were extracted from an epoch. These features were then compared to the same features of 2 previous epochs, which were approximately 60 seconds behind. Therefore, this method attempts to discriminate between seizure and nonseizure using the differences exhibited in the frequency domain. An example of this is shown in frequency domain representations in Figure 1.2, of a nonseizure epoch and a seizure epoch.

Problems with this method result from the assumption of stationarity. Firstly, due to the nonstationary nature of the newborn EEG signal, significant differences in the spectrum of two epochs spaced 60 seconds apart may result even when seizure is not occurring [20, 23]. Therefore, this may lead to false seizure detections. Also, frequency content within the 10 second analysis epoch, which is assumed to be stationary, can be highly time-varying [20]. Therefore, only suboptimal features can be extracted from the frequency domain analysis of a 10 second newborn EEG epoch.

In [1], a model–based approach for seizure detection was proposed. For this detection scheme, a model of newborn EEG, which included both background and seizure, was

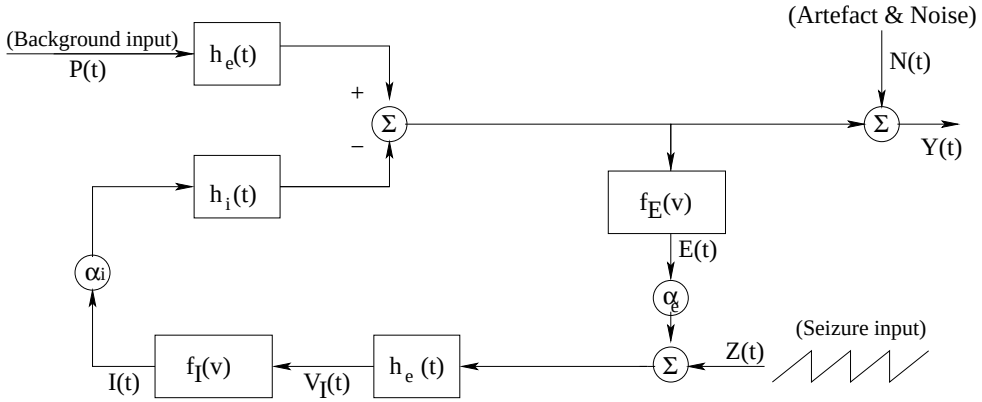

Figure 1.3: Schematic of newborn EEG model proposed by Roessgen et al. [1].

proposed. The model architecture is shown in Figure 1.3, and is an extension to the model proposed by Lopes Da Silva et al. [24]. In the model, $Z(t)$ is used to model the seizure generating signal, and is chosen as a random repetitive waveform. The background generating signal, $P(t)$, is assumed to be stationary, zero mean, white Gaussian noise.

The full EEG model in Figure 1.3 consists of 11 model parameters. To detect seizure events in real newborn EEG, the model parameters are firstly estimated from the real EEG using *Whittle's* approximation. If the estimated model parameters for the real EEG are close to the seizure model parameters, then a seizure detection is scored.

This method had limited success due to the extremely complex system it is trying to model. Assumptions in the model such as generating the background using stationary white Gaussian noise are incorrect as it has been shown that the EEG is nonstationary and non-Gaussian [20, 25]. Another drawback of this model–based approach, as stated in [26], is that the model parameters may never converge accurately when estimating for real EEG signals. It was also shown that the autocorrelation–based technique of Liu et al. [19] and the power spectrum–based technique of Gotman et al. [22] both gave better performance than the model–based parametric approach [26].

A method for detecting seizure in infants using a singular spectrum analysis (SSA) approach was presented in [27]. The motivations for using an SSA approach was its good performance with quasi-periodic signals and the robustness to noise of the singular value decomposition (SVD) process used in the SSA method.

This method begins with a preprocessing stage which attempts to whiten the background signal prior to SSA. A nonlinear function [27] is used to Gaussianize the data before a whitening filter, derived from the inverse of an ARMA model of the newborn EEG background, is used to whiten the background. This process, however, does not

affect the rhythmical characteristics of the newborn EEG seizure. Therefore, seizure detection can be made by detecting the period for which the signal is not Gaussian white noise.

After the whitening preprocessing step, the signal is converted into a trajectory matrix so that the signal part and noise part can be separated. The signal space is related to the n_0 largest singular values in the SVD of the trajectory matrix. The number n_0 is determined using the Rissanen's minimum description length (MDL) method [28]. If the value is $n_0 = 1$, the signal is pure white noise, and if $n_0 > 1$ a nonstochastic component exists. The SSA–based newborn EEG seizure detection algorithm is shown in Figure 1.4.

The SSA approach has a major flaw in that it uses a time-invariant model of the newborn EEG for the whitening preprocessing stage. The newborn EEG is a dynamic nonstationary signal. Therefore, the whitening process may not correctly whiten sections of the background, leading to false alarms.

1.2.2 Nonstationary Techniques

Due to the time–varying frequency content of the EEG signal, signal processing techniques capable of handling nonstationarity in the signal are the best techniques to be used for automatic seizure detection. Joint time-frequency representations (TFRs) can be used to track the frequency content as it evolves over time. Therefore, a number of recent seizure detection algorithms have incorporated time-frequency signal processing (TFSP) techniques. In this section, we briefly introduce the various TFSP techniques that have been used for the detection of EEG seizure in newborns. A thorough review of TFSP will be presented in chapter 3.

Quadratic time-frequency distributions (QTFDs) are a class of methods for obtaining a TFR and have been used in the development of seizure detection algorithms. The general form of a QTFD is given as the convolution of the Wigner-Ville distribution with a time-frequency filter and may be expressed as:

$$E_z(t,f) = \int_{-\infty}^{\infty}\int_{-\infty}^{\infty}\int_{-\infty}^{\infty} g(\nu,\tau)z(u+\tfrac{\tau}{2})z^*(u-\tfrac{\tau}{2})e^{j2\pi(\nu t-\nu u-f\tau)}dud\nu d\tau \qquad (1.3)$$

where $g(\nu,\tau)$ is the Doppler-lag kernel which uniquely defines the QTFD [29].

In [16, 20], the authors characterized seizure patterns in the TF domain using a QTFD. A TF template for seizure was created using observations from their TF analysis. A 2D cross–correlation process in the TF domain, using the seizure template and the TFD of EEG epochs, was then used to identify seizure events.

A limitation of this technique is that a large number of TF seizure templates are

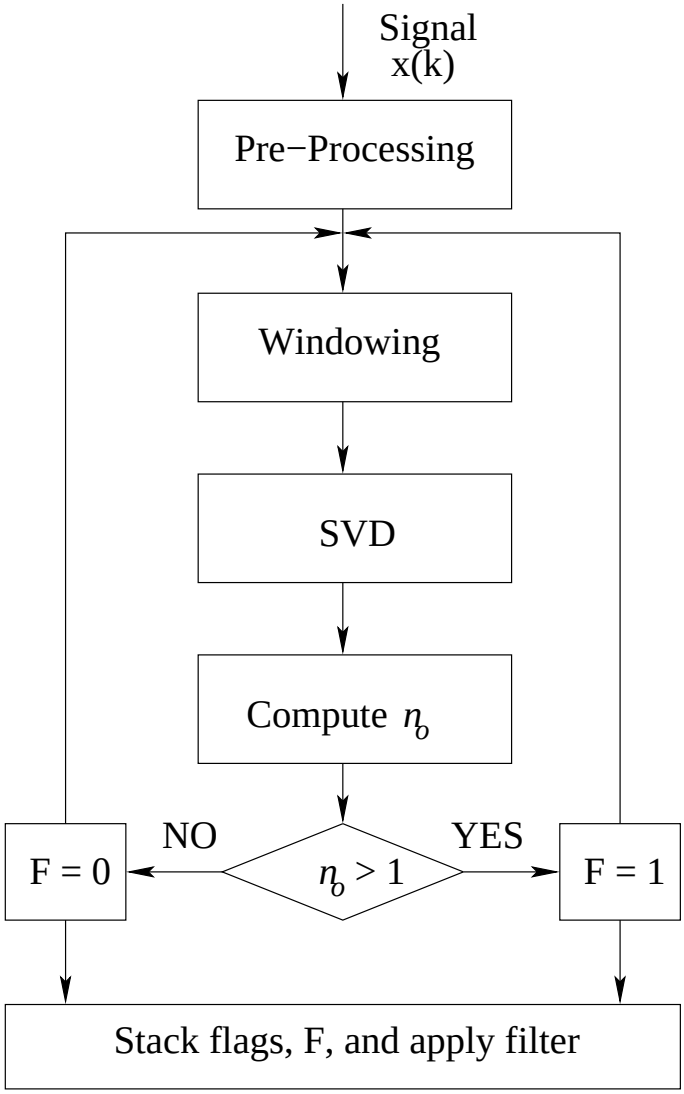

Figure 1.4: Algorithm for seizure detection using SSA-MDL approach.

needed for accurate seizure detection. This then leads to excessive computation times because of the 2D correlation process.

In [30, 31], a method of detecting spikes in the EEG signal using QTFDs was defined. It was shown that the high frequency area of the TF domain could be used to detect spikes and that the distribution of time intervals between successive spikes differed between seizure and nonseizure epochs. The distribution of time intervals between successive spikes were then characterized using a histogram of successive spike intervals (HSSI). A number of HSSI which represented different seizure classes were formed. An automatic seizure detection algorithm, which compared the HSSI of an EEG epoch to the defined HSSI seizure templates using the Jensen function [32] for similarity, was proposed.

In [33], a method of seizure detection based on the SVD of the TFR using a QTFD was proposed. It was shown that the first and second, left and right singular vectors of the TFR differed between seizure and nonseizure epochs. It was suggested that the singular vectors characterized the low frequency signature of newborn EEG seizure. A two-layer feed forward neural network was used to classify the EEG data into seizure and nonseizure.

The SVD-based method was combined with the HSSI-based method to provide a seizure detection algorithm which could detect both the high frequency and low frequency signatures of newborn EEG seizure. However, both methods require training for the template design (i.e. HSSI and singular vectors). This requires a large database of seizures, but these templates were designed using only a small data set. Also, both techniques use QTFDs for TFR but it was shown in [34] that a single QTFD cannot simultaneously show spike activity and long duration slow frequency activity optimally. For this, an adaptive TFR such as the adaptive spectrogram (ASPEC), defined in Chapter 6, is needed.

Wavelet transform (WT) is another nonstationary signal processing technique that has become popular for analyzing transient signals. In [35], features such as the mean and variance of particular coefficients from the WT were chosen as possible features for distinguishing between seizure and nonseizure EEG signals. From these list of features, an optimal subset of features was derived using the mutual information evaluation function [36]. The optimal discriminating features were fed to an artificial neural network classifier for automatic seizure detection. A limitation of this algorithm, however, is that the artificial neural network was only trained using the EEG from one baby. This training set is not adequate as EEG patterns vary significantly within patients and between patients. Therefore, the algorithm would need to be reassessed using a larger database.

Analysis of **adult** EEG using an adaptive time-frequency (TF) method known as matching pursuit [37] has been undertaken in [38, 39, 40, 41, 42]. This method has many benefits such that it can provide high resolution TFRs without crossterms [40, 37], it can provide information about the nonlinearities associated with a signal [39], and provide a TF parameterization of the signal [42]. This technique has recently been incorporated into an algorithm for seizure detection in the adult [43]. Matching pursuit, however, has not previously been used in the analysis of **newborn** EEG or for the development of automatic newborn EEG seizure detection algorithm.

1.3 Scope, Aims and Objectives

The scope of the thesis includes the analysis of newborn EEG using appropriate nonlinear and nonstationary techniques to determine the significant characteristics of various EEG states. It also includes the development of automatic seizure detection algorithms based on appropriate adaptive time-frequency signal processing techniques. These algorithms should outperform other well documented automatic seizure detection algorithms, but are not required to run online.

The specific aim of this thesis, therefore, is to develop a superior automatic newborn EEG seizure detection algorithm which may be used to aid in better monitoring and treatment of sick neonates. This aim can be achieved by specifying the following objectives:

1. To provide a realistic newborn EEG simulation algorithm based on the nonlinear and nonstationary characteristics of the real EEG signal. (Chapter 4)

2. To investigate the use of atomic decomposition techniques, such as matching pursuit and basis pursuit, in analyzing nonstationary signals. (Chapter 5)

3. To extract EEG seizure features from the newborn EEG using matching pursuit decomposition, and develop an automatic seizure detection methodology based on these features. (Chapter 5)

4. To develop a method of spike detection using adaptive TF techniques and implement the method in an automatic seizure detection algorithm. (Chapter 6)

5. To assess the performance of the proposed newborn EEG seizure detection algorithms using synthetic and real EEG data and compare with previous, well documented, newborn EEG seizure detection algorithms. (Chapter 6)

1.4 Thesis Contributions

The work presented in this thesis contain a number of *original contributions* to the field of biomedical signal processing. The contributions are:

1. We provided a new method for simulating newborn EEG data using both nonlinear and nonstationary analysis and synthesis techniques [23, 44, 45]. (*see Chapter 4, sections 4.2, 4.3 and 4.4*)

2. Basis pursuit was proposed as an atomic decomposition technique which provides the sparsest signal representation. In many signal processing applications, however, only an adequate signal approximation is needed. We have shown that basis pursuit does not always provide a sparser signal approximation than matching pursuit. Indeed, we have shown that matching pursuit generally provides a sparser signal approximation than basis pursuit for various levels of approximation [46, 47]. (*see Chapter 5, section 5.2*)

3. We introduced a new signal complexity measure, referred to as "structural complexity", which is a measure of the coherency between the dictionary used for signal decomposition and signal structures. This measure has been used as a basis for detecting changes in signal structure, such as newborn EEG [47, 48, 49, 50]. (*see Chapter 5, section 5.3*)

4. We developed a new TF dictionary that is coherent with the TF structures found in newborn EEG seizure. Using this dictionary and the structural complexity measure, we were able to detect the transition from non–seizure to seizure states [50]. *(see Chapter 5, section 5.4)*

5. We have shown that the signal length is pivotal for detecting periodic and repetitive spikes when using matching pursuit [51, 52]. Without allowing for this relationship, the performance of detecting repetitive spikes becomes poor. (*see Chapter 6, section 6.4*)

6. We have shown that the adaption algorithm for ASPEC, which optimizes the window length at each time instant, can be used for detecting spikes. It was also demonstrated that this method of spike detection outperformed matching pursuit in detecting repetitive spikes [34, 53]. (*see Chapter 6, sections 6.3 and 6.4*)

7. We developed a new automatic seizure detection algorithm based on the detection of seizure spikes using the optimal window scale method [53]. (*see Chapter 6, section 6.5*)

1.5 Organization of Thesis

This thesis is structured as follows:

Chapter 1 describes the motivation for this research and reviews some previous techniques and methods used for detection of newborn EEG seizure. It also details the objectives and major contributions of this research and outlines an overview of the thesis.

Chapter 2 provides an introduction to the EEG signal. This chapter describes many characteristics of the EEG signal from both clinical (i.e. medical) and signal processing perspectives.

Chapter 3 provides a detailed review of current TFR methods. This includes linear and quadratic time-frequency distributions, time-scale transforms, and relevant atomic decomposition techniques. The ability of TFR methods to relay the time–varying information associated with nonstationary signals is demonstrated.

Chapter 4 proposes a new method of simulating the newborn EEG signal. The simulation of background EEG begins with the fractal dimension (FD) analysis of real newborn EEG background. It is assumed that the FD estimate is a random variable and an estimate of the distribution is given. Using FD theory and the estimated distribution, a background EEG simulator is derived. (*Answers Objective 1*)

The proposed method for newborn EEG seizure simulation is based the time-frequency signal synthesis (TFSS) of simulated seizure TFRs. Comparison in the time, frequency and TF domain between real and simulated signals show the validity of the simulation methods. (*Answers Objective 1*)

Chapter 5 compares the sparsity of matching pursuit and basis pursuit signal approximations. It is determined that matching pursuit generally provides a sparser signal approximation. For this reason, matching pursuit is the preferred atomic decomposition technique to be used in this thesis. (*Answers Objective 2*)

A new signal complexity measure, referred to as *structural complexity,* obtained using matching pursuit is defined. A generic method for detecting changes in signal structure is proposed based on a change in the structural complexity. This methodology for detecting changes in signal structure is then applied to newborn EEG. To optimize the use of SC for the newborn EEG case, we create a TF dictionary that is coherent with the newborn EEG seizure structures. (*Answers Objective 3*)

Chapter 6 reviews a number of spike detection algorithms. The ability of TFSP techniques to detect repetitive spikes is investigated. It is demonstrated that epoch length is pivotal in the ability of MP to detect the individual spikes of a repetitively

spiking signal.

ASPEC is shown to be a better TF technique for detecting the individual spikes of a repetitively spiking signal than MP. The adaption algorithm for ASPEC, which determines the optimal window scale at each time instant, was also demonstrated to be a valid spike detection method and shown to outperform the MP-based technique. (*Answers Objective 4*)

A seizure detection algorithm, based on the ability to detect repetitive spikes using the optimal window scale method, is proposed. This algorithm is evaluated using two performance assessment methods and is compared to four well-documented newborn EEG seizure detection algorithms. (*Answers Objective 5*)

Chapter 7 gives a summary of the work undertaken and provides a number of conclusions based on the results in the thesis. It also outlines recommendations for future research in this area.

1.6 Author's Publication List

The following is a list of publications that have been written by or in conjunction with the author during his PhD candidacy:

1. ([46]) L.J. Rankine and M. Mesbah, "Significant Atom Determination of Basis Pursuit Decomposition," *Proc. International Symposium on Signal Processing and its Applications,* Paris, France, July 2003, pp. 573-576

2. ([49]) L.J. Rankine, M. Mesbah and B. Boashash, "Atomic Decomposition Complexity for Seizure Detection in Neonates," *Proc. International Federation for Medical and Biological Engineering,* Sydney, Australia, Aug. 2003, CD-ROM

3. ([47]) L. Rankine, M. Mesbah and B. Boashash, "Atomic Decomposition for Detecting Changes in Signal Structure: Application to EEG," *International Conference on Biomedical Engineering,* Innsbruck, Austria, Feb. 2004, pp. 285-288

4. ([50]) L. Rankine, M. Mesbah and B. Boashash, "A Novel Algorithm for Newborn EEG Seizure Detection using Matching Pursuits with a Coherent Time-Frequency Dictionary," *Proc. International Conference on Scientific and Engineering Computation,* Singapore, July 2004, CD-ROM

5. ([48]) L. Rankine, M. Mesbah and B. Boashash, "Newborn Seizure Detection using Signal Structural Complexity," *EUSIPCO 2004,* Vienna, Austria, Sept. 2004, pp. 2207-2210

6. ([45]) N. Stevenson, L. Rankine, M. Mesbah and B. Boashash, "Newborn EEG seizure simulation," *Workshop on Digital Image Computing,* Brisbane, Australia, Feb. 2005, pp. 145-150

7. ([23]) L. Rankine, H. Hassanpour, M. Mesbah and B. Boashash, "EEG simulation using fractal dimension analysis," *Thirteenth Iranian Conference on Electrical Engineering,* vol. 3, Zanjan, Iran, May 2005

8. ([34]) L. Rankine, N. Stevenson, M. Mesbah, and B. Boashash, "A Quantitative Comparison of Non-Parametric Time-Frequency Representations," *EUSIPCO 2005* Antalya Turkey, Sept. 2005, CD-Rom

9. ([51]) H. Hassanpour, L. Rankine, M. Mesbah and B. Boashash, "Comparative Performance of Time-Frequency Based EEG Spike Detection," *EUSIPCO 2005* Antalya Turkey, Sept. 2005, CD-Rom

10. ([52]) L. Rankine, M. Mesbah and B. Boashash, "Improving the Ability of Matching Pursuit Algorithm in Detecting Spikes," *EUSIPCO 2005,* Antalya Turkey, Sept. 2005, CD-Rom

11. ([53]) L. Rankine, M. Mesbah and B. Boashash, "Automatic newborn EEG seizure spike and event detection using adaptive window optimization," *Proc. IEEE International Symposium on Signal Processing and its Applications,* vol. I, Syndey, Australia, Aug. 2005, pp. 187-190

12. ([44]) L. Rankine, H. Hassanpour, M. Mesbah and B. Boashash, "Newborn EEG Simulation from Nonlinear Analysis," *Proc. International Symposium on Signal Processing and its Applications,* vol. I, Syndey, Australia, Aug. 2005, pp. 191-194

1.6.1 Publications in Preparation

The following is a list of publications currently under preparation for submission.

1. L. Rankine, N. Stevenson, H. Hassanpour, M. Mesbah and B. Boashash, "Simulation of the Newborn EEG Background and Seizure States," *To be submitted to the International Journal of Modelling and Simulation*

2. L. Rankine, M. Mesbah and B. Boashash, "Automatic Newborn EEG Seizure Detection using Adaptive Time-Frequency Signal Processing," *To be submitted to the IEEE Transactions on Biomedical Engineering*

Chapter 2

Newborn EEG Signal Characteristics

2.1 Introduction

Richard Caton's discovery in the late 19th century, that *"feeble currents of varying direction pass through the multiplier when electrodes are placed on two points of the external surface, or one electrode on the grey matter and one on the surface of the scull"* of rabbits and other animals is believed to be the beginning of the EEG [54]. However, it wasn't until 1929 that Hans Berger first demonstrated electrical activity in the human brain [54, 55].

The EEG has many uses as a diagnostic and prognostic tool. Primarily, the EEG is used in the assessment of the CNS and diagnosis of neurological diseases [56]. The EEG is extremely useful in the management of epileptic patients. Other uses of the EEG include localization of abnormal brain structures [57], investigation of patients with neurological and psychiatric disorders [58] and the monitoring of patients with metabolic disorders [59]. The EEG is also used for studying sleep disorders and for evaluating states of consciousness [59, 60].

In this chapter we review the characteristics of the newborn EEG signal. In section 2.2 we summarize the neurophysiological mechanisms responsible for the newborn EEG signal. The methods of recording the EEG signal are presented in section 2.3. The characteristics of the newborn EEG signal associated with the normal and abnormal background EEG state, along with the characteristics of the seizure state, are then presented in section 2.4.

2.2 EEG Neurophysiology

The basic mechanism of the CNS is the neuron (nerve cell). CNS functioning results from the depolarization and hyperpolarization of the neuron membrane, which is caused by ion flux across the membrane. The depolarization of membranes causes an action potential generation. This releases neurotransmitters from presynaptic regions to either excitatory or inhibitory postsynaptic receptors resulting in excitatory postsynaptic potentials or inhibitory postsynaptic potentials respectively [4, 61]. Figure 2.1 shows a diagram of a CNS neuron and displays a zoomed picture of the synapse, demonstrating the presynaptic and postsynaptic regions. Figure 2.2 illustrates the neurotransmitter process, with the density of ions, shown by the number of '+' and '-' signs, indicating the polarization. In normal brain functioning there is an equilibrium between excitatory and inhibitory processes [4], and, as a consequence, neurons fire randomly and asynchronously.

2.3 Recording Methods

Significant differences exist in the EEG recorded from the scalp and the cerebral cortex[1]. The cortical EEG, also referred to as the electrocorticogram (ECoG), is a measure of neural activity in the neighbourhood of the electrode whereas the scalp EEG is an average of the diverse activities of many small regions of the cortical surface in proximity to the scalp electrode [64]. The amplitude of the scalp EEG is generally much smaller than the ECoG unless a significant area of the cortical region under the scalp electrode is synchronized. This then results in comparable amplitudes between the scalp and cortical EEG.

Differences in frequency content exist between the scalp EEG and ECoG. Observations have revealed that the ECoG contained more power in higher frequencies than the scalp EEG due to the higher frequencies tendency to be spatially coherent over small cortical surface areas and the scull acting as a low pass filter [65, 66]. Also, the ECoG is generally unaffected by artifacts resulting from eye movements and muscle contractions, unlike the scalp EEG [67]. However, the invasive nature of the ECoG restricts its clinical use, leaving the scalp EEG as the primary method of analyzing the CNS of the newborn.

[1] The brain has three major parts, the cerebrum, cerebellum and brain stem. The cerebrum consists of two hemispheres and the cerebral cortex, which is the extensive outer layer of gray matter. The cerebral cortex is responsible for higher brain functions such as mathematical abilities, voluntary muscle movement, reasoning, and perception [62, 63]. A detailed description of human brain anatomy is given in [64].

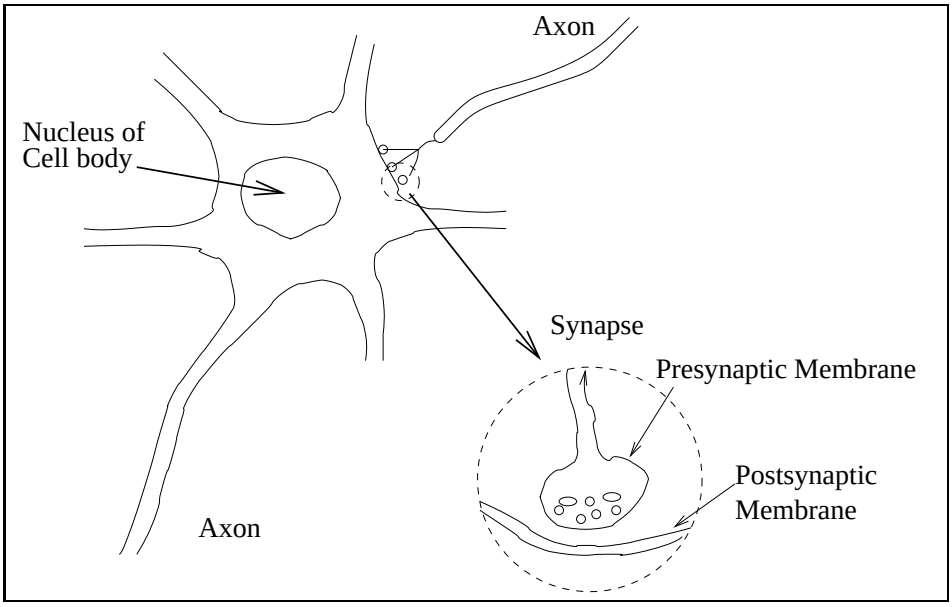

Figure 2.1: A neuron of the CNS, with a zoomed view of the synapse.

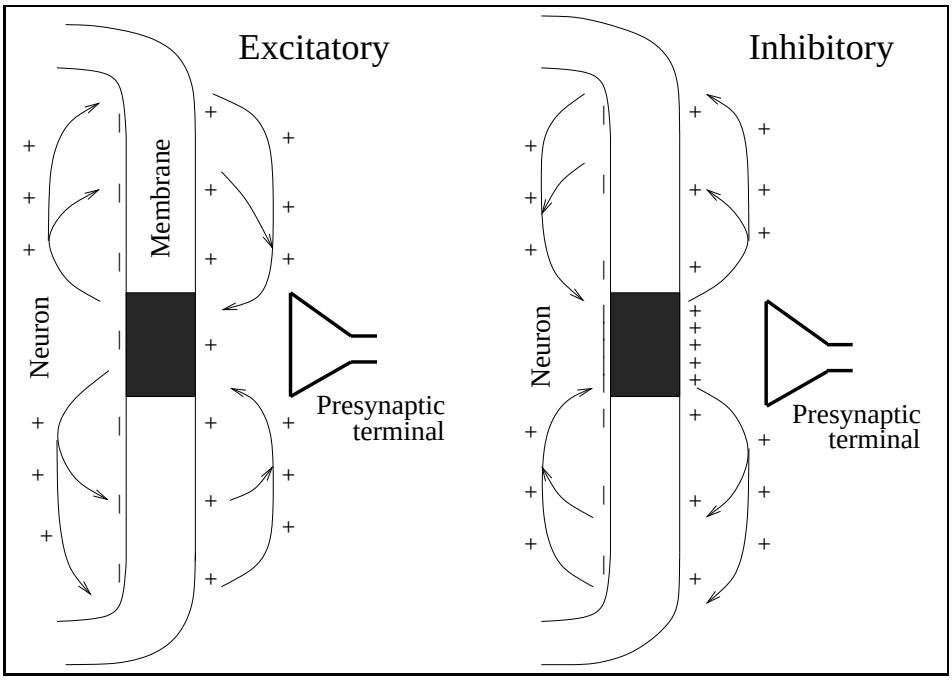

Figure 2.2: The ionic current flows around the synapse (shown in Figure 2.1) through the neuronal membrane and along the membrane, demonstrated by the arrows.

Most recordings of scalp EEG involve the placement of electrodes over the head according to the International 10-20 standard. Twenty one electrode sites are defined under the 10-20 standard [68] and they are determined by four standard positions on the

head: the nasion, inion, and left and right preauricular points [59]. The 10-20 standard of electrode placement is shown in Figure 2.3 where odd numbers refer to the left side and even numbers refer to the right side.

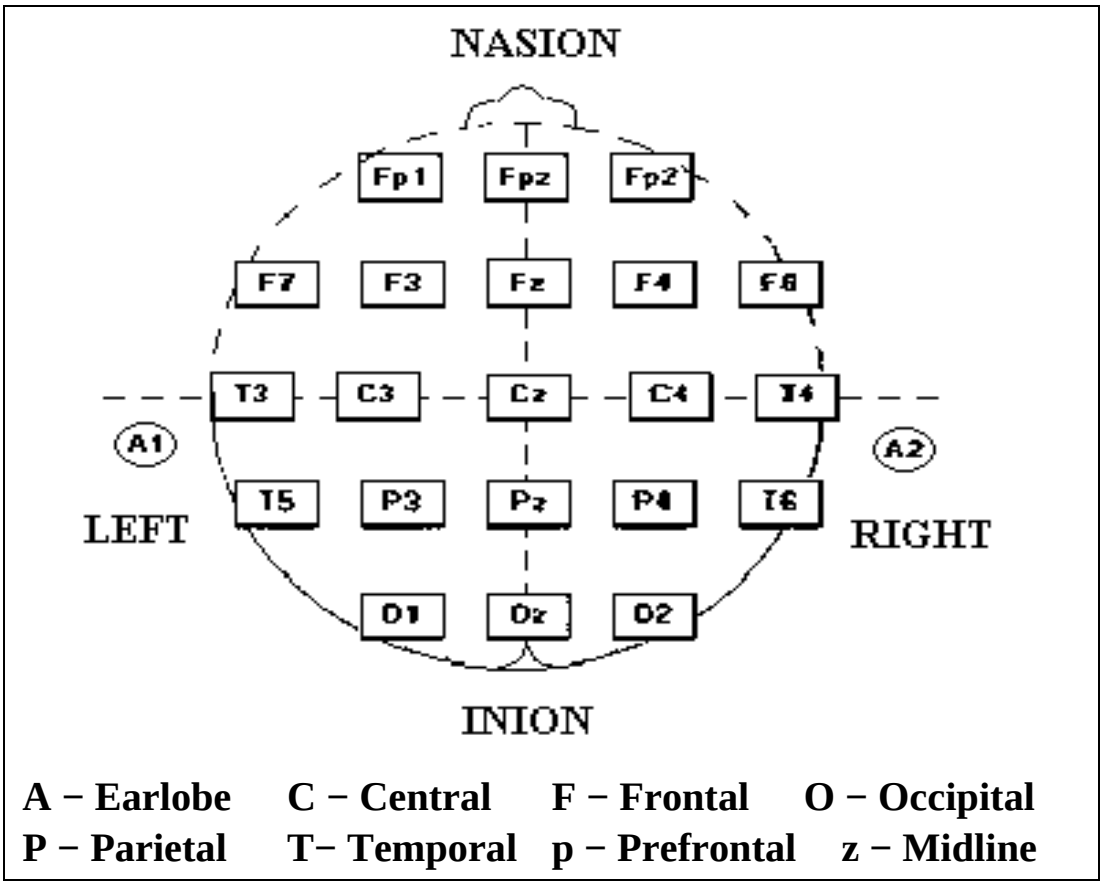

Figure 2.3: International 10-20 standard of electrode placement.

The EEG is a voltage measurement, which infers that a potential difference is recorded. The *montage* is the method by which the potential difference between electrode sites are selected as EEG channels. Two montages recommended by the American EEG society are bipolar and referential (monopolar) montages [68]. In bipolar montage, an EEG channel is obtained by measuring the potential difference between two adjacent electrode sites. This method of recording removes common electrical activity between the two electrode sites such as unwanted artefacts, but may exclude some important EEG information localized around either of the recording sites. In the referential method, a common reference electrode to all EEG channels is used. Usually, it is placed away from the scalp on either the chin, nose or ear to minimize the possibility of including potentials from the brain [62]. This method of recording provides a localized

representation of electrical activity but may be hindered by its susceptibility to noise and artefact.

2.4 Characteristics of Newborn EEG

2.4.1 Background

The EEG signal is a complex waveform that, in the first instance, appears to be some form of noisy signal. For epileptic patients, the EEG can be divided into a background state (i.e. when seizure is not occurring) and a seizure state. The background EEG activity is characterized by patterns that are relatively stable, and is generally without major temporal changes in frequency and voltage [69, 9].

The frequency content of the background EEG has no clear upper and lower boundaries. However, current EEG measuring equipment generally concentrate on capturing the clinically relevant range of between 0.1Hz to 100Hz [70]. This frequency range is divided into a number of bands. These bands, designated by Greek letters, are defined as:

- Delta (δ) 0.1–3.5Hz
- Theta (θ) 4–7.5Hz
- Alpha (α) 8–13Hz
- Beta (β) 13–30Hz
- Gamma (γ) above 30Hz

Delta activity is the predominant range in infants and is normal during deep sleep stages in the adult. It is considered abnormal in the EEG of awake adults. Theta activity, if focal or lateralized, with excessive amplitude is an indicator of possible localized cerebral pathology in the adult patient. However, it is often seen in normal children. The Alpha rhythm is best seen when the adult patient is resting with closed eyes and is the classical EEG correlate of wakefulness [59, 70]. The Beta and Gamma activities are just regarded as a fast variant of the alpha activity (i.e. higher frequency).

The EEG characteristics differ considerably from the adult and older child to the newborn, particularly in frequency content. In the adult and older child, the predominant frequency range is between 8-30Hz (Alpha and Beta activity). Frequencies between 0.3-7Hz and above 30Hz are sparsely represented [70]. The newborn EEG has most of its power in the low frequency range of between 0.4-7.5Hz [71, 72]. Also, the variations in newborn EEG are more rapid, the stages of sleep-wake cycle are unstable, the reaction to opening eyes is missing, an interhemispheric asymmetry is observable and

certain adult features of EEG are missing (e.g. spindles and K-complexes)[2] [73]. The amplitude of EEG in the adult is most commonly between 10–50μV [70]. This range is also common to the newborn EEG [73]. Observations show that the maximum amplitudes of various EEG rhythms, from the defined frequency bands, tend to be inversely related to their frequency [62].

A comparison between 2 seconds of background EEG of the adult and newborn is shown in Figures 2.4 (a) and (b) respectively. From these plots, it is clear that the adult EEG has much more high frequency activity than the newborn. The amplitudes of the EEGs are comparable in magnitude.

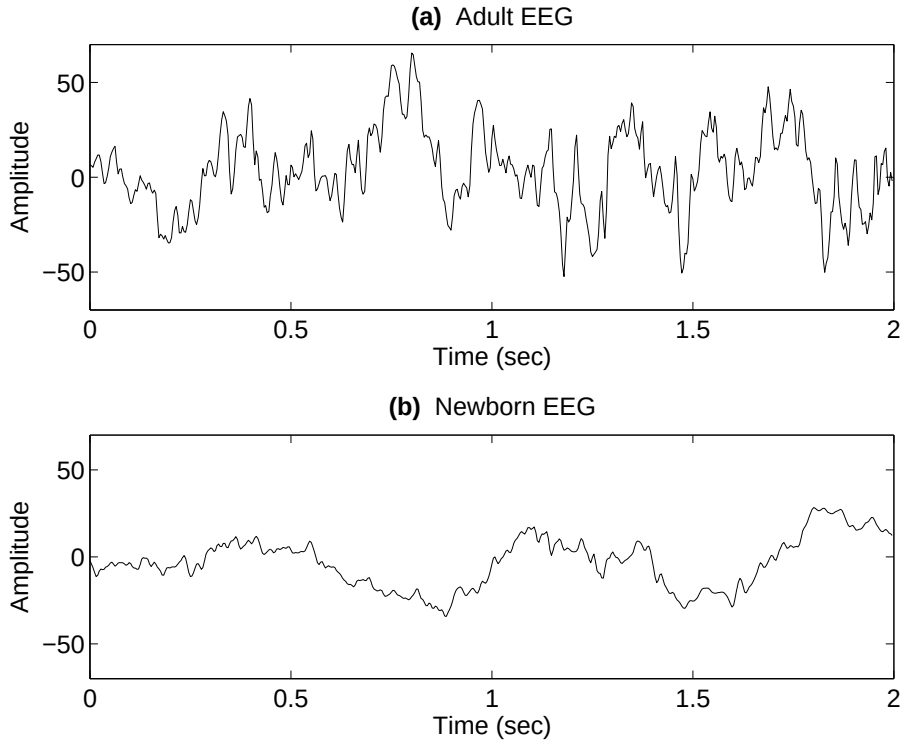

Figure 2.4: The background EEG signals of the (a) Adult and (b) Newborn.

2.4.2 Abnormal Background Patterns

Abnormalities occurring in the EEG signal can be specifically associated with some underlying pathology. Therefore, these types of abnormalities are labeled as *specific abnormalities*. The abnormalities which are not related to any pathology are labeled as

[2]Spindles are rhythmic waves at approximately 14Hz occurring during sleep stages. K-complexes are transient complex waveforms consisting of slow waves associated with sharp components [62].

nonspecific abnormalities. The majority of abnormalities in the EEG are nonspecific. Specific and nonspecific EEG abnormalities can been classified into three groups [74]:

(a) Distortion or disappearance of normal patterns

(b) Appearance or increase of abnormal patterns

(c) Disappearance of all patterns

Abnormalities can be further classified in terms of the spatial coverage and period of persistence. The term *paroxysmal* has been given to abnormalities that are characterized by an abrupt onset and termination and is significantly different to the background activity in frequency and amplitude [59]. Usually, specific EEG abnormalities occur paroxysmally [74].

A number of abnormal EEG patterns are common to the adult and newborn. Two such patterns are the *spike* and *sharp wave* patterns. A spike is defined as *"a transient, clearly distinguishable from the background activity, with a pointed peak at conventional paper speed and a duration from 20 to under 70msec. Main component is generally negative to other areas. Amplitude is variable"* [62, 75]. This broad definition is due to the large variations between spikes within an individual, and between individuals, making more precise definition difficult.

Similar to the spike pattern, a generalized definition of a sharp wave is given as *"a transient, clearly distinguishable from background activity, with pointed peak at conventional paper speeds and duration of between 70-200msec. The main component is generally negative to other areas"* [62, 75]. Another difference between spikes and sharp waves, not mentioned in the definition above, is that the starting phase of the sharp wave has a similar duration as a spike, but the finishing phase is longer. This is shown in Figures 2.5 (a) and (b), which show a spike and sharp wave respectively.

Isoelectric pattern, which can be referred to as electrocerebral inactivity pattern, is an abnormal pattern characterized by extremely low voltage patterns. The majority of patients exhibiting this EEG abnormality generally die, (e.g. An isoelectric EEG pattern occurs at the moment of cardiac arrest [76]). Otherwise these type of patterns indicate a poor prognosis for the patient, as those who survive are left with severe neurological sequelae [59].

Burst–Suppression pattern is characterized by a burst of high voltage lasting approximately 1-10 seconds followed by periods of quiescence or inactivity (i.e. isoelectric patterns) lasting 2-10 seconds [9, 59].

Runs of rapid spikes is an abnormal pattern that is particular to only adult and older children EEG. This abnormal pattern consists of bursts of spikes occurring at

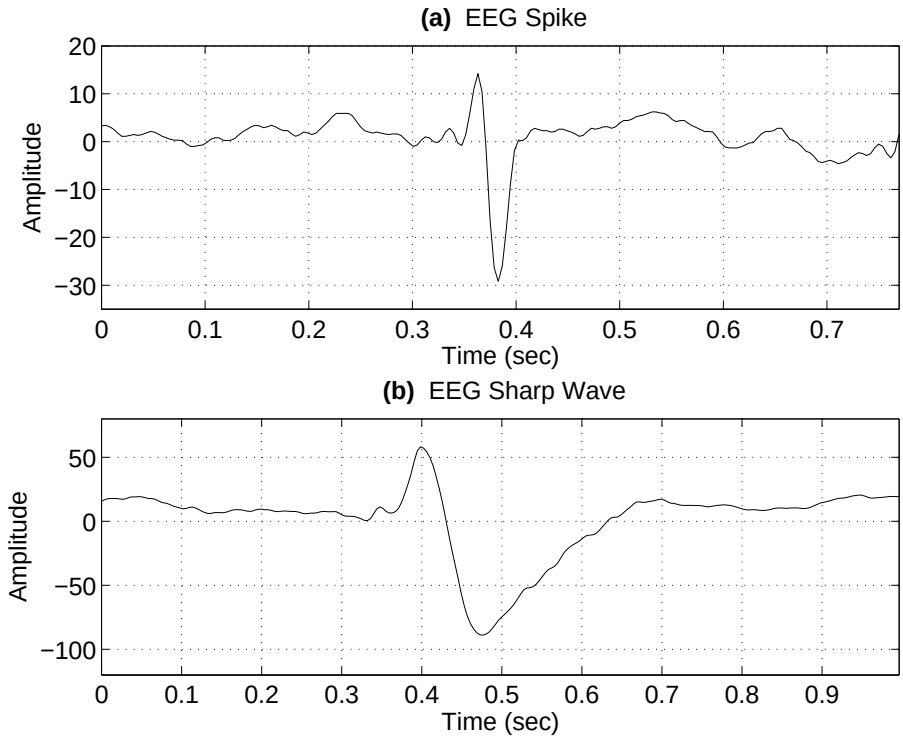

Figure 2.5: Two abnormal paroxysmal EEG events: (a) Spike and (b) Sharp wave.

rates between 10 to 25/sec. Various forms of *Spike wave complex*, which are classified according to the rate they occur, are also specific to the adult and older child patients. For example, the classic 3/sec spike wave complex is almost never seen before the age of 4 [75].

2.4.3 Normal Paroxysmal Patterns in Newborns

The assessment of paroxysmal patterns occurring in the newborn EEG is much more complicated than for the adult and older child. This is due to some paroxysmal patterns being normal variants for newborns at specific conceptional ages (CA)[3] [9].

Delta brushes, also called spindle-shaped bursts, refer to patterns containing spindles of varying frequencies and voltages along with a delta wave. They are highly representative of prematurity, and mostly disappear at term [9].

Fast transients are spikes and sharp waves, described previously. These patterns, which are nearly always abnormal patterns in the adult and older child, may be normal ontogenetic events in the newborn. For example, spikes in the frontal region may be normal for newborns between 35 weeks on to 40 weeks CA. Also, sharp transients

[3]Conceptional age refers to the time in weeks since conception.

consisting of 3-8 sharp, rhythmic waves with high voltages in the temporal region are common to newborns aged between 30 and 32 weeks CA [9].

Slow transient patterns consist of short runs of rhythmic delta waves with high amplitude. The delta waves are approximately between 0.5-1Hz for ages 29-31 weeks CA and appear as 1-2Hz delta waves from 37-40 weeks CA [9].

2.4.4 Ictal EEG

Ictal or seizure patterns in the EEG are the most significant EEG abnormalities. Seizures are abnormal reactions of the brain and are the result of a number of diseases such as, but not limited to, measles encephalitis, tuberculous meningitis, neurosyphilis, Rickettsia disease and herpes simplex encephalitis [77]. Seizures may also be a result of craniocerebral trauma or brain damage.

The neurophysiological mechanism for seizure generation is the imbalance between excitatory and inhibitory processes [4], as described in section 2.2 and shown in Figure 2.2. This results in an excessive synchronous discharge of neurons within the CNS [4, 14]. The continuance and propagation of seizure requires the recruitment of a critical mass of neurons within the region of onset and functionally intact pathways between neurons.

The ictal patterns in the newborn are highly variable, with complex and varied morphology and cover a variety of frequencies [8]. However, in broad terms, ictal patterns in the newborn are generally characterized by periods of rhythmic spiking or repetitive sharp waves [22]. An example of newborn EEG seizure activity is shown in Figure 2.6, clearly indicating the repetitive spiking characteristic.

The newborn EEG seizure event is generally characterized by a gradual, progressive build up of ictal activity. The EEG seizures in newborns are generally focal[4] and spread across the brain in various ways [9]. However, newborn seizures which have highly rhythmical spiking are often multifocal with slow migration of the spike activity from one area to another [77].

The minimum duration of ictal patterns in the newborn EEG used to define a seizure event is a highly debated topic among neurologists. Some require that a seizure event display ictal patterns for no less than 10 seconds. However, others require a duration of at least 20 seconds [9]. Evidence from a recent study has shown that even shorter durations than 10 seconds are clinically significant and provide prognostic value [78]. In a study of 487 neonatal electrographic seizures, the average seizure duration was 137 seconds, with a range of between 10 seconds to 46 minutes. An important result of this study was that 97% of all seizure events were less than 9 minutes [79].

[4]Localized to a particular area of the brain.

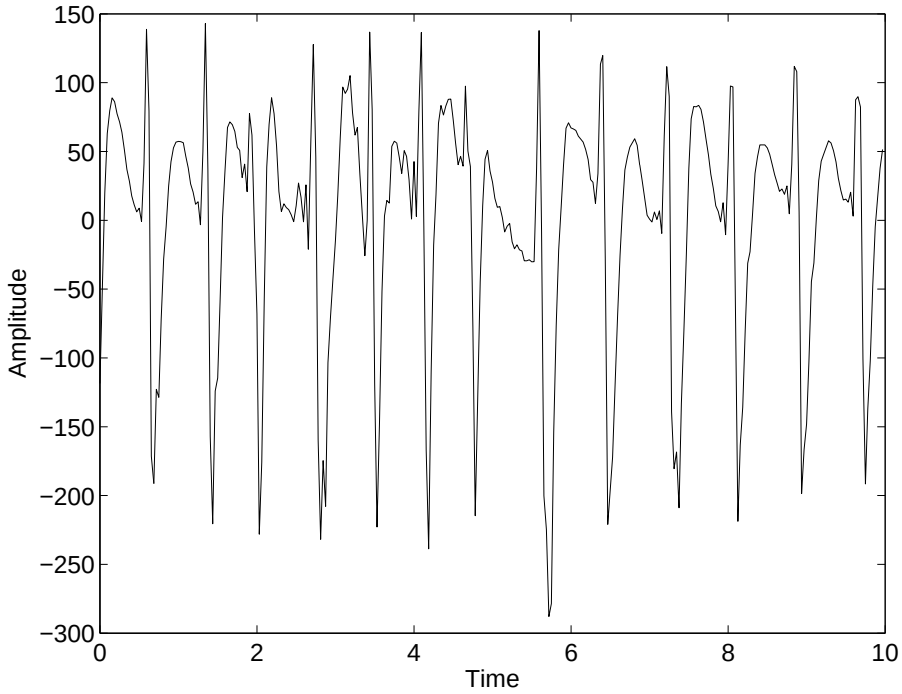

Figure 2.6: Repetitive, rhythmical spiking, characteristic of newborn EEG seizure.

The newborn EEG has been shown to be a nonstationary signal, particularly the ictal patterns. Therefore, representation of the rhythmic seizure patterns in the frequency domain, as shown in Figure 2.7, does not clearly illustrate any of the important time–varying information. Due to this, time–frequency signal analysis (TFSA) has recently been applied to the newborn EEG. Many significant time–varying patterns, such as piecewise linear components, were found to exist in the EEG seizure. This is demonstrated in Figure 2.8, which starts off with a single increasing linear component. The same component then begins to decrease for approximately 3 seconds before the signal becomes a multicomponent signal with constant frequency. This clearly emphasizes the superiority of TFSA in analyzing nonstationary signals.

2.5 Summary

This chapter provided an overview of the EEG signal. The neurophysiological mechanism of EEG generation involves the generation of inhibitory and excitatory postsynaptic potentials. Recordings of the EEG can be obtained through electrodes placed on the scalp or directly on the cerebral cortex. The recording of newborn EEG, however, is always through scalp electrodes because of the fragility of the brain during the

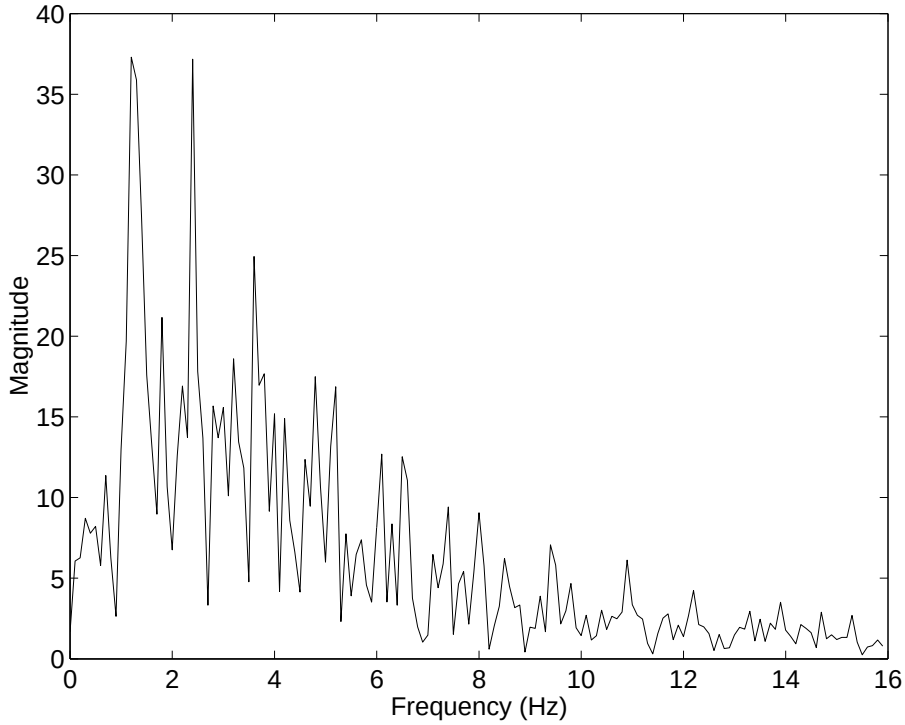

Figure 2.7: Frequency domain representation of the signal in Figure 2.6.

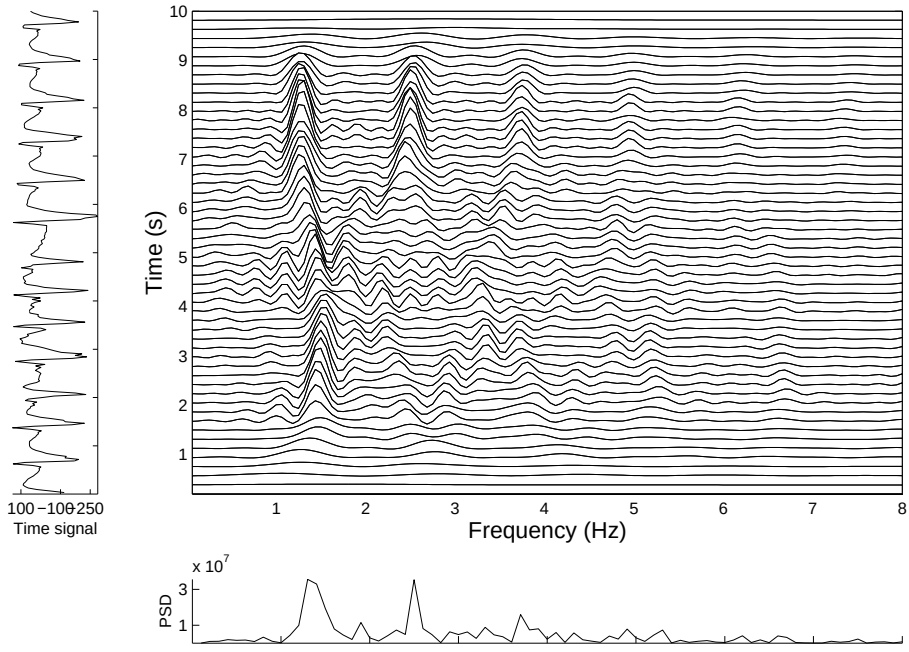

Figure 2.8: TF domain representation of the signal in Figure 2.6.

neonatal period.

The newborn EEG activity is concentrated in the 0.4-7.5Hz frequency band. Paroxysmal patterns that are abnormal in the adult EEG are sometimes normal ontogenetic events in the newborn. Ictal patterns in the EEG are the most notable EEG abnormality. The ictal pattern is a result of the excessive synchronous discharge of neurons and is a primary indicator of CNS dysfunction. TFSA clearly demonstrates the important time–varying information in the nonstationary EEG signal and is superior to both the time domain representation (i.e. raw time series) and frequency domain representation.

Chapter 3

An Overview of Time–Frequency Signal Representations

3.1 Introduction

Traditionally, signal analysis has been done in either the time domain or frequency domain. These representations can provide adequate information about stationary signals. However, most real life signals are nonstationary, exhibiting time–varying spectra. For nonstationary signals, neither the time domain nor frequency domain representations can clearly illustrate all relevant signal information [80].

Time–frequency signal analysis (TFSA) involves analyzing signals in a joint TF domain. From a TFR, important information about the instantaneous frequency (IF) content of a signal can be extracted. This gives the signal analyst the ability to observe how frequency content of a signal is changing over time.

Joint TFR can be obtained through a number of techniques. In this chapter, we present an overview of various TFRs that are relevant to this thesis. In section 3.2, we demonstrate the need for joint TFR of nonstationary signals. Linear TF transforms are reviewed in section 3.3, followed by an introduction to quadratic time–frequency distributions (QTFDs) in section 3.4. Finally, in section 3.5, we outline various methods of atomic decomposition and how they can be used to provide joint TFR.

3.2 The Need for Joint Time–Frequency Representation

The recording of real life signals involves the measurement of a parameter, which we can generalize with the term *amplitude*, as it changes in time. Hence, this signal representation is often referred to as the *time* domain representation. Signal analysis almost

always begins with this type of representation, yet only minimal information about the signal can be easily extracted.

One of the most frequently used methods of signal analysis is through the transformation of the time domain signal into the *frequency* domain. The frequency domain representation provides information regarding the energy and phase of particular frequency components in the signal. The FT is the most widely used method to obtain the frequency domain representation. The FT of a signal, $x(t)$, given in (1.2), is repeated here for convenience

$$X(f) = \mathcal{F}\{x(t)\} = \int_{-\infty}^{\infty} x(t)e^{-j2\pi ft}dt \tag{3.1}$$

The magnitude of the frequency content, called the *magnitude spectrum*, is the most common, and often useful, method of frequency analysis. The magnitude spectrum is obtained by taking the absolute value of the FT (i.e. $|X(f)|$).

Although the FT is a powerful tool and often used in many signal processing applications, it suffers from the inability to exhibit all relevant signal information for many nonstationary signals. Instead, the FT provides an average of frequency content over the signal period without providing any temporal information.

To show the limitation of the FT in the analysis of nonstationary signals, we consider the case of two linear frequency modulated (LFM) signals, given in Figure 3.1(a). Figure 3.1(b) shows that, on average, over the entire signal length, both signals contain the same magnitude spectrum[1]. Figure 3.1(b) also shows that the magnitude spectrum does not provide any temporal information about the frequency content of the nonstationary signals in Figure 3.1(a). However, by analyzing these signals in the TF domain, we can clearly see how the frequency content varies in the signal. This is demonstrated in Figures 3.2(a) and (b), which are the TFR of signal 1 and signal 2 respectively. The Wigner–Ville distribution, which will be discussed in section 3.4, was used to provide the TFR in this example.

The plots in Figures 3.2(a) and (b), clearly show how the frequency content of the signal varies with time, illustrating the differences between the two LFMs. The TFRs also provide all information available from the time domain and frequency domain representations, such as signal duration and frequencies, contained in the signal. Therefore, from this example, the powerful nature of TFR in the analysis of nonstationary signals is clearly demonstrated.

[1]It should be noted that the discriminating information for these signals is contained in the phase of the frequency components, which has been discarded in obtaining the magnitude spectrum.

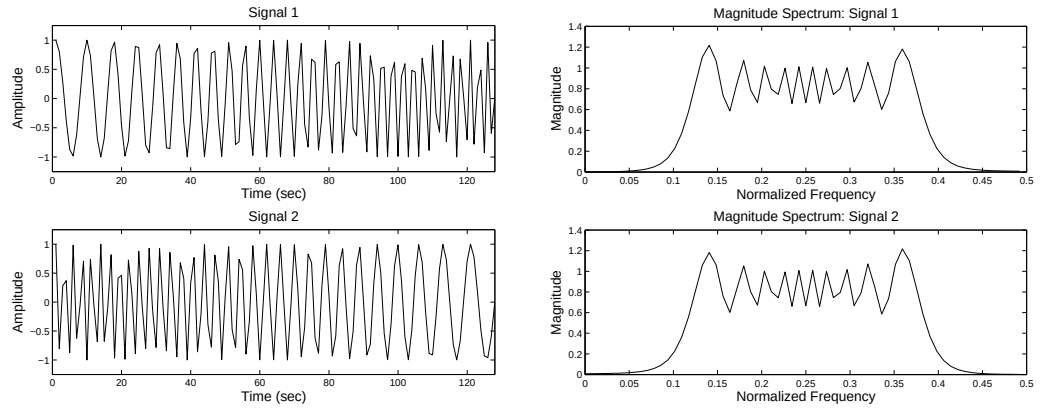

(a) (b)

Figure 3.1: (a) The time domain representation and (b) frequency domain representation of two different LFMs.

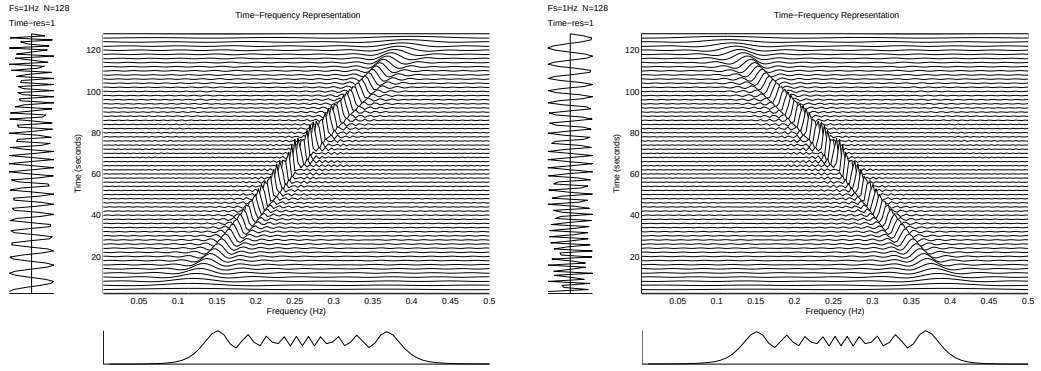

(a) (b)

Figure 3.2: The TFR of (a) signal 1 and (b) signal 2. A clear distinction between the two signals is apparent from their TFRs.

3.3 Linear Time-Frequency Transforms

Linear TF transforms are achieved by using the inner product[2] concept to correlate the signal with a collection of waveforms (atoms) that are highly concentrated in time and frequency [81]. Unlike the FT, which correlates the signal with complex sinusoidal functions that spread the entire time domain, these concentrated TF atoms can indicate

[2]The inner product of two functions $f(t)$ and $g(t)$ is given by $\langle f, g\rangle = \int_{-\infty}^{\infty} f(t)g^*(t)dt$. The ℓ^2 norm of a function f is given by $\langle f, f\rangle = ||f||_2 = \int_{-\infty}^{\infty} f(t)f^*(t)dt$.

how much signal energy is located in a particular TF region of the TF domain. This then provides the ability to analyze the frequency content as it evolves over time [17]. The general linear TF transform of a signal, $x(t)$, is given by

$$T\{x(t)\} = E_x(t,f) = \int_{-\infty}^{\infty} x(\tau)\phi_{t,f}^*(\tau)d\tau \tag{3.2}$$

where $T\{\cdot\}$ is a linear TF operator, $E_x(t,f)$ is the TFR and $\phi_{t,f}(\tau)$ is a TF atom concentrated around time t and frequency f[3].

The short–time Fourier transform (STFT) is an example of a linear TFR that has found wide application in different areas of science and engineering. For the STFT, the TF atoms in (3.2) are

$$\phi_{t,f}(\tau) = w(\tau - t)e^{j2\pi f\tau} \tag{3.3}$$

where the function $w(\tau)$ is generally a real even function with relatively short duration. It is often referred to as a window function [17]. Therefore, the STFT is expressed as

$$STFT(t,f) = \int_{-\infty}^{\infty} x(\tau)w(\tau - t)e^{-j2\pi f\tau}d\tau \tag{3.4}$$

The wavelet transform (WT) is another method which can be used to obtain a TFR. It was proposed as a method of analyzing signals with structures of differing time durations by correlating the signal with TF atoms that have varying time supports [81]. The atoms are created by scaling and translating a function $\phi(\tau)$ which is referred to as the *mother wavelet*. The WT is given as

$$WT(t,s) = \int_{-\infty}^{\infty} x(\tau)\frac{1}{\sqrt{s}}\phi^*\left(\frac{\tau - t}{s}\right)d\tau \tag{3.5}$$

which, in essence, is a time-scale representation. A TFR can be obtained from the WT as a result of the relationship between scale and frequency. That is, if f_0 is the center frequency of $\phi(\tau)$, then all center frequencies for the time-scaled atoms can be given as $f = f_0/s$ [17, 81]. Therefore, the TFR using the WT is given by

$$E_x(t,f) = WT(t,s)|_{s=\frac{f_0}{f}} \tag{3.6}$$

For both the WT and the STFT, time and frequency resolution is restricted by the resolution of the TF atoms used in the transform [81]. This TF resolution is bounded by the Heisenberg *uncertainty principle*

[3]The symbol $'*'$ in (3.2) represents the complex conjugate.

$$\triangle t \triangle f \geq \frac{1}{4\pi} \tag{3.7}$$

where $\triangle t$ and $\triangle f$ are the effective duration and effective bandwidth of the TF atoms respectively [21]. It can be seen from (3.7) that the uncertainty principle puts a lower limit on the spread or concentration of a function in time and frequency.

3.4 Quadratic Time-Frequency Distributions

QTFDs are commonly used methods for obtaining joint TFR. A QTFD is a special form of bilinear transform [82, 83]. The most basic QTFD is the Wigner-Ville distribution (WVD). All other QTFDs can be obtained by a TF averaging or smoothing of the WVD [81, 29].

The WVD of a signal, $x(t)$, is defined using its analytic associate $z(t)$. The analytic associate of $x(t)$ is obtained using the Hilbert transform, shown as [84, 21]

$$\mathcal{H}\{x(t)\} = X_H(\kappa) = \frac{1}{\pi} \oint_{-\infty}^{\infty} \frac{x(t)}{t-\kappa} dt, \tag{3.8}$$

such that $z(t) = x(t) + j\mathcal{H}\{x(t)\}$. The instantaneous autocorrelation function (IAF) of $z(t)$ is then defined as

$$K_z(t,\tau) = z(t+\tfrac{\tau}{2}) z^*(t-\tfrac{\tau}{2}) \tag{3.9}$$

and the WVD is expressed as

$$W_z(t,f) = \underset{\tau \to f}{\mathcal{F}}\{K_z(t,\tau)\} = \int_{-\infty}^{\infty} z(t+\tfrac{\tau}{2}) z^*(t-\tfrac{\tau}{2}) e^{-j2\pi f\tau} d\tau \tag{3.10}$$

As a TFR, the WVD has a number of remarkable properties. For this reason, the WVD is the most widely studied QTFD. Some of the important properties include[4]:

- Realness: $W_z(t,f)$ is always real
- Time-shift invariance: A time shift in the signal causes the same shift in the WVD such that

$$z(t-t_0) \rightarrow W_z(t-t_0, f) \tag{3.11}$$

- Frequency-shift invariance: Frequency modulation of a signal causes the same frequency shift in the WVD as the modulating frequency. That is

$$z(t) e^{j2\pi f_0 t} \rightarrow W_z(t, f-f_0) \tag{3.12}$$

[4] A detailed description of properties can be found in [29].

- Time marginal: Integrating the WVD with respect to f gives the instantaneous power

$$|z(t)|^2 = \int_{-\infty}^{\infty} W_z(t,f)df \tag{3.13}$$

- Frequency marginal: Integrating the WVD with respect to t gives the energy spectrum

$$|Z(f)|^2 = \int_{-\infty}^{\infty} W_z(t,f)dt \tag{3.14}$$

- IF: The first moment of the WVD with respect to f is the IF

$$\frac{\int_{-\infty}^{\infty} fW_z(t,f)df}{\int_{-\infty}^{\infty} W_z(t,f)df} = \frac{1}{2\pi}\frac{d\{\arg z(t)\}}{dt} \tag{3.15}$$

3.4.1 Crossterm Interference of the WVD

Among all of the QTFDs, the WVD also provides the highest TF resolution for LFM monocomponent signals (see Figure 3.2) and provides a positive two dimensional Gaussian for a Gaussian signal. However, despite these desirable properties, the application of the WVD is limited by the interference terms occurring as a result of the bilinear transformation. These interferences or crossterms occur in the case of nonlinear FM monocomponent signals and multicomponent signals [29].

The crossterms resulting from WVD of a nonlinear FM monocomponent signal can be explained as follows. Consider a finite duration signal with a time–varying amplitude such that

$$z(t) = a(t)e^{j\theta(t)} \tag{3.16}$$

where $a(t)$ is real. Therefore, the IAF (see (3.9)) can be written as

$$K_z(t,\tau) = K_a(t,\tau)e^{j\psi(t,\tau)} \tag{3.17}$$

where

$$K_a(t,\tau) = a(t+\tfrac{\tau}{2})a(t-\tfrac{\tau}{2}) \tag{3.18}$$

$$\psi(t,\tau) = \theta(t+\tfrac{\tau}{2}) - \theta(t-\tfrac{\tau}{2}) \tag{3.19}$$

If the phase function $\theta(t)$ is quadratic, relating to a linear IF function $f_i(t)$[5], then the central finite difference approximation in (3.19) is exact and gives $\psi(t,\tau) = \frac{d\theta}{dt}\tau =$

[5]The IF, $f_i(t)$, is defined as the derivative of the phase such that $f_i(t) = \frac{1}{2\pi}\frac{d\theta(t)}{dt}$.

$2\pi f_i(t)\tau$, which leads to [21]

$$K_z(t,\tau) = K_a(t,\tau)e^{j2\pi f_i(t)\tau} \tag{3.20}$$

Therefore, $K_z(t,\tau)$, when considered as a function of τ only, has a constant frequency equal to $f_i(t)$. This process is referred as dechirping [21]. When the signal has a nonlinear IF function, the central finite difference approximation is not exact and the IAF is not dechirped, resulting in the formation of crossterms called *inner artefacts* [29].

Crossterms resulting from multi-component signals can be explained as follows. Consider a multicomponent analytic signal

$$z(t) = z_1(t) + z_2(t) \tag{3.21}$$

The IAF for $z(t)$ can then be shown to be [29]

$$K_z(t,\tau) = K_{z_1}(t,\tau) + K_{z_2}(t,\tau) + K_{z_1z_2}(t,\tau) + K_{z_2z_1}(t,\tau) \tag{3.22}$$

where $K_{z_1z_2}(t,\tau)$ and $K_{z_2z_1}(t,\tau)$ are the instantaneous cross-correlation functions between the two components. Taking the FT of (3.22), with respect to τ, we obtain the WVD of the multicomponent signal, such that

$$W_z(t,f) = W_{z_1}(t,f) + W_{z_2}(t,f) + 2\mathrm{Re}\{W_{z_1z2}(t,f)\} \tag{3.23}$$

It can be seen in (3.23), that the WVD of the multicomponent signal is the sum of the WVD of each component plus some interference term which is related to the cross-WVD of the two components [29]. These crossterms are referred to as *outer artefacts.*

Figures 3.3(a) and 3.3(b) show the WVD of a nonlinear FM signal and a multicomponent signal respectively, along with their associated IFs for individual components. From these TFR plots, it is clear that the information regarding the IFs is masked by unwanted cross-terms, reducing the effectiveness of the TFR.

3.4.2 Suppression of Crossterms

All QTFDs can be formulated by smoothing the WVD with a time–lag kernel, $G(t,\tau)$. By correctly designing $G(t,\tau)$, we can define QTFDs that attenuate the cross-terms associated with the WVD. QTFDs which have the cross–terms attenuated in comparison to the desired terms are often called *reduced interference distributions* (RIDs) [29]. The general form of QTFDs, including all RIDs, which are defined by the time–lag kernel, is shown as

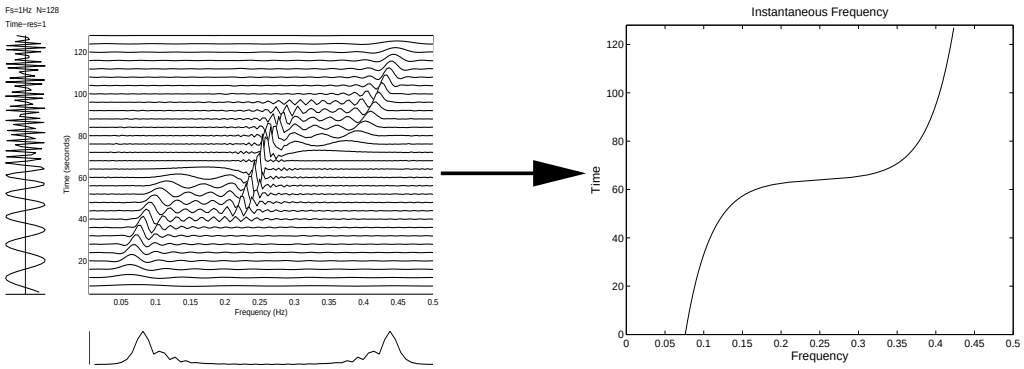

(a) Nonlinear FM Monocomponent

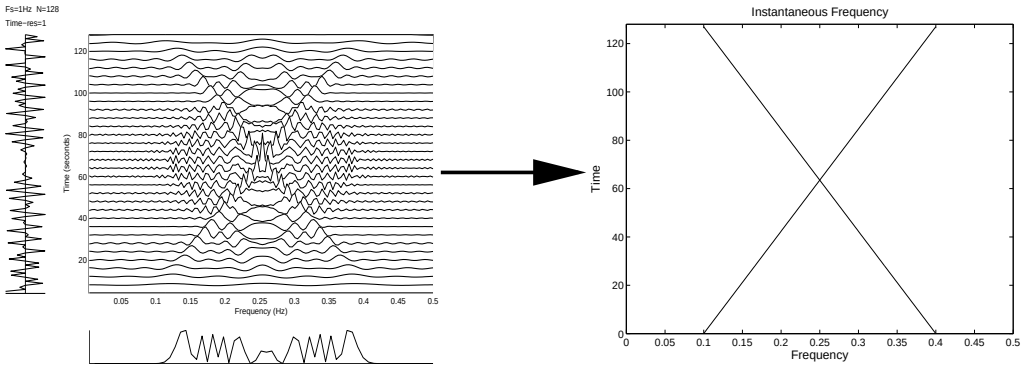

(b) Multicomponent

Figure 3.3: The TFR and corresponding IF of (a) a nonlinear FM monocomponent signal and (b) a multicomponent signal made up of two LFMs components.

$$E_z(t,f) = \int_{-\infty}^{\infty}\int_{-\infty}^{\infty} G(t-u,\tau)z(u+\tfrac{\tau}{2})z^*(u-\tfrac{\tau}{2})e^{-j2\pi f\tau}dud\tau \tag{3.24}$$

The spectrogram, defined as the square magnitude of the STFT (i.e. $|STFT(t,f)|^2$) is another important QTFD. However, it can also be obtained from (3.24) by using the time–lag kernel

$$G_{spec}(t,\tau) = w(t+\tfrac{\tau}{2})w(t-\tfrac{\tau}{2}) \tag{3.25}$$

where $w(\tau)$ is the window function used in the STFT. The spectrogram can be thought of as a RID with almost no interference terms. However, this interference reduction also results in poor TF resolution [29]. Therefore other RIDs attempt to provide the

resolution of the WVD with the crossterm reduction of the spectrogram. Table 3.1 shows the time–lag kernels, $G(t,\tau)$ of some QTFDs. It can be seen from Table 3.1 that the Choi-Williams (CW) [85], B [86] and Modified B (MB) [87] distributions have tunable parameters (i.e. σ for CW and β for B and MB). The parameters can be changed for various signals to improve the TFR obtained by these distributions.

Distribution	Kernel $G(t,\tau)$
Wigner-Ville	$\delta(t)$
Choi-Williams	$\frac{\sqrt{\pi\sigma}}{\lvert\tau\rvert}e^{-\pi^2\sigma t^2/\tau^2}$
B	$\lvert\tau\rvert^{\beta}\cosh^{-2\beta}t$
Modified B	$\frac{\cosh^{-2\beta}t}{\int_{-\infty}^{\infty}\cosh^{-2\beta}t dt}$

Table 3.1: QTFDs and their associated time-lag kernels

Figure 3.4 shows the WVD, spectrogram, B-distribution and CW for a multicomponent signal made up of two LFM signals. It can be seen that the WVD gives high resolution for the LFM components but is corrupted by a number of interference terms. However, the spectrogram does not display any interference terms but has low resolution for the signal components. For both the B-distribution and the CW, we can see that they provide high resolution and minimal crossterm interference.

3.5 Atomic Decomposition Techniques with Time-Frequency Dictionaries

In reviewing atomic decomposition techniques as methods for TFSA, there is terminology particular to these methods which must first be addressed. The term *atom,* which was previously referred to in section 3.3, is used to describe an elementary waveform, $\phi_\gamma(t)$, which is used for signal representation. A collection of atoms used for signal representation is called the *dictionary,* represented as $\Phi = \{\phi_\gamma\}_{\gamma\in\Gamma}$. The dictionary atoms are generally obtained through transformations of a fundamental waveform $\phi(t)$. The transformations are indicated by "γ", which can be a single or multi-index parameter. Therefore, Γ represents the entire set of parameters used to create Φ.

Time–frequency atom generally refers to those atoms which are highly concentrated in time and frequency. However, we also use this term to describe atoms which have specific TF characteristics (i.e. LFM atoms, hyperbolic FM atoms etc.).

If Φ spans the Hilbert space, H, the dictionary is said to be *complete* [37]. For a finite dimension signal space, the dictionary may have more atoms than are needed to

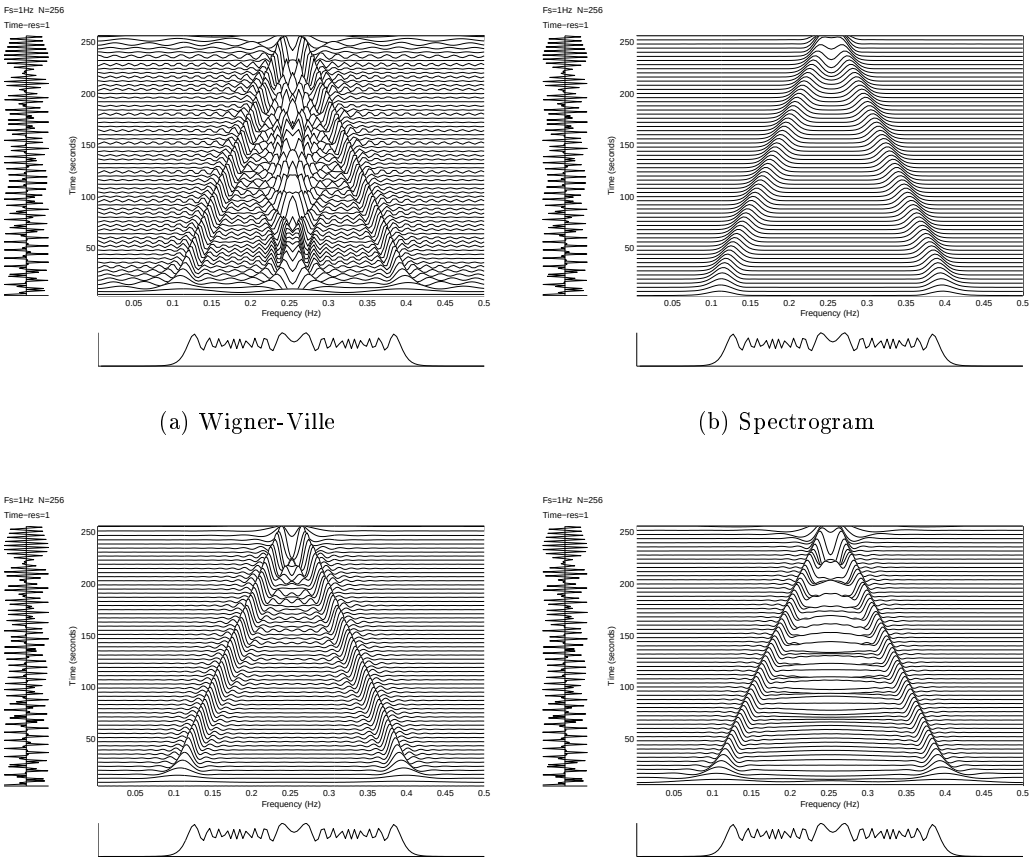

(a) Wigner-Ville

(b) Spectrogram

(c) B-distribution

(d) Choi-Williams

Figure 3.4: The TFR of a multicomponent signal using (a) Wigner-Ville distribution, (b) Spectrogram, (c) B–distribution and (d) Choi–Williams distribution.

span the space. This is a *redundant* dictionary[6]. *Orthogonal bases*, such as the Fourier basis and orthogonal wavelet bases, can be thought of as dictionaries which have the minimum number of atoms needed to span the finite Hilbert space (i.e. the minimum number of atoms to make the dictionary complete).

Traditional analysis techniques involving orthogonal bases provide a unique representation. However, these analysis techniques are limited in the information they provide. For example, the Fourier basis provides poor representations of signals with structures well localized in time, and WTs give poor frequency resolution for signals with narrow high frequency support [37]. Therefore, it would be desirable to have a

[6]It should be noted that a redundant dictionary is complete, but due to its redundancy it is often referred to as *overcomplete* [88].

dictionary with TF atoms capable of representing all types of signal structures with high resolution. This is possible with redundant TF dictionaries. However, because of this redundancy, there are many possible signal representations, (i.e. unlike the unique representation from an orthonormal basis). Therefore, a method of choosing atoms that are best adapted to signal structures is required [37].

Atomic decomposition techniques are methods for selecting atoms ϕ_γ from a redundant dictionary, $\Phi = \{\phi_\gamma\}_{\gamma\in\Gamma}$, to provide a signal representation, (or approximation), as a linear superposition of the selected atoms. A representation of signal, x, can be given using atoms from Φ as

$$x = \sum_{\gamma\in\Gamma} \alpha_\gamma \phi_\gamma \tag{3.26}$$

where α_γ is the coefficient associated with ϕ_γ. An approximation of x using m atoms can also be given by

$$\hat{x} = \sum_{i=0}^{m-1} \alpha_{\gamma i} \phi_{\gamma i} \tag{3.27}$$

The signal left over from the approximation, $R^m x = x - \hat{x}$, is often referred to as the residual. The method of selecting the atoms for signal representation or approximation constitutes an atomic decomposition technique. A number of atomic decomposition techniques are available, including: best orthogonal basis, method of frames, matching pursuit (MP) and basis pursuit (BP) [89, 90, 37, 88].

For certain redundant dictionaries, such as the cosine packet (CP) and wavelet packet (WP) dictionaries, it is possible to have subcollections of atoms which form orthogonal bases. Using these dictionaries, the best orthogonal basis algorithm finds the orthogonal basis whose corresponding coefficients have the minimum entropy [88]. However, by choosing a single basis, the representation still cannot provide high resolution for signals with structures that have highly varying TF supports.

Method of frames picks out the representation, given in (3.26), whose coefficients have the minimum ℓ^2 norm; expressed as [88]

$$\min \ ||\alpha||_2 \quad \text{subject to} \quad x = \sum_{\gamma\in\Gamma} \alpha_\gamma \phi_\gamma \tag{3.28}$$

However, there are two major problems with this atomic decomposition technique. First, its representation is generally not very sparse[7], which is a desirable characteristic for

[7] A sparse representation is defined as one with the minimum number of significant atoms [88]. Sparse representations will be discussed in detail in chapter 5.

atomic decomposition techniques. Second, examples have shown that method of frames gives poor resolution in its representations for a variety of signals [88].

MP is currently finding application in a multitude of engineering areas. MP is an iterative algorithm that selects the atom which best represents (i.e. correlates with) the signal residue at each iteration. That is, the atom selected at each iteration is the one for which the projection of the residual, using the inner product, is largest. The objective function for each iteration of MP is given by

$$\gamma i = \arg\{\sup_{\gamma\in\Gamma}\langle R^i x, \phi_\gamma\rangle\} \tag{3.29}$$

Using (3.29) at each iteration, the MP decomposition of a signal, x, approximating with m atoms, is given as

$$x = \sum_{i=0}^{m-1}\langle R^i x, \phi_{\gamma i}\rangle\phi_{\gamma i} + R^m x \tag{3.30}$$

where the inner product, $\langle R^i x, \phi_{\gamma i}\rangle$, is taken as the coefficient value associated with the atom $\phi_{\gamma i}$. It should also be clearly noted that at $i = 0$ we have $R^0 x = x$.

Each atom in Φ is generally normalized such that

$$||\phi_\gamma(t)||_2 = 1; \quad \forall\gamma \tag{3.31}$$

The normalization of the dictionary removes any magnitude bias in the projection of the residual vector onto the dictionary vectors. A thorough description of the MP algorithm is provided in [37].

BP is a recently proposed atomic decomposition technique [88]. It was introduced as an alternative to previous decomposition techniques in an attempt to provide the sparsest representation and with the ability to resolve signal structures that are close in time and frequency. BP decomposition is an optimization method which tries to solve the following problem:

$$\min\ ||\alpha||_1 \quad \text{subject to} \quad x = \sum_{\gamma\in\Gamma}\alpha_\gamma\phi_\gamma \tag{3.32}$$

This optimization problem can be expressed in terms of a linear programming problem of standard form. Any available linear programming technique can be used to solve the BP optimization problem. The simplex method and interior point method were proposed in [88]. Finding a solution to the linear programming problem as applied to BP criteria is equivalent to finding the basis with the minimum ℓ^1 norm of coefficients

such that

$$x = \sum_{i=0}^{N-1} \alpha_{\gamma i} \phi_{\gamma i} \tag{3.33}$$

where N is the length of the discrete signal x. For the BP representations, the selected atoms are linearly independent, but are not necessarily orthogonal.

The simplex method initially chooses N atoms from the dictionary as the first guess of the optimal basis. The next step is to swap the atoms from this basis with other atoms from the dictionary so as to improve the objective function (i. e. minimum ℓ^1 norm of coefficients). Using the simplex method there is always a swap that can improve the objective function until the optimal solution is found. This can be thought of as jumping from one vertex to another on the boundary of the simplex until the optimal solution is found. The interior point method begins by choosing a point inside the simplex. The first vector of coefficients $\alpha^{(0)}$, which gives the initial point inside the simplex, also provides the initial overcomplete representation $\Phi\alpha^{(0)} = f$. The interior point method iteratively modifies the coefficients in a way that moves the point in the simplex toward the outer vertex which is the optimal solution. The iterations continue until there are $\leq N$ atoms which are significantly non-zero [88].

3.5.1 Time–Frequency Representation from Atomic Decompositions

Joint TFR of a signal can be derived from the TF atoms selected in the atomic decomposition. The TFR is obtained by the summation of the estimated TF contribution of each of the selected atoms such that

$$E_x(t,f) = \sum_{\gamma \in \Gamma_{AD}} |\alpha_\gamma|^2 E_{\phi_\gamma}(t,f) \tag{3.34}$$

where Γ_{AD} is the set of atom parameters relating to the atoms chosen in the decomposition to represent the signal.

There are various methods of estimating the TF contribution of each TF atom. Two such methods include:

1. The WVD of TF atoms, (see (3.10)).

2. Heisenberg boxes [37, 81].

A Heisenberg box is formed by evaluating the spread of the atom in time and frequency and assigning a rectangle to cover that area of the TF domain. This is shown in Figure

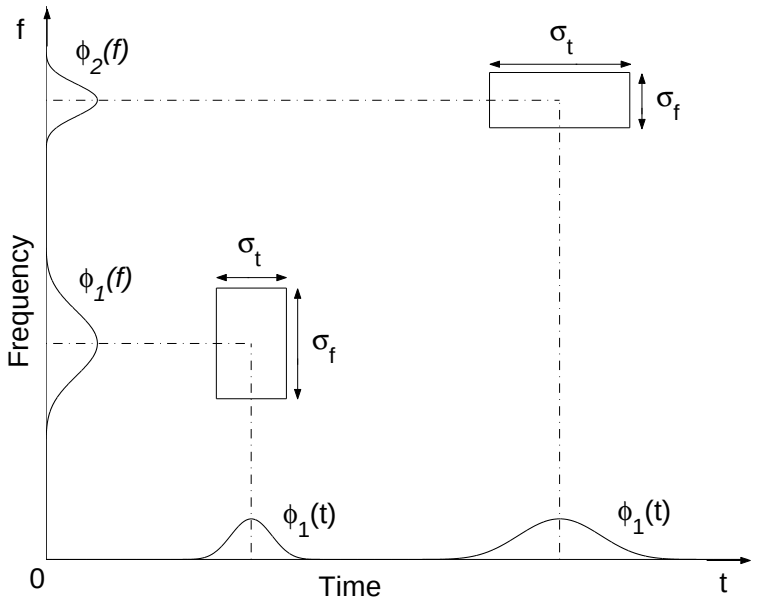

Figure 3.5: Heisenberg boxes of two TF atoms.

3.5 with two TF atoms[8] localized around different time and frequency positions and with different bandwidths and durations.

A TF dictionary that is regularly used is the Gabor TF dictionary. This dictionary consists of dilated, s, translated, u, and modulated, ξ, Gaussian windows $\phi(t)$, such that the dictionary atoms are expressed as

$$\phi_\gamma(t) = \frac{1}{\sqrt{s}}\phi\left(\frac{t-u}{s}\right)e^{j2\pi\xi t} \tag{3.35}$$

where $\gamma = [s, u, \xi]$ and $\Gamma = \mathbb{R}^+ \times \mathbb{R}^2$. The WVD distribution is highly suitable for estimating the TF contribution of the Gabor atoms. This is because the WVD of a Gaussian signal is a positive 2D Gaussian centered at the time and frequency position of the translation and modulation parameters and shaped by the scale parameter. Using the time and frequency shift invariance properties of the WVD, the Gabor TF atom has a WVD [37]

$$W_{\phi_\gamma}(t,f) = W_\phi\left(\frac{t-u}{s}, s(f-\xi)\right) \tag{3.36}$$

[8]Note that the windows in Figure 3.5 only indicate the durations, bandwidths and time and frequency centers of the atoms, not the actual atom functions.

The Gaussian window, which is usually chosen, and its corresponding WVD are [17, 37]

$$\phi(t) = 2^{1/4} e^{-\pi t^2} \longrightarrow W_\phi(t,f) = 2e^{-2\pi(t^2+f^2)} \tag{3.37}$$

where $W_\phi(t,f)$ is the WVD of the Gaussian window $\phi(t)$.

Other TF Dictionaries that are regularly used for decomposition by MP and BP include the CP and WP dictionaries [37, 81, 88]. WP and CP dictionaries generally use Heisenberg boxes to estimate the TF contribution of atoms. Figure 3.6(a) and 3.6(b) show the TFR of the multicomponent signal shown in Figure 3.4, using MP and BP respectively. The Gabor dictionary has been used with MP and the CP dictionary has been used with BP. It can be seen that the Gabor dictionary using the WVD to estimate atom contribution provides a more aesthetic TFR than the CP dictionary using Heisenberg boxes. This is due to the smooth 2D Gaussian nature of the WVD of the Gabor atom. However, from both representations it is obvious that no crossterms exist.

The crossterm free representation is simply explained by the formulation of the TFR. By adding, individually, the TF contribution of the selected atoms, the crossterms between the selected atoms is neglected and therefore not added into the representation. This can be explained with a simple example. Consider a signal with a decomposition which contains two Gabor atoms. If we use the WVD to estimate the TF contributions, using (3.34), the TFR would be

$$E_x(t,f) = \sum_{i=0}^{1} |\alpha_{\gamma i}|^2 \, WVD_{\phi_{\gamma i}}(t,f) \tag{3.38}$$

It can be seen that the TFR in (3.38) does not include $WVD_{\phi_{\gamma 0}\phi_{\gamma 1}}(t,f)$, which is the interference term produced in the traditional WVD (see (3.23)).

Another benefit of using atomic decomposition is that the signal decomposition also provides a TF parameterization of the signal [42]. That is, TF parameters such as dilation, translation and modulation associated with the selected TF atoms also provide information about signal characteristics. Also, for noisy signals, approximations using atomic decomposition techniques can lead to lower signal to noise ratios (SNR) in the TF plane [37, 88].

3.6 Summary

The analysis and processing of nonstationary signals requires techniques that can show the time–varying spectrum characteristic of these signals. This chapter has demonstrated that TFSA is appropriate for the analysis of nonstationary signals. However,

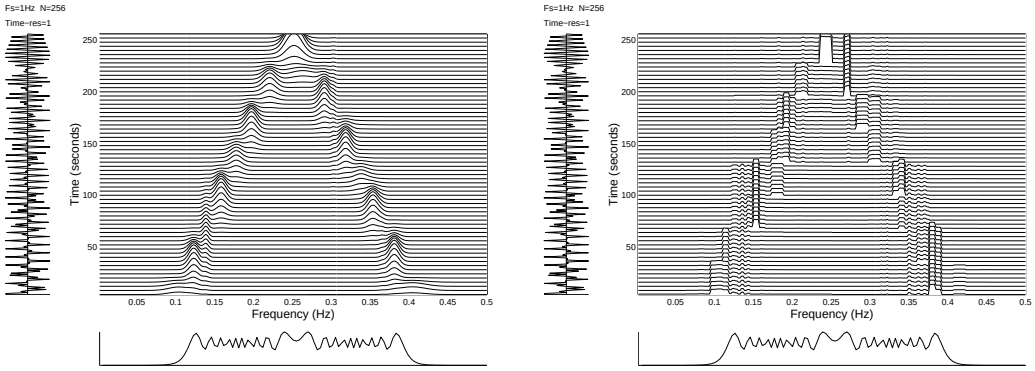

(a) Matching Pursuit (b) Basis Pursuit

Figure 3.6: TFRs of a multicomponent signal using (a) MP with a Gabor dictionary and (b) BP with a CP dictionary.

there are many different techniques for obtaining a TFR.

Linear TF transforms were introduced as a method of TFSA. Although they are widely used, these methods are restricted because of the limited TF resolution attainable in their TFR. A review of QTFDs was given, beginning with the WVD. Despite the desirable properties of the WVD, it was shown that its representation was not suitable for nonlinear FM signals and multicomponent signals due to the crossterms produced by the bilinear transform. The spectrogram was explained and shown to be related to the WVD. Although it was not severely affected by crossterms, it was shown that the lower TF resolution of signal components was attained from the spectrogram. It was then demonstrated that smoothing of the WVD, to provide RIDs, could produce much more comprehendible TFRs. Finally, we presented an overview of atomic decomposition techniques and illustrated their ability to provide a joint TFR. We also demonstrated how atomic decomposition can be used as methods of TF parameterization.

Chapter 4

Newborn EEG Simulation

4.1 Introduction

The newborn EEG is a highly complex signal, which has been shown to exhibit nonstationarities as well nonlinearities [20, 91]. Therefore, different signal processing techniques such as TFSA techniques (for nonstationarity) and nonlinear techniques (for nonlinear and chaotic behaviour), are required for analysis of these various characteristics.

Nonlinear behaviour is a significant characteristic of the newborn EEG background [27, 91], which has also been shown to exhibit nonstationarities [19, 20]. The prominent characteristic of the newborn EEG seizure is its nonstationarity [20]. Therefore, in developing a method for newborn EEG simulation, the nonlinear nonstationary behaviour of the newborn EEG background and prominent nonstationary behaviour of the newborn EEG seizure must be carefully considered.

In this chapter, we develop a method for simulating newborn EEG background and a method for simulating newborn EEG seizure, which can be combined to provide a method of artefact free, newborn EEG simulation. In section 4.2, we provide an introduction to nonlinear time series analysis and review fractional dimension as a nonlinear measure. It is then demonstrated in section 4.3, that the background newborn EEG exhibits nonlinear characteristics and we analyze real newborn EEG background using fractal dimension (FD). Using the results from the FD analysis and fractal theory, we propose a method of simulating newborn background EEG. In section 4.4, we propose a method of simulating newborn EEG seizure using the TF characteristics of real newborn EEG seizure. This method incorporates a time–frequency signal synthesis (TFSS) process which transforms the simulated newborn EEG seizure TFR into a newborn EEG seizure time domain signal.

4.2 Nonlinear Analysis Techniques

Linear models for signal analysis are suitable as an initial approximation in most engineering applications. However, linear equations can only lead to exponential growth/decay or periodically oscillating solutions [92, 93]. All other irregular behaviours of a linear system are considered as a result of randomness in the signal. Chaos theory, however, demonstrates that irregular outputs of a system are not only a result of irregular input to a system, but can also be obtained through nonlinear systems with deterministic equations [93]. In this section, we give a brief overview of nonlinear signal analysis techniques.

The *phase space* reconstruction of discrete time series is the focal tool used in nonlinear analysis. The phase space is created using various lag samples of the time series to form a d–dimensional multivariate space such that for a discrete signal $x(n)$, the d–dimensional vectors are [92]

$$\mathbf{y}(n) = [x(n), x(n+T), x(n+2T), \ldots, x(n+(d-1)T)] \tag{4.1}$$

where T is the time lag interval for the state space in samples. This process is referred to as phase space reconstruction by method of delays [93]. The dimension, d, is called the embedding dimension of the phase space. A typical phase portrait with embedding dimension two and time lag of one sample for the nonlinear Hénon map, described by

$$x(n) = 1.4 - x^2(n-1) + 0.3x(n-2) \tag{4.2}$$

is given in Figure 4.1. This time series is not periodic, but instead *chaotic* [93]. The random nature of the chaotic signal becomes structured in the phase portrait.

A number of nonlinear signal measures can be calculated from the phase space reconstruction of a time series. These measures are methods of quantifying the nonlinear properties of the signal in the hope of enhancing the knowledge of the underlying system [93]. One such measure is fractional dimension of a time series.

4.2.1 Fractal Dimension

Fractal signals with fractional dimension are typical of chaotic systems [93]. Correlation dimension is one of several methods used to quantify self–similarity associated with fractal signals. It is defined by the correlation sum, $C(\epsilon)$, for a collection of points $\mathbf{y}_n$ in a vector space, (i.e. the phase space). The correlation sum is the fraction of points that are closer than a defined distance ϵ according to a particular norm and is given as

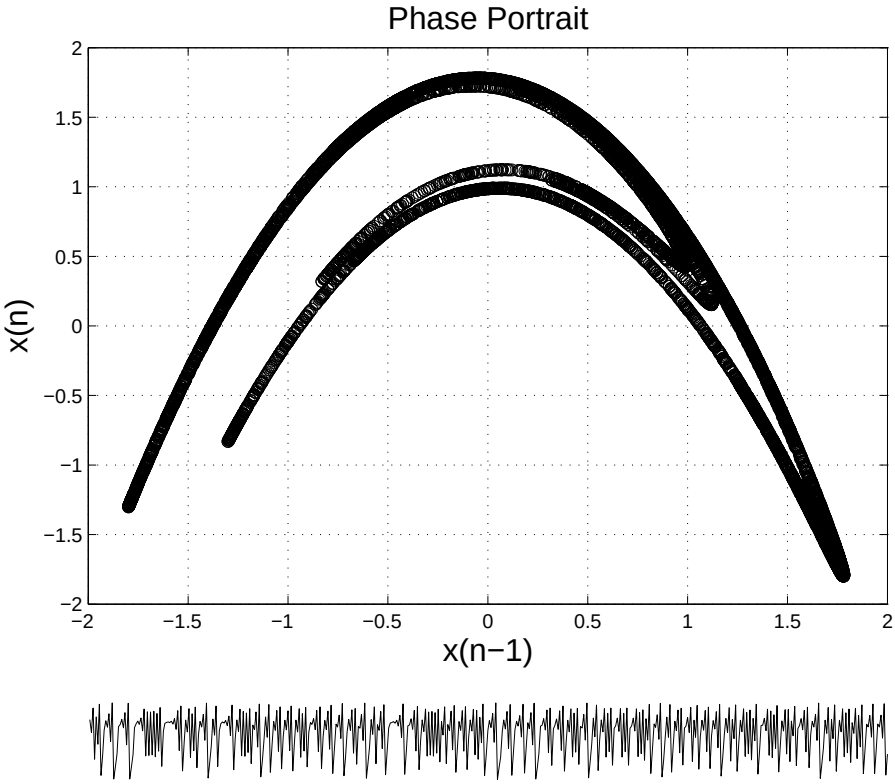

Figure 4.1: The phase portrait of a Hénon map time series.

$$C(\epsilon) = \frac{2}{N(N-1)} \sum_{i=1}^{N} \sum_{j=i+1}^{N} \Theta(\epsilon - ||\mathbf{y}_i - \mathbf{y}_j||) \tag{4.3}$$

where Θ is the Heaviside step function

$$\Theta(x) = \begin{cases} 1 : x > 0 \\ 0 : x \leq 0 \end{cases} \tag{4.4}$$

and N is the number of vectors. In essence, the double sum of the Heaviside function in (4.3) counts the pairs of $(\mathbf{y}_i, \mathbf{y}_j)$ whose distance are less than ϵ. The correlation dimension is then given as the power law relating ϵ to $C(\epsilon)$ such that

$$D = \frac{d \ln C(\epsilon)}{d \ln \epsilon} \tag{4.5}$$

The use of the correlation dimension, however, is limited to stationary signals as it suffers considerably from nonstationarities in the signal [93].

Previous to the development of these nonlinear techniques based on the phase space

reconstruction, the power spectrum was used as the dominant means of analyzing irregular time series. When a signal spectrum, $S(f)$, exhibits a power law such that

$$S(f) \propto |f|^{-\gamma} \tag{4.6}$$

the power law exponent, γ, can be used as a measure of irregularity or complexity. To obtain the power law, an ensemble average of power spectra over a long time period has been used, assuming that the signal is statistically stationary [94]. This method of analysis is therefore, inappropriate for nonstationary signals such as the newborn EEG.

There is a relationship between a signal with a spectral power law of $|f|^{-\gamma}$ and the theoretical FD of the signal. It can be shown that the FD of a signal with a spectrum

$$S(f) = \frac{c}{|f|^{\gamma}} \tag{4.7}$$

where c is a constant, will have a FD of [95]

$$D = \frac{5-\gamma}{2} \tag{4.8}$$

If the FD can be accurately estimated over short periods, it may be used to track nonstationarities in the signal[1]. It could also provide much better time resolution of signal complexity than the power law exponent γ.

In [96], a comparison between FD estimators was performed. The comparison found that the Higuchi method provided the most accurate results for estimating the FD. Therefore, in our analysis of the newborn EEG we have only used the Higuchi method [94] for FD estimation.

Higuchi FD Estimation

Consider a discrete time series $x(n)$ of length N. From this time series we can construct k new time series, x_k^m, for each value m such that

$$x_k^m = \left[x(m), x(m+k), x(m+2k), \ldots, x\left(m + \left\lfloor \frac{N-m}{k} \right\rfloor \cdot k\right)\right] \tag{4.9}$$

where m and k are integers that indicate the initial time and time interval respectively. The function $\lfloor u \rfloor$ gives the integer part of u. The length of the constructed time series in (4.9) is defined as

[1] A time–varying FD relates to a time–varying power spectrum, or nonstantionary signal.

$$L_m(k) = \sum_{i=1}^{\lfloor (N-m)/k \rfloor} |x(m+ik) - x(m+(i-1)k)| \times \frac{N-1}{\lfloor \frac{N-m}{k} \rfloor \cdot k} \tag{4.10}$$

The term $(N-1)/\lfloor (N-m)/k \rfloor \cdot k$ is a normalization factor for the curve length of the subset time series.

The length of the signal for the time interval k, $< L(k) >$, is then defined as the average value over k sets of $L_m(k)$ such that

$$< L(k) >= \frac{\sum_{m=1}^{k} L_m(k)}{k} \tag{4.11}$$

If $< L(k) > \propto k^{-D}$, then the signal will have dimension D. For Higuchi's method, the FD can be found from a linear least squares fit of the curve, $\log(< L(k) >)$ versus $\log(k)$. This technique gives stable indices and time scale from a small number of data [94], giving it the ability to track nonstationarities in a signal.

4.3 Newborn EEG Background Simulation

Power spectrum analysis has been a major tool in the analysis of the newborn EEG. However, as demonstrated previously in chapter 3, it cannot display all relevant information from nonstationary signals, nor can it give accurate information regarding the nonlinearities of nonlinear, nonstationary signals. However on inspection of the newborn EEG background power spectra, we can see that it follows some form of power law. This is demonstrated in Figure 4.2(a) and 4.2(b), which gives the power spectra of two background EEG epochs.

The fact that the newborn EEG background exhibits some form of power law in the power spectrum infers that it may be fractal in nature. Along with its demonstrated nonstationarity, this suggests that FD estimation using the Higuchi method is appropriate for analysis of the newborn EEG background.

4.3.1 Fractal Dimension Analysis of the Background EEG

The EEG data used in this analysis was acquired at the Royal Womens Hospital, Brisbane, Australia, using the MEDELEC[2] system[3]. Electrodes were placed on the scalp according to the 10–20 international standard of electrode placement and twenty EEG channels were obtained using bipolar montage. Signals were bandpass filtered with cutoff frequencies at 0.5Hz and 30Hz, with a sampling frequency of 64Hz. The recordings

[2]MEDELEC is a product of oxford instruments (see www.oxford-instruments.com)
[3]A detailed description of the EEG data acquisition is given in Appendix A.

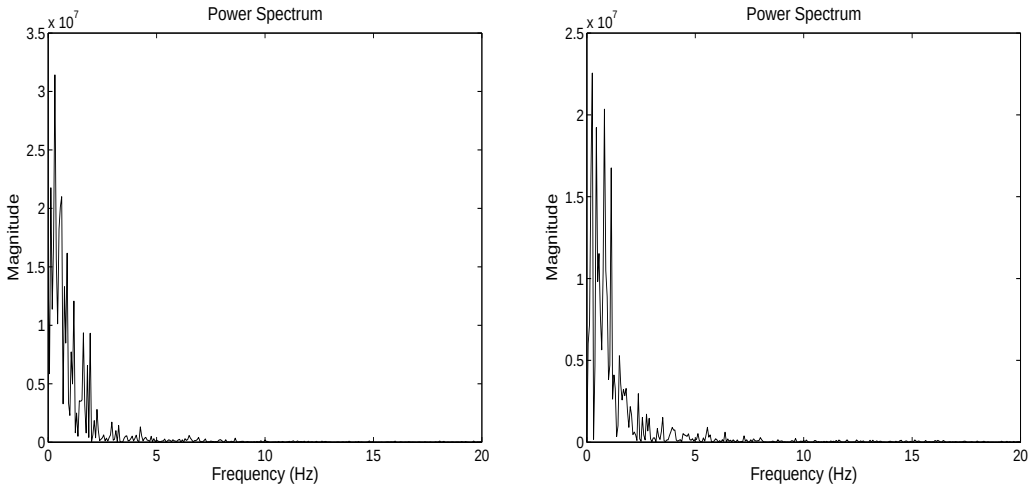

(a) Epoch 1

(b) Epoch 2

Figure 4.2: The power spectrum of two newborn EEG background epochs, demonstrating the power law associated with the spectrum.

from three newborns were used in this analysis and were marked as seizure free periods by a neurologist.

As a result of the bandpass filtering, the lowest significant frequency in the recorded newborn EEG is 0.5Hz. For a fractal signal to be considered stationary it must be at least twice as long as the period of the lowest significant frequency component [93]. It was shown that the newborn EEG can be significantly nonstationary for periods as low as 6 seconds [20]. Therefore, using this information, we decided to segment the EEG recordings into epochs of 256 samples (i.e. 4 seconds) which fits the requirements of a quasi–stationary period for the newborn EEG background.

A total of 5000 epochs from three newborns were assessed using the Higuchi method of FD. The FD estimates appeared to be random with an estimate of the probability density function (pdf) shown in Figure 4.3.

The Lilliefors and Jarque-Bera tests for goodness–of–fit to a normal distribution were applied to the FD estimates. Both tests indicate that the FD estimates were not normally distributed at the 5% significance level. Therefore, we assumed that the distribution was a Beta distribution. Using the *betafit* function in Matlab, we estimated the parameters α and β for the Beta distribution, along with there 95% confidence intervals to be

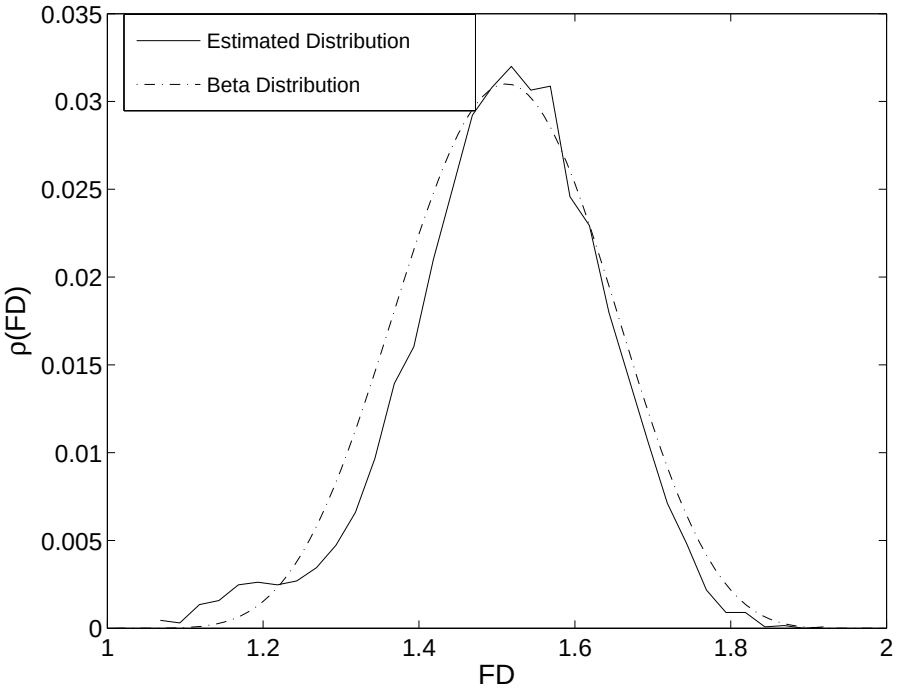

Figure 4.3: An estimate of the pdf for the FD of real newborn EEG background.

$$\alpha = 7.3471 \begin{cases} 7.5620 \\ 7.1323 \end{cases} \qquad \beta = 7.1321 \begin{cases} 7.3770 \\ 6.8873 \end{cases} \tag{4.12}$$

The relatively small confidence intervals indicate the likeness of the estimated Beta distribution to the dataset. The distribution has a mean of 1.51 and a standard deviation of 0.125, which can both be derived from α and β. The theoretical pdf for the defined Beta distribution[4] of the FD estimates is also shown in Figure 4.3.

[4]The Beta distribution is a two parameter (i.e. α and β) distribution which has a finite density if $\alpha, \beta \geq 1$, and the integral is finite if $\alpha, \beta > 0$.The density function for the Beta distribution is expressed as [97]

$$\begin{aligned} \rho(\theta) &= \frac{\Gamma(\alpha+\beta)}{\Gamma(\alpha)\Gamma(\beta)}\theta^{\alpha-1}(1-\theta)^{\beta-1} \\ \theta &\in [0,1] \end{aligned}$$

where

$$\mathcal{E}(\theta) = \frac{\alpha}{\alpha+\beta}, \qquad \text{var}(\theta) = \frac{\alpha\beta}{(\alpha+\beta)^2(\alpha+\beta+1)} \tag{4.13}$$

4.3.2 Background Simulation Algorithm

The simulation of the newborn EEG background is based on the formation of signals which have similar fractal and time–varying characteristics as the real newborn EEG background. To create the desired fractal signals with known FD, we start with a power spectrum $S_w(f)$ representative of a white sequence, such that

$$S_w(f) = r^2 \tag{4.14}$$

where r is a positive constant. We then multiply the power spectrum in (4.14) by the power law sequence that relates to the desired theoretical FD to give the power spectrum of the fractal signal,

$$S_F(f) = \frac{r^2}{|f|^\gamma} = X_F(f)X_F^*(f) \tag{4.15}$$

where

$$X_F(f) = \frac{r}{|f|^{\gamma/2}} e^{j\theta(f)} \tag{4.16}$$

is the FT of the fractal signal, $x_F(t)$. The mapping from $S_F(f) \rightarrow X_F(f)$ is not unique because the phase information $\theta(f)$ has been discarded in power spectrum. Therefore, in generating our desired fractal signals we have chosen $\theta(f)$ to be a realization of stationary random process $\Theta(f)$, with uniform distribution on the interval $[0, 2\pi)$. The hypothesis of a uniform distribution was tested using the Kolmogorov-Smirnov test on five hundred newborn EEG background epochs and could not be rejected at the 5% significance level.

The FT of a real signal gives a function with Hermitian symmetry[5]. This means that for the realization of the random process, $\theta(f)$, we only need the frequency variable f to be positive (i.e. $f \in \mathbb{R}^+$), as this will also provide us with the negative frequency values of $\theta(f)$. Once $\theta(f)$ has been obtained, we can obtain the fractal signal by taking the inverse FT of (4.16), such that

$$x_F(t) = \int_{-\infty}^{\infty} X_F(f) e^{j2\pi ft} df \tag{4.17}$$

Insignificant power in frequencies less than 0.5Hz, is generally removed from the EEG by highpass or bandpass filtering [71, 98]. Therefore, to simulate EEG data, our next step was to highpass filter the fractal signal. To investigate the effect of filtering on the synthetic fractal signal, we plotted the FD estimate of the non–filtered signal versus the FD estimate of the filtered signal in Figure 4.4.

[5] A function, $g(t)$, is Hermitian if $g(t) = g^*(-t)$.

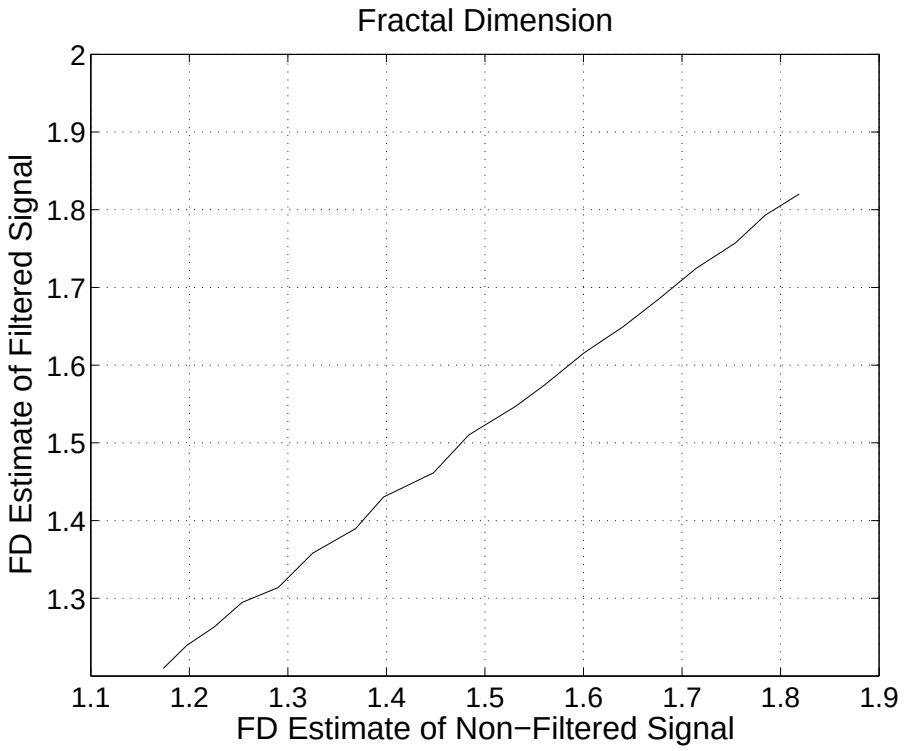

Figure 4.4: FD estimate of the non–filtered signal versus the FD estimate of the filtered signal.

The plot in Figure 4.4 shows that the FD estimate of the filtered signal is approximately equal to the FD estimate of the non–filtered signal from 1.2 to 1.8, for which a large proportion of the real EEG is estimated (see Figure 4.3).

To simulate the newborn background EEG, we chose to create synthetic epochs of length 256 samples, which is the same length used in the analysis of the real newborn EEG background. The theoretical FD of each epoch was randomly chosen according to the Beta distribution with parameters $\alpha = 7.35$ and $\beta = 7.13$, as was explained in section 4.3.1. The epochs were then highpass filtered with cutoff frequency randomly selected according to a uniform distribution on the interval $[0.4, 0.6]$Hz to vary the peak frequency. The synthetic epochs were then concatenated to form the synthetic signal. The synthesized signals are therefore nonstationary as a result of the epochs having varying FD and peak frequencies.

Figures 4.5(a) and 4.5(b), show an epoch of the simulated newborn EEG and real newborn EEG, in the time and frequency domains respectively. It is clear from Figure 4.5(b) that both the simulated and real EEG have similar spectral power laws. It should also be noted that the simulated signal in Figure 4.5(a) is free of artefacts, as are all

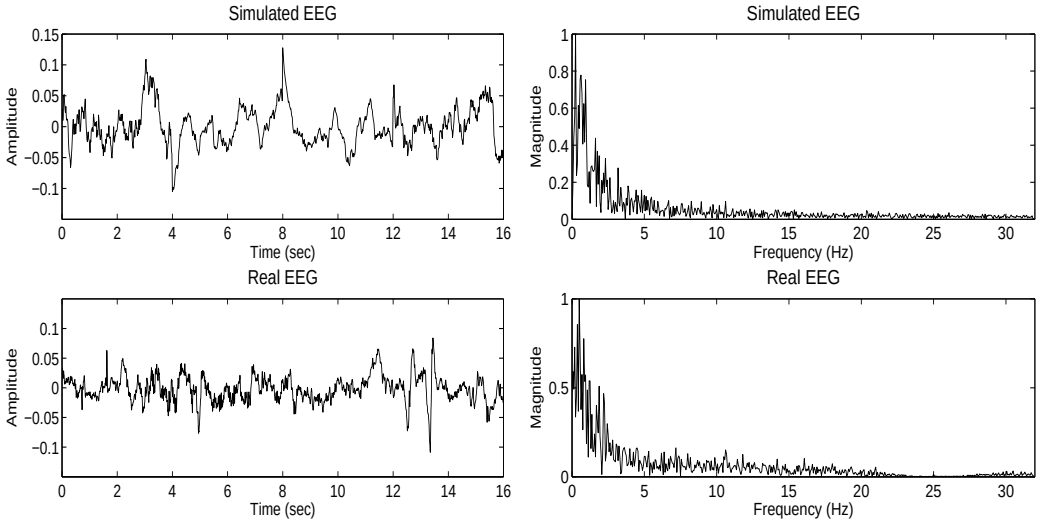

(a) Time domain

(b) Frequency domain

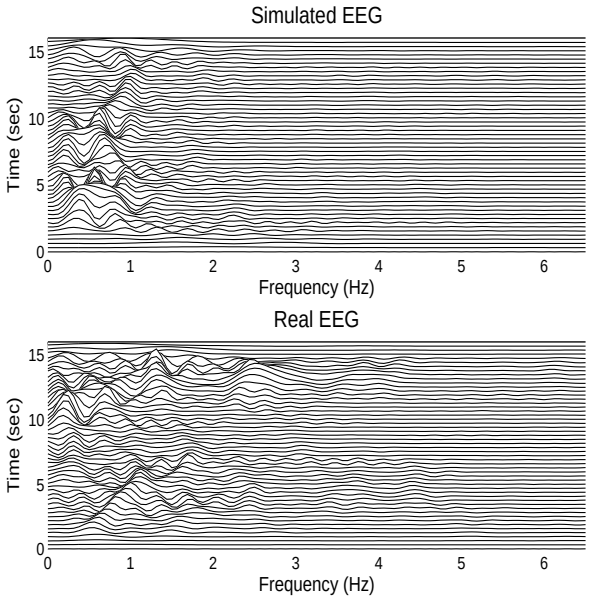

(c) TF Domain

Figure 4.5: Similarities between the simulated and real EEG in the (a) time domain, (b) frequency domain, and (c) TF domain.

the simulated newborn EEG background using this technique. This is desirable for the initial evaluation of some detection algorithms.

A comparison between the real and simulated EEG in the TF domain, using the B–distribution [21], is shown in Figure 4.5(c). These plots show the nonstationarity of the real and simulated EEG. Figure 4.5(c) also shows that neither the real or simulated EEG have any clear pattern in the TF domain. Instead they both exhibit random fluctuations in the IF content which is a known characteristic of the newborn EEG background [16].

Evaluating newborn EEG simulation algorithms is a difficult task. However, this method of simulation allows for both the nonlinear and nonstationary characteristics of the newborn EEG background where previous methods of newborn EEG background simulation, such as [1, 27], make the invalid assumption of stationarity.

4.4 Newborn EEG Seizure Simulation

A prominent characteristic of newborn EEG seizure is its nonstationarity. The TF patterns of the nonstationary newborn EEG seizure have been extensively studied and classified in [16, 20, 99]. This indicates that the simulated newborn EEG seizure should somehow incorporate the general TF characteristics found in the newborn EEG seizure.

Two models for newborn EEG seizure simulation have previously been proposed. The first technique developed by Roessgen in [1] is based on some physiological parameters of the brain and utilizes a stationary sawtooth waveform. This technique was recently extended by Boashash and Mesbah in [16] to incorporate a single LFM signal. Celka and Colditz have also developed a piecewise LFM model of seizure based on a Weiner filter with sawtooth inputs and nonlinear gain [27].

The Roessgen model lacks the incorporation of nonstationarity, while Boashash's and Mesbah's addition only handles single LFM behaviour, not the piecewise LFM often seen in seizure. The method proposed by Celka and Colditz lacks time–dependent signal shape and time–dependent harmonic magnitude variation. It is also unable to simulate the sharp repetitive spikes often associated with newborn EEG seizure.

Our proposed method of newborn EEG seizure simulation makes use of the piecewise LFM patterns outlined in [16, 20, 99], as well as the results from our own TF investigation. Using these defined patterns, we generate various TF templates of newborn EEG seizure. The TF templates are then mapped to the time domain using the modified short–time Fourier transform (MSTFT) magnitude method [100]. We refer to this operation as time–frequency signal synthesis (TFSS).

4.4.1 Seizure Simulation Algorithm

Initially, the desired seizure length is determined. The parameters for the seizure are chosen from their specific sampling distribution, which were based on our TF analysis of newborn EEG seizure. These parameters include the number of LFM pieces in the IF law, the slope of the LFM pieces, the seizure start frequency, the envelope of each harmonic component (relative amplitude and frequency), the SNR and seizure to background ratio (SBR). The parameter range and parameter sampling distribution are specified in Table 4.1. Note, as the beta distribution ranges from 0 to 1, the range value is used to correctly scale the sampling distribution. We have chosen the beta distribution because the distribution can be skewed and shaped using the chosen parameters, to match the observations from our TF analysis[6].

Table 4.1: Parameter ranges and distribution

parameter	**range**	**distribution**
LFM slope (Hz/sec): $\{a\}$	-0.07:0.07	Beta(2,4)
LFM pieces: $\{N\}$	1:4	Beta(3,3)
LFM envelope amplitude	-0.25:0.25	Beta(1,1)
SNR (dB)	10:20	Beta(1,1)
SBR (dB)	10:15	Beta(1,1)
seizure start frequency (Hz)	0.5:3.5	Beta(2,4)

The initial IF law of the fundamental component is generated from the selected parameters according to,

$$f(t) = \sum_{i=1}^{N} a_i t_i + c_i, \tag{4.18}$$

where,

$$t_i = \begin{cases} 0 & \text{for } t < t^i_{\text{lo}}, \\ t & \text{for } t^i_{\text{lo}} \leq t \leq t^i_{\text{hi}}, \\ 0 & \text{for } t > t^i_{\text{hi}}, \end{cases} \tag{4.19}$$

where $f_i(t)$ is the IF law, a_i is the slope of the i^{th} LFM piece, c_i is a constant to correctly align the pieces of the IF law, N is the number of pieces in the piecewise LFM and t^i_{lo} and t^i_{hi} are uniform random variables ranging across the epoch with t^i_{hi} conditioned on t^i_{lo} such that $t^i_{\text{hi}} > t^i_{\text{lo}}$ (see Figure 4.7).

The TF image is initially constructed, using the IF law, with a number of harmonics. The magnitude of each harmonic component, including the fundamental component, is multiplied by a specific, oscillating, random amplitude envelope that is estimated

[6] A special case of the Beta distribution is Beta(1,1), which is the uniform distribution.

using cubic spline interpolation ($f_{\text{envelope}}(t) << f(t)$). The TF image is smoothed, along the frequency axis, using a one–dimensional Hamming window that is scaled according to the seizure length. The two–dimensional, TF image is then synthesized into a one–dimensional, time domain signal using the MSTFT magnitude method assuming a sampling frequency of 10Hz. The seizure simulation protocol is outlined in Figure 4.6.

The MSTFT magnitude method uses an iterative technique developed by Griffin and Lim, [100], to estimate the discrete time domain signal $x[n]$. The difference between

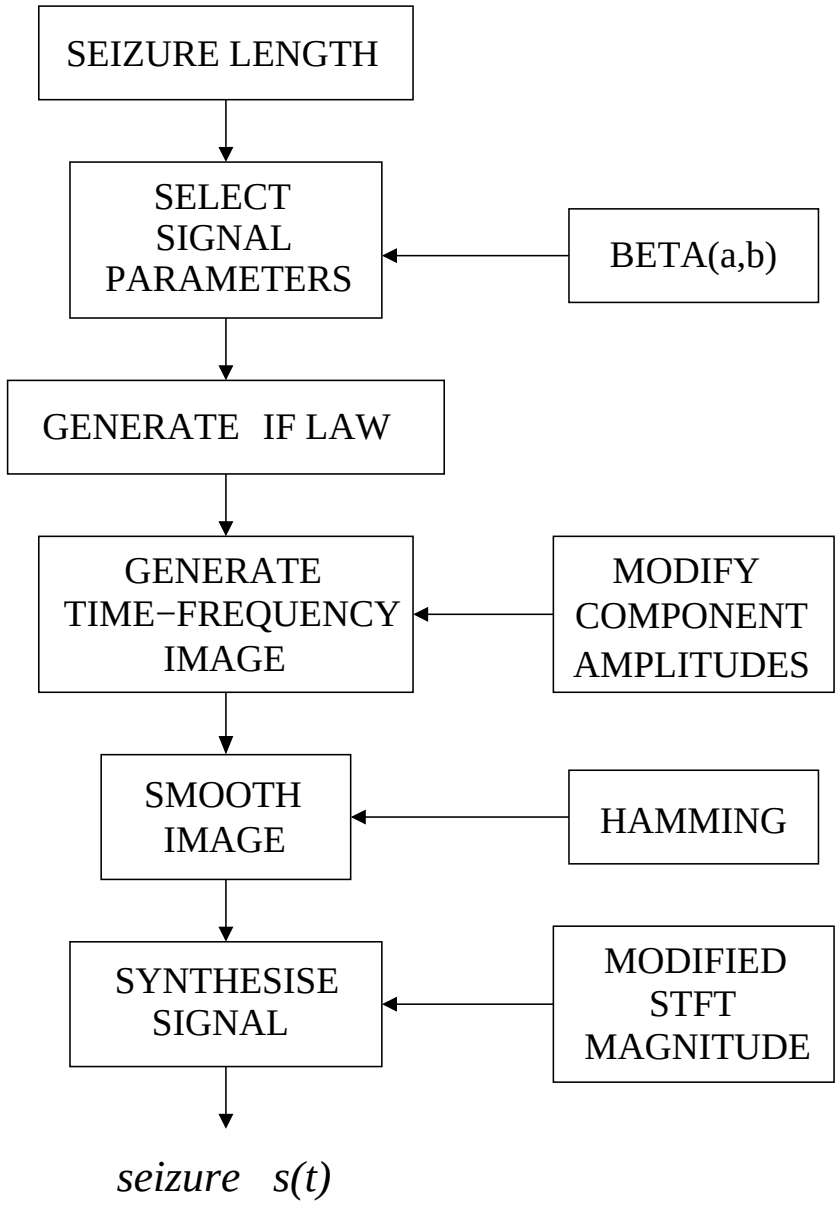

Figure 4.6: Block diagram of newborn EEG seizure simulation algorithm.

the desired STFT and the update STFT is minimized in this procedure. The update equation is as follows,

$$x_{i+1}[n] = \frac{\sum_{m=-\infty}^{\infty} w[n-m] \int_{-0.5}^{0.5} \hat{X}_i[n,f] e^{j2\pi fm}\, df}{\sum_{m=-\infty}^{\infty} w^2[n-m]} \tag{4.20}$$

where,

$$\hat{X}_i[n,f] = |Y[n,f]| \frac{X_i[n,f)}{|X_i[n,f)|}, \tag{4.21}$$

$Y[n,f)$ is the desired STFT, $X_i[n,f)$ is the i^{th} update STFT, $x_i[n]$ is the i^{th} update synthesized signal, $w[n-m]$ is the STFT window, n is discrete time, f is continuous frequency and m is the discrete time lag. The signal is synthesized with an initial $x[n]$ of white Gaussian noise. In this case, the stopping criterion of the MSTFT magnitude method is the iteration number ($i_{\max} = 200$). Further details on the convergence of the algorithm can be found in [100].

This method of signal synthesis was chosen over other available techniques as the signal synthesis is performed on a much simpler image than other techniques, which require the incorporation of crossterms in the original image. Also, the MSTFT magnitude method does not require any knowledge of the synthesized signal's initial phase.

An example of the TF template and its associated TF seizure image are shown in Figures 4.7(a) and 4.7(b) respectively. The one–dimensional simulated seizure signal using the TF image in Figure 4.7(b) is shown in Figure 4.8(a). It can be seen that the simulated EEG signal exhibits similar characteristics, in the time domain, to the real seizure signal in Figure 4.8(b).

For a more quantitative analysis, specific segments of real EEG seizure were analyzed with the intention of extracting an approximation to the piecewise LFM law and the component envelope. These values were fed into the seizure simulation algorithm and the TF images were then correlated to assess the similarity between simulated and real seizure. The results of this experiment, conducted on five seizure epochs, are shown in Table 4.2.

Table 4.2: The results of the seizure simulation technique, $\mu = 0.8$, $\sigma^2 = 0.03$.

trial	**correlation**
1	0.861
2	0.920
3	0.943
4	0.486
5	0.789

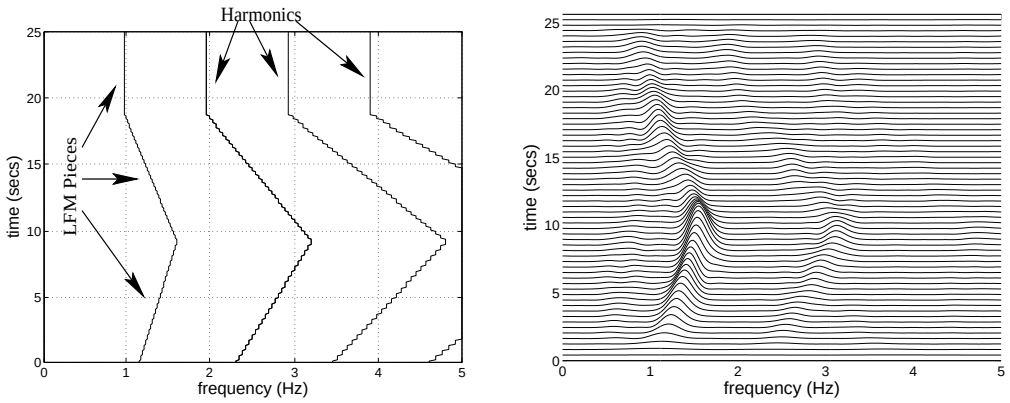

(a) generate IF law (b) Simulated TF image

Figure 4.7: The seizure synthesis procedure beginning with the (a) generated IF law and its harmonics then (b) the formation of the TF image

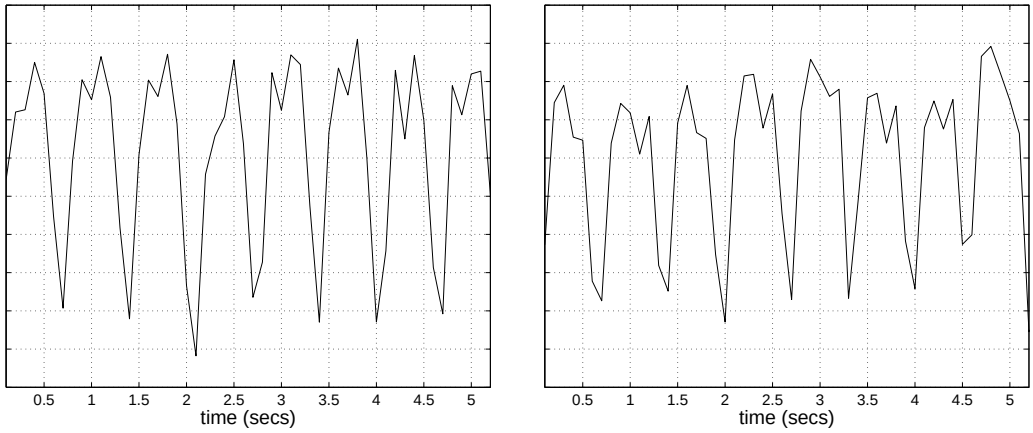

(a) synthesized seizure (b) real seizure

Figure 4.8: Comparison between the (a) synthesized seizure and (b) real seizure signals

An example of the TF output of the experiment is shown in Figure 4.9. The synthesized seizure is plotted above the real seizure in Figure 4.10. The general shape of the simulated TF image conforms to the seizure epoch with a correlation coefficient of 0.94. In the time domain the signal has the general characteristics required of a simulated signal, [16, 27], notably, nonstationary frequency content, moderate "spiky" behaviour, asymmetric oscillation and envelope amplitude variation.

The simulated EEG provides the essential signal structures seen in EEG seizure,

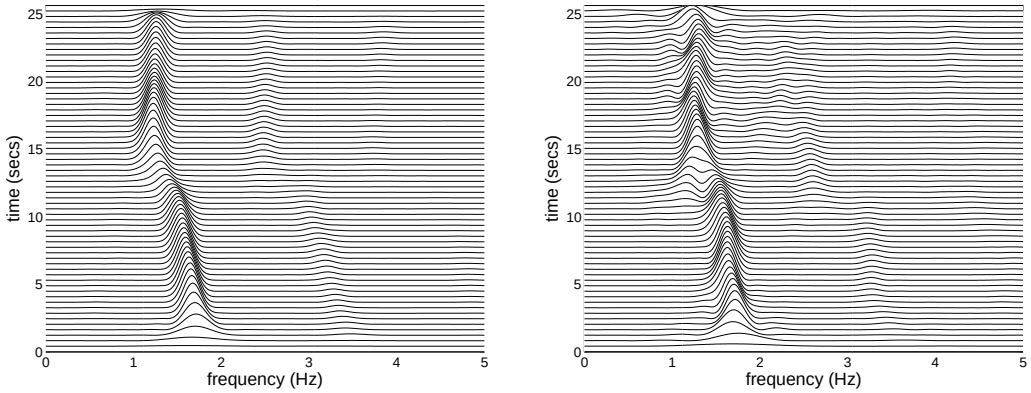

(a) simulated seizure (b) real seizure

Figure 4.9: TF domain comparison of real and simulated seizure, $\rho = 0.94$.

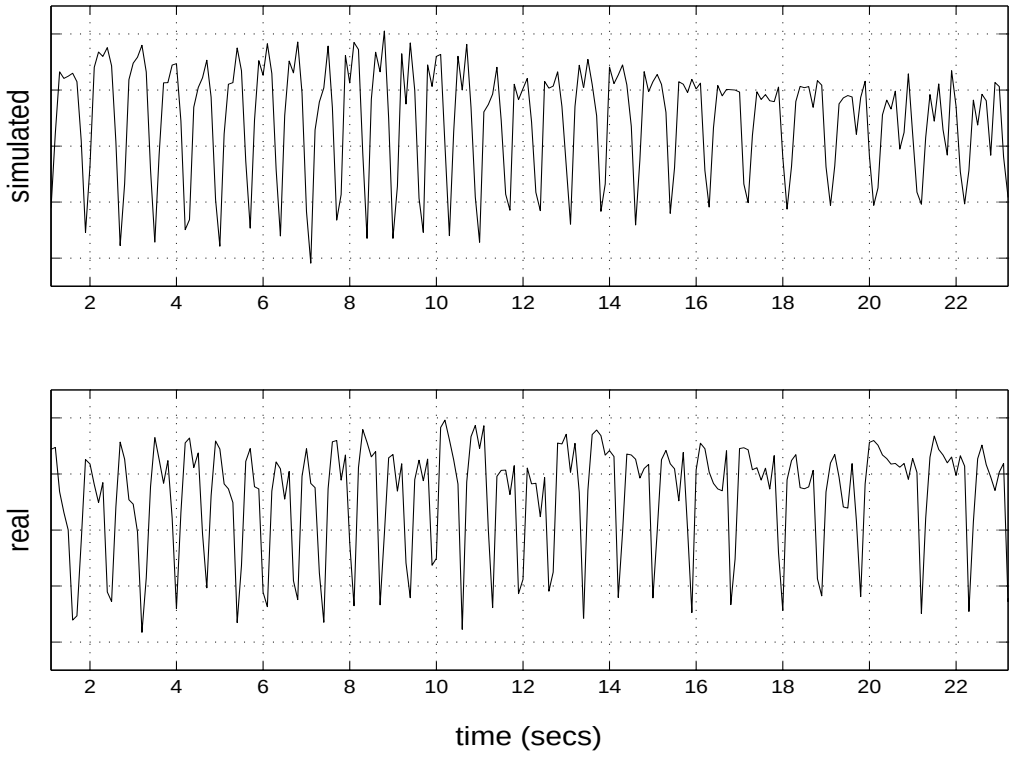

Figure 4.10: Time domain comparison of real and simulated seizure.

particularly in the TF domain, as outlined in [16]. This is shown in the high two–dimensional correlation coefficients between real and simulated signals. However, not all forms of seizure fit into this general piecewise LFM pattern of behaviour. This can be

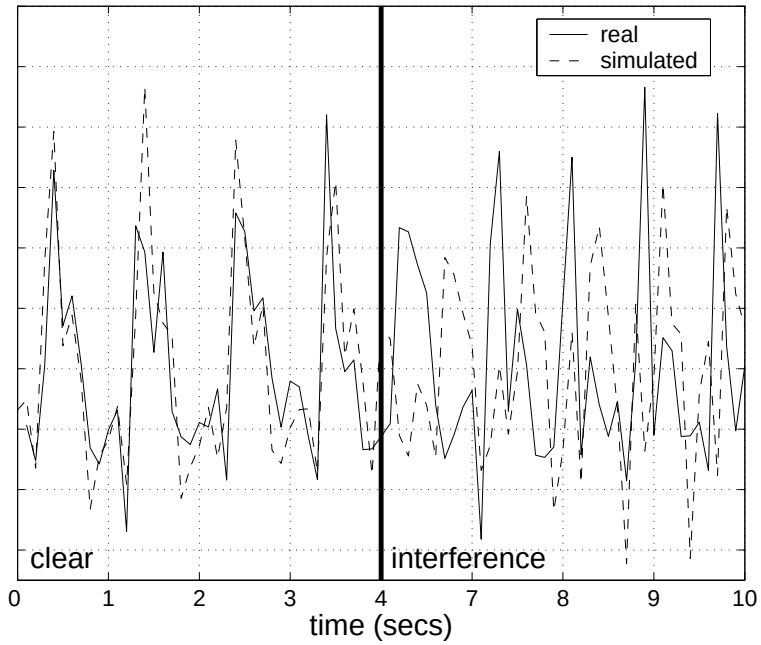

Figure 4.11: Simulated and real seizure.

seen by the low coefficient in trial 4. This particular form of seizure has a higher relative noise component, a non–piecewise LFM IF law, more transient events and contains severe "spiky" behaviour compared to other seizures. These phenomenon contribute to an effective whitening of the spectrum which interferes with the simulative capacity of a piecewise LFM model. Nonetheless, the synthesized seizure still has sections that provide a good approximation, in addition to poor approximation sections. This is shown in Figure 4.11.

The advantage of using TFSS over other techniques is its relative simplicity, its ability to handle spectral distortion and the discontinuities of the piecewise IF law. In addition, this technique can provide a larger variety of seizure waveforms, within BT[7] product limits, depending on the fundamental TF template or templates chosen. This modularity has an advantage over a method such as Celka's which would require additional complexity to incorporate other forms of seizure.

By combining the simulation algorithm for the newborn EEG background and newborn EEG seizure, we develop a complete newborn EEG simulator. This system for EEG simulation is demonstrated in Figure 4.12. During seizure periods the range for the gain values are given in Table 4.1 via the SBR. The seizure plus background is the new signal used as the signal in the evaluation of the SNR and the noise is additive

[7]The BT product refers to the value of the effective bandwidth of the signal multiplied by the effective duration of a signal and is a measure of signal richness [80].

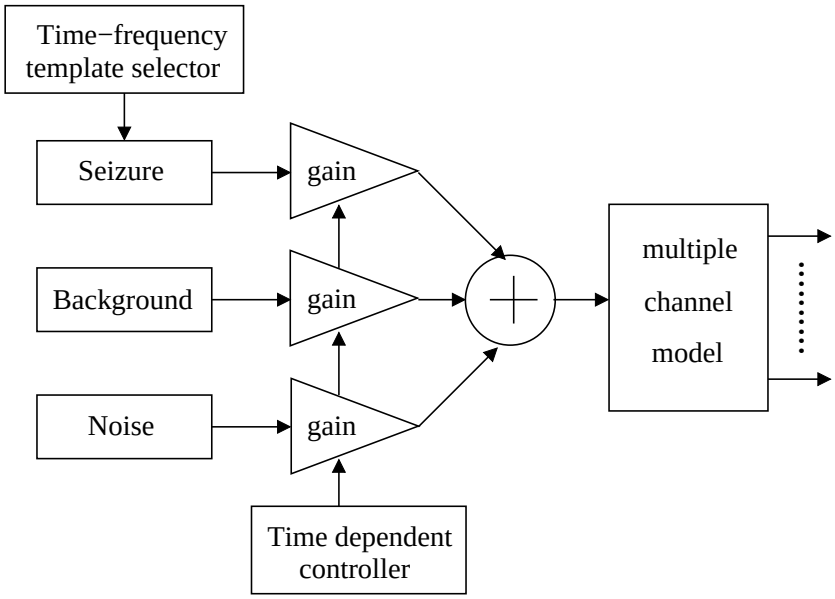

Figure 4.12: Complete newborn EEG simulator.

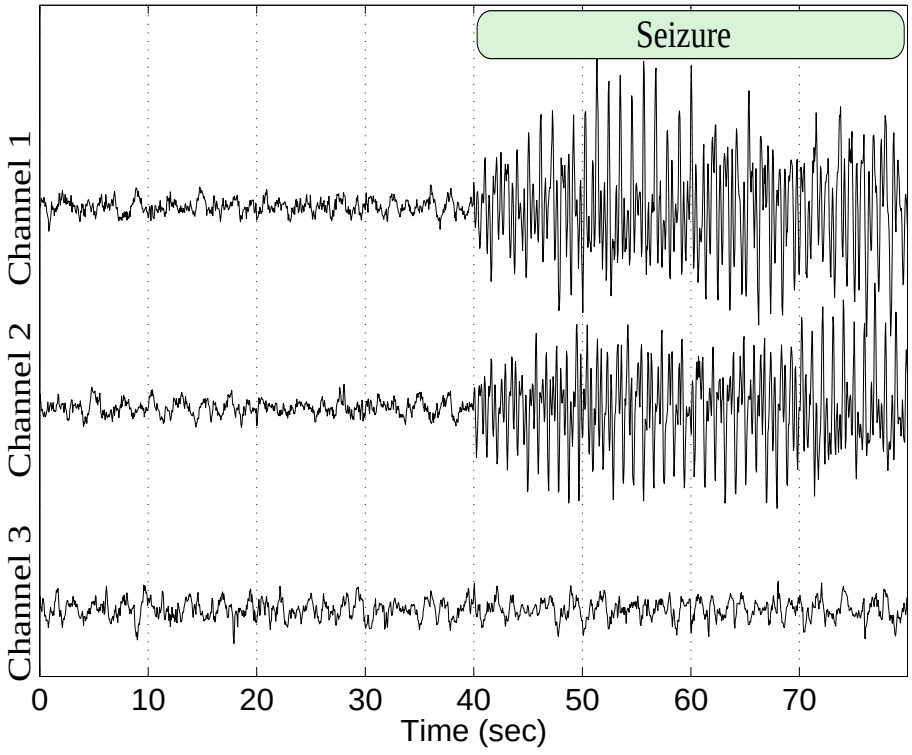

Figure 4.13: Simulated EEG channels which include background and seizure EEG.

Gaussian white noise. During nonseizure periods, the gain associated with the seizure signal is zero and the background is the signal used for the SNR.

Figure 4.13 shows an example of simulated EEG using the combination of the two proposed algorithms. Channel 1 and 2 both contain seizure starting at 40 seconds and lasting until 80 seconds. However, channel 3 does not contain any seizure. This example is simulative of a real EEG seizure event in the newborn and could be used for assessing automatic seizure detection algorithms.

4.5 Summary

This chapter presents a method for simulating newborn EEG background and a method for simulating newborn EEG seizure. It was shown that the power spectrum of real newborn EEG background closely follows a power law of the form $S(f) \propto |f|^{-\gamma}$. Using this result, it was assumed that the newborn EEG background exhibited fractal characteristics. Therefore, we analyzed real newborn EEG background using a FD estimate obtained from the Higuchi method [94]. It was then assumed that the FD of the newborn EEG background was random and it was estimated that the distribution was a Beta distribution with $\alpha = 7.35$ and $\beta = 7.13$. The simulated newborn EEG background was then created by concatenating fractal epochs, randomly chosen according to the defined Beta distribution, with peak frequencies between [0.4,0.6]Hz, also chosen randomly. Previous background EEG simulation methods have assumed stationarity. However, our proposed newborn EEG background simulation algorithm has allowed for the nonlinear and nonstationary characteristics observed in real newborn background EEG.

The proposed newborn EEG seizure simulation algorithm was developed by taking into account the prominent TF characteristics that have been observed in the TFSA of real newborn EEG seizure. The algorithm begins by creating a TF template of newborn EEG seizure that mimics the observed TF seizure characteristics of real newborn EEG seizure. The TF templates are then mapped to the time domain using a TFSS technique called the MSTFT magnitude method. It was then demonstrated how the background and seizure simulation algorithms could be combined to form a complete newborn EEG simulator which can be used for the testing and comparison of automatic newborn EEG seizure detection algorithms.

Chapter 5

Detecting Signal State Changes Using MP-Based Structural Complexity

5.1 Introduction

Atomic decomposition techniques using redundant dictionaries have become increasingly popular alternatives to traditional signal representations which make use of orthogonal bases. By incorporating redundant dictionaries, these techniques can adaptively select optimal waveforms to represent the signal. This can lead to higher resolution and sparser signal representations.

The MP algorithm, proposed by Mallat and Zhang [37], is one such decomposition technique which is gaining popularity. It has been applied in many different signal processing areas. In particular, it has been recently used for the analysis of adult EEG [38, 39, 40, 42] and has been incorporated into an automatic adult EEG seizure detection algorithm [43]. The MP algorithm using TF dictionaries has a number of advantages over classical analysis techniques. It can provide information about the time–varying characteristics of nonstationary signals without introducing crossterms, as in the case of QTFDs [37]. It can also provide information on the nonlinearities in the signal [39]. Another advantage of the MP algorithm is that it can be used as a denoising tool.

The denoising technique of MP relies on the TF dictionary being more coherent with the desired signal structures than the noise component. This means that the atoms representing the desired signal structures will be chosen first in the MP decomposition. Therefore, if the iterations are stopped before the noise component is represented, we can reconstruct a signal or obtain a TFR with less noise. The change in exponential

decay of the absolute value of the atom coefficient value is generally used as a stopping criterion for denoising with MP [37].

Another atomic decomposition which has only recently been proposed is the BP decomposition technique [88]. Like the MP algorithm, BP can also provide crossterm free TFRs and has denoising capabilities. BP decomposition was proposed with the goal of providing a sparser signal representation than MP. However, in many signal processing applications, such as signal and image compression and denoising, only an adequate signal approximation is required instead of a complete signal representation.

In this chapter, we begin by comparing the sparsity of signal approximations from both MP and BP decompositions. This comparison is done in order to determine which of the two decomposition techniques generally provides the sparsest signal approximation.

We then introduce a new signal complexity measure in section 5.3, referred to as signal *structural complexity* (SC). The measure is shown to be a quantification of the coherency between the decomposition dictionary's atoms and the structures within a signal.

Often, if the underlying process generating the signal undergoes some type of change, this will generally reflect on the signal itself. Through synthetic examples in section 5.3, we demonstrate how the SC measure can be incorporated as a method of detecting changes in signal structure and, therefore, state of the underlying process.

The generic detection methodology based on the change in the SC measured is then applied to the automatic detection of newborn EEG seizure in section 5.4. To optimize this automatic detection method, we develop a TF dictionary that is coherent with newborn EEG seizure structures. The automatic detection method is demonstrated firstly using synthetic newborn EEG data and then confirmed using real newborn EEG data.

5.2 Sparsity Comparison of MP and BP Approximations

There are three desirable attributes of a decomposition technique that have been defined by Chen et al. [88]. The first attribute is *speed,* which means that a decomposition algorithm should run in the order of $O(N)$ or $O(N \log_2(N))$ time. Secondly, it is desirable for a decomposition technique to be able to resolve components that are close in time and frequency (i.e. *superresolution*). Thirdly, a decomposition technique should aim to provide the *sparsest* (most compact) representation, which is the representation

with the fewest significant coefficients[1].

It has been shown through a number of computational examples that BP provides a sparser signal *representation* than MP [88]. Also, for some specific redundant dictionaries, it has been shown that the ℓ^1 optimization of the BP algorithm results in the optimally sparse representation, which has been referred to as the *ideal signal representation* [101]. However, in many signal processing applications we only require an adequate signal *approximation* instead of a complete signal representation.

An approximation of the signal $x(t)$ using MP or BP can be written as:

$$\hat{x} = x - e_a \tag{5.1}$$

where e_a is the approximation error (n.b. it was previously referred to as the residual in Chapter 3). A relative measure of approximation accuracy is defined through the signal to error ratio (SER), expressed as

$$SER = 10 \log_{10} \left(\frac{E_x}{E_{e_a}} \right) \text{dB} \tag{5.2}$$

where E_x and E_{e_a} represent the energy in the signal and energy in the error signal, e_a, respectively.

If a desired level of signal approximation, SER_D, is predefined, it can be used as a stopping criterion for MP. That is, at iteration i of the MP algorithm, $SER^i_{\hat{x}}$ is compared with SER_D. If $SER^i_{\hat{x}} \geq SER_D$ the iterations are stopped, otherwise, the iterations are continued. The atoms selected in the approximation are referred to as the *significant atoms*.

Determining the significant atoms from a BP decomposition differs slightly from MP. The BP decomposition technique does not select its atoms iteratively like MP, but instead iteratively improves the signal representation according to the objective function (see Chapter 3). Therefore, after BP has obtained its optimal signal representation, we then iteratively add the selected atoms in order of their coefficient value (i.e. largest coefficient to smallest) until the signal approximation achieves $SER_{\hat{x}} \geq SER_D$.

5.2.1 Comparison Experiment

To compare the sparsity of signal approximations using MP and BP, we developed an experiment using two real life signals; a whale song and a newborn EEG recording. In this experiment we segmented the real life signals into 50 epochs of length 512 samples.

[1] It should be noted that *significant coefficients* and *significant atoms* are used interchangeably to represent the number of atoms (coefficients) in a signal representation.

The WP dictionary was used for both decomposition techniques. The range of desired signal approximations levels were, $SER_D = [7.5, 10, 12.5, 15, 17.5, 20]$.

Figures 5.1(a) and (b) show the average number of significant atoms needed by MP and BP, at each approximation level, for the whale signal and EEG recording respectively. It can be seen from the plots in Figures 5.1(a) and (b) that the BP decomposition, on average, requires more atoms than MP to approximate both the whale song and EEG recording. These two examples indicate that MP provides the sparsest signal approximation. In fact, extensive testing using different types of real life and synthetic signals show that MP generally provides a sparser approximation than BP [46, 47].

Recently, it has also been proven that for *quasi-incoherent*[2] dictionaries, the orthogonal MP (OMP)[3] provides a sparser approximation than BP [102]. For this reason, as well as our experimental results shown in this section and in [46, 47, 49], we have adopted MP as the preferred signal decomposition method in this thesis.

5.3 Structural Complexity

An important feature from an MP decomposition is the number of significant atoms. This feature can provide information about the structure of the signal under analysis in relation to the decomposition dictionary. For example, if a signal has components that have strong correlation with the decomposition dictionary's atoms, fewer significant atoms will be needed to approximate the signal. We qualify this by saying that the signal complexity is low. These signal components are referred to as *coherent structures* [37]. If the signal structures change such that their correlation with the decomposition dictionary's atoms is reduced, the number of significant atoms needed for the approximation will increase, which indicates that the signal complexity has become higher. Therefore, we can use the number of significant atoms in a signal approximation to quantify the complexity of a signal. We refer to this measure of complexity as *structural complexity* (SC).

Figure 5.2 shows the basic methodology for obtaining the SC measure. It can be seen from Figure 5.2 that the SC measure is a function of:

1. Desired level of accuracy of the approximation (SER_D)

[2]The definition of coherent and incoherent here is based on the coherency between atoms within the decomposition dictionary. This should not be confused with our definition of coherent which is based on how much atoms from the decomposition dictionary correlate with signal structures. Our definition is the same as the definition provided in the original MP paper by Mallat and Zhang [37].

[3]OMP has an added criterion which requires that the selected atoms in the decomposition be orthogonal.

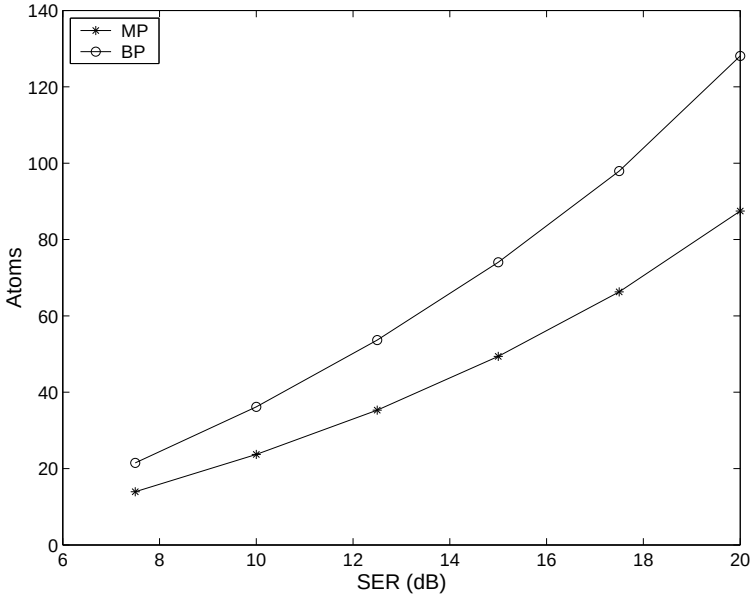

(a) Whale song

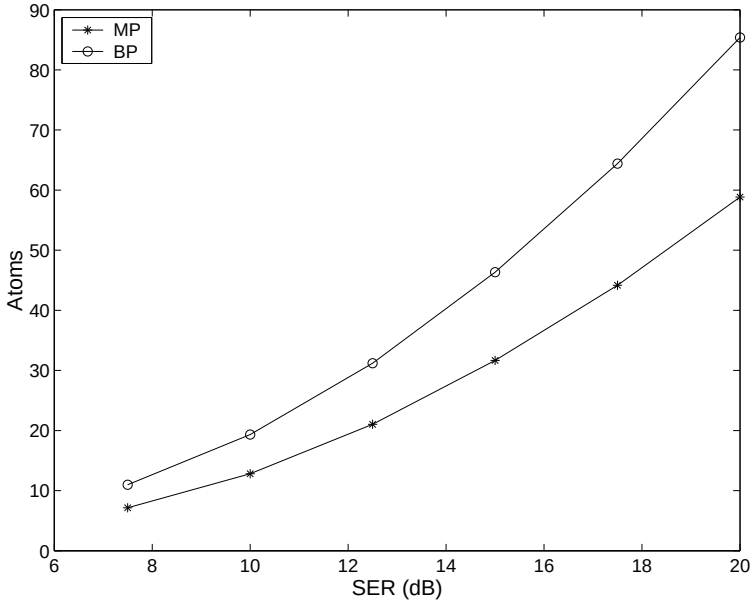

(b) Newborn EEG recording

Figure 5.1: The average number of significant atoms needed by MP and BP for (a) a whale song and (b) newborn EEG recording.

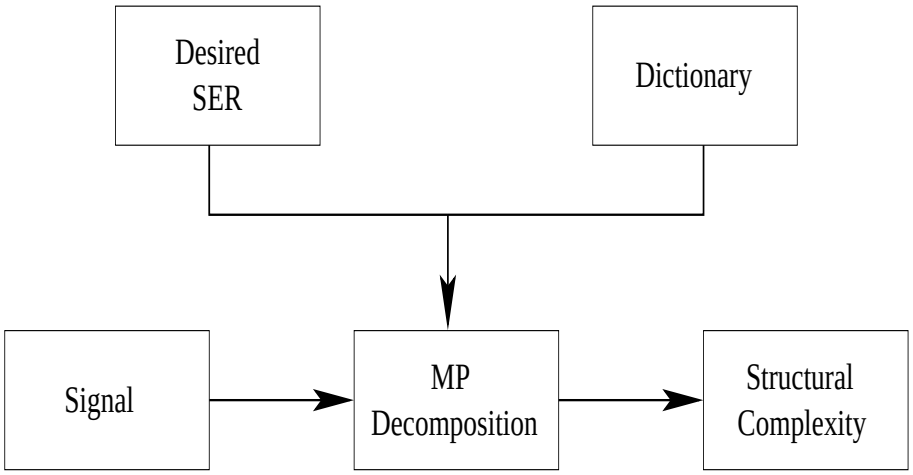

Figure 5.2: Methodology for obtaining the SC measure.

2. Type of decomposition dictionary

Therefore, we emphasize that the SC measure is not an absolute measure, but rather a relative measure that strongly depends on the nature of the decomposition dictionary.

5.3.1 Detection of Signal Transitions using SC

A change in the SC relates to a change in the coherency between the decomposition dictionary atoms and the signal structures. If the SC is changing, this implies that the structures making up the signal are changing. This may be the result of a new event taking place or the system under analysis is undergoing a change. Therefore, the proposed SC measure can be used to detect changes in the state of signals. To demonstrate the use of SC in detecting signal state transitions, we have developed two experiments.

Experiment 1:

In this experiment, we created a number of synthetic signals which have varying levels of coherency with the decomposition dictionary (i.e. different SC levels). To do this, we firstly chose two different TF dictionaries. Atoms were selected from both of these dictionaries to synthesize the signals. However one of the dictionaries chosen to create the synthetic signals was also used for signal decomposition. This dictionary is referred to as the decomposition dictionary, Φ_D. The second dictionary, not used for signal decomposition is referred to as the alternative dictionary, Φ_A. By using varying numbers of atoms from Φ_D and Φ_A, we created a number of synthetic signals with varying levels

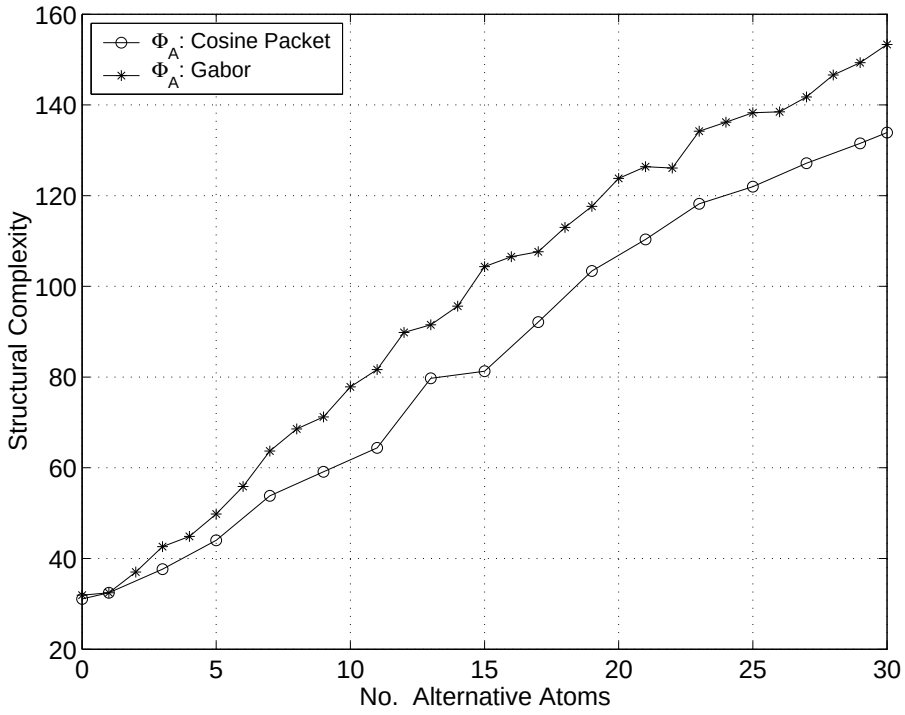

Figure 5.3: Demonstrates how the signal complexity changes as the decomposition dictionary becomes less coherent with signal structures.

of SC. That is, if a signal was constructed with a large number of Φ_D atoms and a small number of Φ_A atoms, the signal would be more coherent with Φ_D and therefore have low SC. However, if a signal was constructed using a large number of Φ_A atoms and a small number of Φ_D atoms, the signal would be less coherent with Φ_D and would result in high SC. For ease of reference, this is shown in Table 5.1

Atoms	Coherency	SC
$\Phi_D >> \Phi_A$	High	Low
$\Phi_A >> \Phi_D$	Low	High

Table 5.1: Relationship between signal structures, coherency and SC

For this experiment, the synthetic signals, of length N, were constructed using k randomly selected atoms of which $k - l$ were selected from Φ_D and l from Φ_A. The number, l, was increased from 0 to k, resulting in synthetic signals with varying levels of SC. Atoms in both dictionaries were normalized such that their ℓ_2 norm was equal to 1. This was done to remove any amplitude biasing of components.

The results of this experiment are shown in Figure 5.3. In this experiment we chose the signal length, $N = 512$, number of atoms, $k = 30$, a WP dictionary as Φ_D and

$SER_D = 13$dB. In this experiment, two alternative dictionaries:

1. Φ_A : CP dictionary
2. Φ_A : Gabor dictionary

were used to provide two separate subexperiments so that the results could be validated. In the first subexperiment, we used the CP dictionary as the alternative dictionary for synthesizing signals. It can be seen from Figure 5.3 that as the number of alternative atoms is increased (i.e. l) the level of SC also increases. This explicitly shows that the SC measure of a signal is related to the coherency between the decomposition dictionary and signal structures. For the second subexperiment, we used a Gabor dictionary as the alternative dictionary. It can be observed from Figure 5.3 that similar results have been obtained as with the CP dictionary.

As a secondary result from the two subexperiments, we can see that the CP atoms are slightly more coherent with the WP atoms than the Gabor atoms. This is indicated by slower rate of rise in SC measure.

Experiment 2:

In this experiment, we show how a change in SC can be used to detect a change in signal structure or a change in signal state. Epochs of length $N = 1024$ samples were created using 100 atoms. The atoms were randomly selected from Φ_D and Φ_A, which were chosen as the redundant WP dictionary and CP dictionary respectively. A complete signal was created by the concatenation of 300 epochs. The epochs for the signal were designed as follows:

- Epochs $1 \rightarrow 100$: $\{15$ atoms $\in \Phi_D$ & 85 atoms $\in \Phi_A\}$, randomly chosen for each epoch
- Epochs $101 \rightarrow 200$: $\{50$ atoms $\in \Phi_D$ & 50 atoms $\in \Phi_A\}$, randomly chosen for each epoch
- Epochs $201 \rightarrow 300$: $\{85$ atoms $\in \Phi_D$ & 15 atoms $\in \Phi_A\}$, randomly chosen for each epoch

The synthetic signal formed by the concatenation of synthesized epochs is shown in Figure 5.4(b). The SC measure for the synthetic signal is shown in Figure 5.4(a). It can be seen from the SC measure that there are two significant changes, separating the signal into three distinct states. The first significant change is a drop in SC which occurs at Epoch 101. The second significant change is a drop occurring at Epoch 201. These

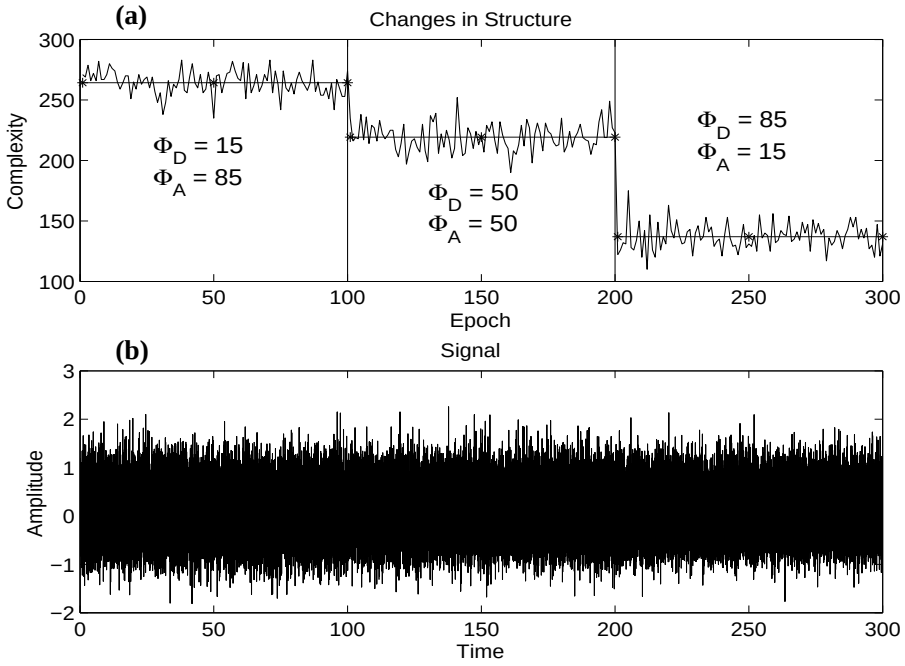

Figure 5.4: The (a) SC measure of the (b) synthetic signal which has three distinct states, as indicated by the SC measure.

are exactly the two places in which we designed the synthetic signal to have change in structure.

In Figure 5.4(a), we have also plotted the average SC value for the three signal states, indicated by '*-*'. This further emphasizes where the significant changes in SC occur. Therefore, the example in Figure 5.4 clearly illustrates the applicability of SC in detecting changes in signal state.

To demonstrate the significance of the SC measure in detecting changes in signal structure, we have also plotted the time domain and frequency domain representations of epochs from the three signal states. Figures 5.5(a)-(c) show Epoch number 50, 150 and 250, respectively. These epochs have been chosen to represent the three states of the synthetic signal. However, from these plots, the change in signal structure is not easily distinguishable. The frequency domain representations of Epoch 50, 150 and 250 are shown in the plots of Figures 5.5(d)-(f). Again, the change in signal structure between the three signal states is not clearly visible in the frequency domain. This indicates the superiority of the SC measure in detecting changes in signal structure.

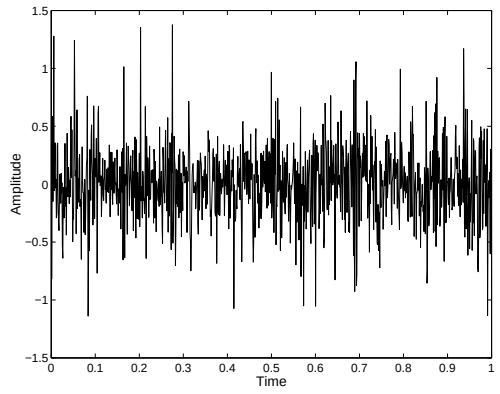

(a) Time domain; Epoch 50

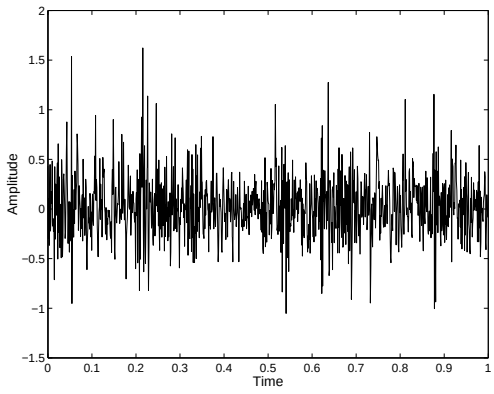

(b) Time domain; Epoch 150

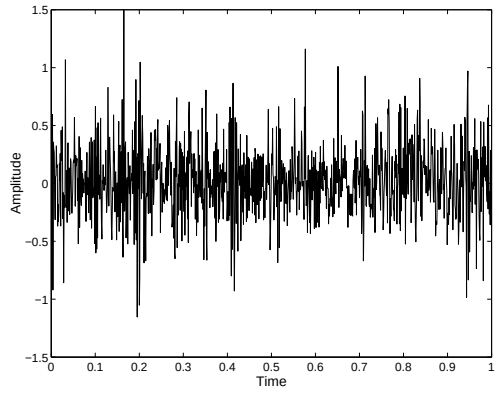

(c) Time domain; Epoch 250

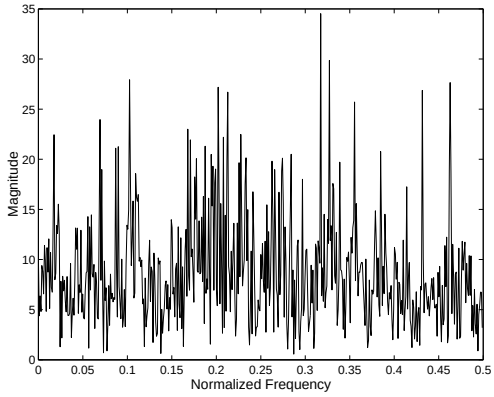

(d) Frequency domain; Epoch 50

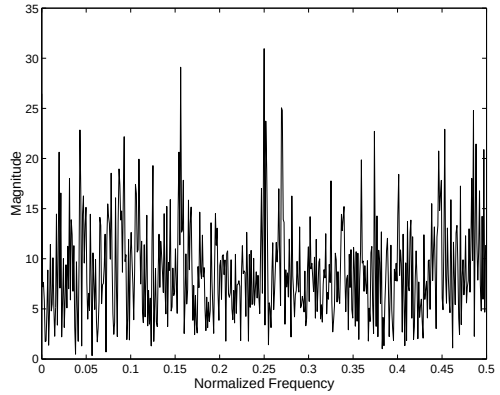

(e) Frequency domain; Epoch 150

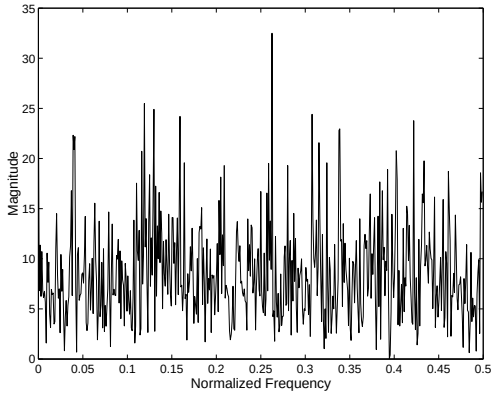

(f) Frequency domain; Epoch 250

Figure 5.5: Time domain representation (a-c) and frequency domain representation (d-f) of the three states of the signal in Figure 5.4(b). No clear difference in states is visible from either the time domain or frequency domain.

5.4 Newborn EEG State Transition Detection using SC

In the previous section, it was shown that if a signal had structures that were highly coherent with the decomposition dictionary, then the SC measure for the signal was low. As the signal structures became less coherent with the decomposition dictionary, the SC measure increased. Therefore, we demonstrated that SC could be used to detect changes in signal structure or transitions in signal state.

In the previous experiments, we designed signals with varying levels of coherency with the decomposition dictionary. This assumed that we had a decomposition dictionary that was highly coherent with a particular signal state. However, in real life applications, decomposition dictionaries that are coherent with a particular signal state may not be readily available. The reason is that the structures (or models) of these signals are generally unknown. In this case, a decomposition dictionary, coherent with a particular signal state, may have to be designed. Our method of designing coherent dictionaries involves creating TF atoms that match the TF patterns observed in a particular signal state. The TF patterns in the signal state of interest may be used to construct dictionary atoms that are coherent with the signal structures for that particular state.

5.4.1 Time-Frequency Analysis of Newborn EEG

The newborn EEG of patients who experience seizure events is one example of a real life signal which has two specific states. The first EEG state is the background (nonseizure) and the second state is the ictal or seizure state. Therefore, the automatic detection of the transition between these two states is a possible application of the SC detection methodology.

An investigation into the TF characteristics of the newborn EEG was previously undertaken by Boashash et al. [16, 103]. In this investigation, the authors looked at both the seizure state and background state of the neonatal EEG. The analysis was done using the B-distribution (described in chapter 3). It was concluded from their TF analysis that the IF of the newborn EEG seizure could be broadly characterized by piecewise LFM with slowly varying amplitude. In their analysis, it was also quite often observed that the newborn EEG seizure was multicomponent in nature. Both these characteristics can be seen in the TFRs of seizure epochs in Figures 5.6(a) and (b).

In Figure 5.6(a), it can clearly be seen that the IF slope changes significantly at around the 8 second mark. This is a demonstration of the piecewise LFM nature of the newborn EEG seizure. In contrast, the seizure epoch in Figure 5.6(b) has an almost constant IF.

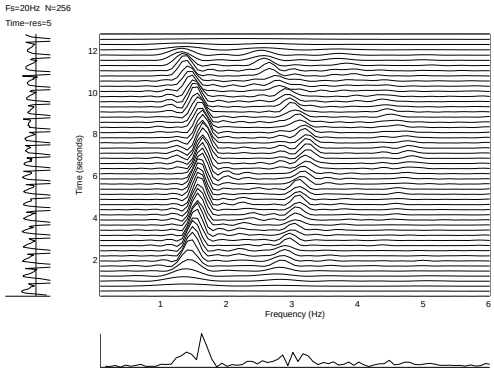

(a) Seizure exhibiting piecewise LFM, multicomponent

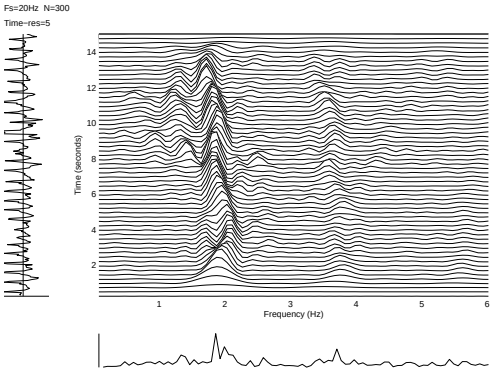

(b) Seizure exhibiting quasi-constant, multicomponent

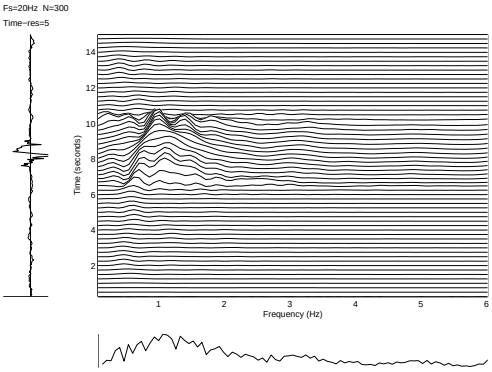

(c) Background, burst-suppression pattern

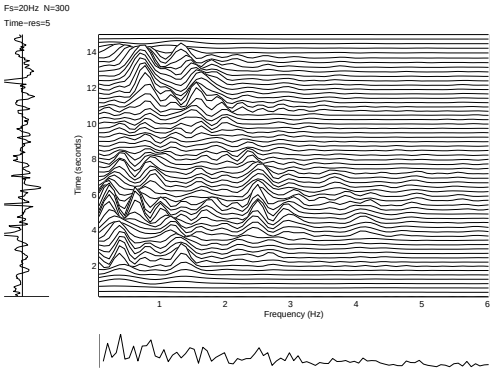

(d) Background lacking specific pattern

Figure 5.6: TFR of various seizure patterns (a-b) and nonseizure patterns (c-d).

In the analysis of the newborn EEG background, it was found that there were only two significant types of patterns in the TF domain. The first pattern is related to the burst-suppression background abnormality. In the time domain, this pattern is characterized by a burst of high voltage activity lasting 1-10 seconds followed by a period of quiescence or inactivity [59], which was discussed in detail in chapter 2. Figure 5.6(c) illustrates a burst-suppression pattern in the TF domain. It can be seen that the burst of high energy masks all other patterns in the TFR. The second class of pattern found in the TFR of newborn EEG background is the EEG activity *lacking a specific TF pattern* [103]. In this background state, there does not exist a dominant TF component which follows any specific IF law. An example of this type of background is shown in Figure 5.6(d).

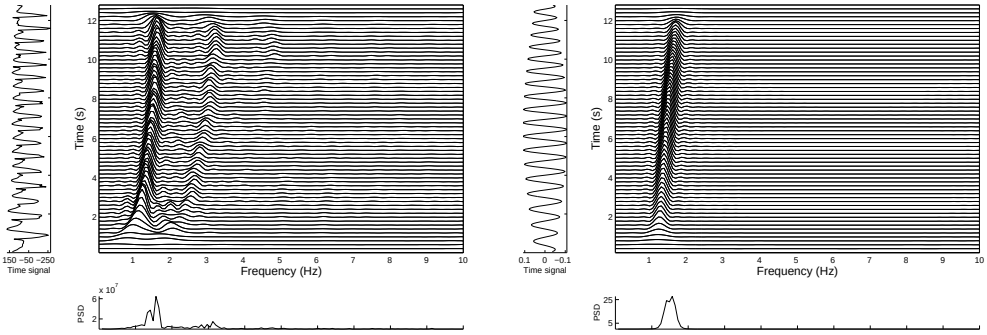

(a) Seizure epoch

(b) Atom 1

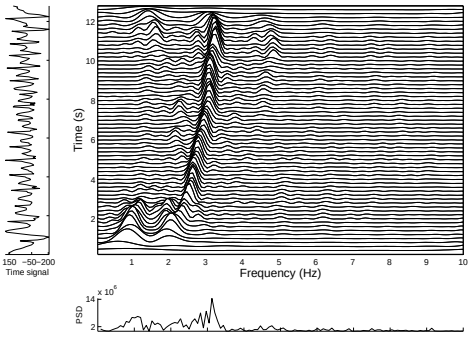

(c) Residual: R^1x

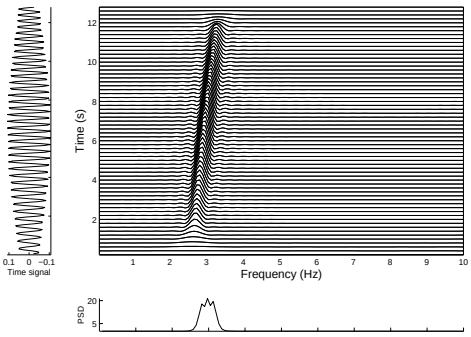

(d) Atom 2

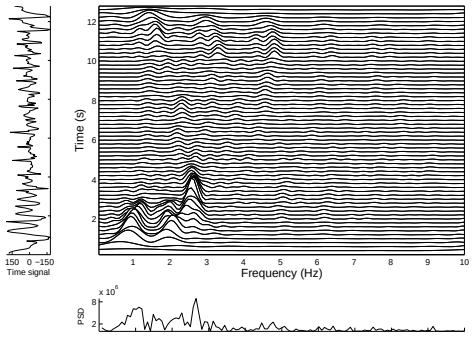

(e) Residual: R^2x

Figure 5.7: The MP decomposition of a seizure epoch using the proposed TF dictionary. The first two atoms selected by the MP algorithm, (b) and (d), are clearly coherent with the seizure signal structures (a) and (c). The residual after two iterations (d) has no clear, dominant TF patterns.

5.4.2 Coherent Dictionary Design

In the TF analysis of the newborn EEG seizure by Boashash et al. [16], the authors determined that LFM nature of seizure patterns had starting frequencies of between [1.5,5]Hz and an LFM frequency slope of between [-0.06,0]Hz/sec. However, in our TF analysis of newborn EEG seizure, also using the B–distribution, we have found that LFM components have a wider range than that presented in [16]. It was found that a more appropriate range for the starting frequency of newborn EEG seizure components was between [0.65,5]Hz with LFM slopes of between [-0.06,0.06]Hz/sec. Figure 5.7(a) shows an epoch of newborn EEG seizure which has two components with increasing frequency (i.e. positive LFM slope) verifying the inclusion of these positive rates.

It was concluded from the TF analysis that the coherent TF dictionary must include LFM atoms which cover the defined ranges in starting frequency and LFM slopes. It was also decided that only LFM atoms were to be included in the dictionary and not piecewise LFM, which would cause a combinational explosion for constructing atoms, making the decomposition dictionary excessively large and causing unrealistic processing times.

The set of LFM atoms to be included in the proposed dictionary were of the form

$$\phi_{\gamma LFM}(n) = \cos\left(\frac{2\pi(\xi_i + \frac{\xi_r}{2}n)n}{F_s} + \theta\right) \tag{5.3}$$

where F_s is the sampling frequency and $\theta = [0, 2\pi)$ is the starting phase. As mentioned before, the initial frequency ξ_i ranged between [0.65,5]Hz and the frequency rate, ξ_r, ranged between [-0.06,0.06]Hz/sec. The sampling frequency chosen was 20Hz as frequencies above 10Hz did not exhibit significant LFM components. The epoch length chosen was $N = 256$ samples (equivalent to 12.8 seconds).

Since the described set of LFM atoms do not form a complete dictionary, we combined this set of LFM atoms with a redundant Gabor dictionary so that the constructed dictionary spanned the N dimensional Hilbert space, forming an overcomplete dictionary.

To illustrate the coherency between the signal structures of the newborn EEG seizure state and the proposed TF dictionary, we applied MP decomposition on the EEG signal whose TFR is shown in Figure 5.7(a). The atom chosen in the first iteration of MP decomposition using the newly proposed TF dictionary is shown in Figure 5.7(b). It can be seen that the atom chosen clearly resembles the dominant LFM component in the newborn EEG seizure signal. The selected atom represents approximately 50% of the energy in the seizure epoch. The residual after the first MP iteration is shown in

Figure 5.7(c)[4]. The TFR of the atom chosen in the second MP iteration is shown in Figure 5.7(d). This atom closely resembles the second LFM component in the EEG seizure epoch and accounts for approximately 10% of the signal energy. Therefore, approximately 60% of the epoch energy is represented with two coherent atoms, resulting in extremely low SC. The residual after two iterations, R^2x, is shown in Figure 5.7(e), which illustrates that no clear TF patterns remain in the residual.

5.4.3 EEG Seizure Detection using SC: Synthetic EEG Data

For the initial validation of the SC methodology for detecting changes in newborn EEG signal structure, we began testing using artefact free synthetic EEG data. The simulation process described in Chapter 4 was used to generate the synthetic newborn EEG data. By testing initially on synthetic data, we could produce long EEG signals for which we knew the exact time location where the EEG signal had changed from background to seizure.

Signal Generation

In the testing of our SC state detection method applied to newborn EEG, we created twenty five synthetic newborn EEG recordings. All synthetic EEG data was created with a sampling rate of 20Hz. For each recording, a 10 minute period of newborn EEG background was created so that an estimate of the baseline for the background period could be attained. Further to this 10 minute period of newborn EEG background, another 10 minute period of background was synthesized for testing of the false detection rate (FDR). Therefore, in total, more than 8 hours of synthetic newborn EEG background was created.

A seizure state was then added to the synthetic recordings. The seizure durations ranged between 25 seconds and 345 seconds. All seizures generated were characterized by piecewise LFM and were all multicomponent. The time-varying amplitudes of the various components of the synthetic EEG seizure were randomly selected. An example of a synthetic newborn EEG recording containing 180 seconds of seizure is displayed in Figure 5.8. In the recording, we have also marked exactly the time period for which the seizure has occurred, mimicking the marking of real EEG data by a neurologist. We have also shown which part of the background state has been used for estimating the baseline background value.

[4]It should be noted that the TFR in this plot has been rescaled to clearly show how the remaining signal energy, R^1x, is distributed in the TF domain. This is why the second LFM component appears to have larger amplitude in Figure 5.7(c) than in Figure 5.7(a).

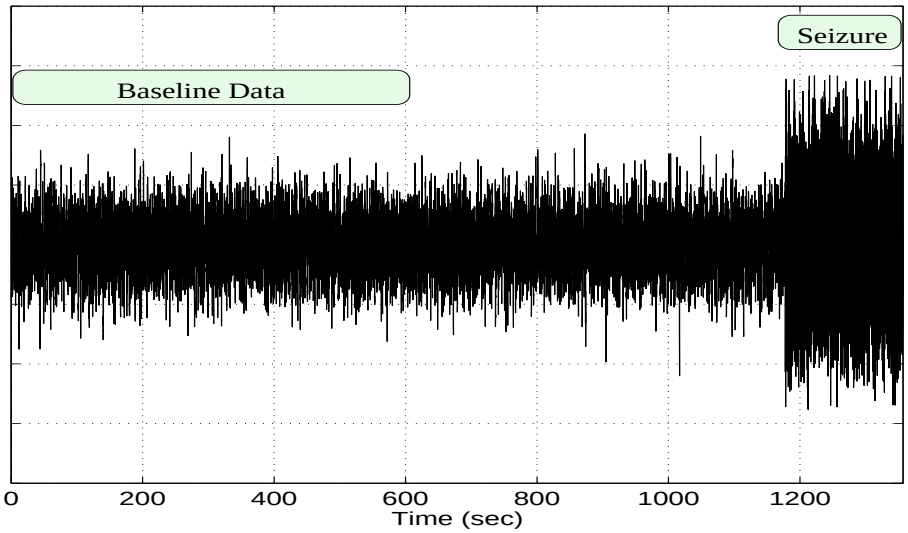

Figure 5.8: Synthetic newborn EEG recording containing background and seizure states.

Results and Discussion

The automatic detection of newborn EEG seizure using SC requires a threshold value to be set to distinguish between seizure and non seizure periods. We determine the threshold value using the baseline data, shown in Figure 5.8.

The minimum SC value for the baseline data was used as the threshold value for the seizure detection algorithm. If the SC was above the threshold value the EEG epoch was deemed a background epoch. If the SC value was less than the threshold value, then an epoch was judged to be seizure.

An example of the SC analysis of the synthetic newborn EEG data is shown in Figure 5.9. The SC measure, displayed in Figure 5.9(a), clearly shows a change in signal structure of the synthetic EEG signal in Figure 5.9(b). The threshold value for the seizure detection method was set to the minimum SC value for the first 10 minutes of the recording (i.e. first 600 seconds), and is clearly shown in Figure 5.9(a) as "*-*". However, it can be seen that a false detection is made. In this case, it is a result of some dominant structures being highly coherent with the Gabor dictionary atoms. Therefore, an extra criterion, such as *"An LFM atom must be selected first for a seizure detection to be made,"* may be included to discard these false detections.

The accuracy of the seizure detection algorithm was measured by considering the sensitivity, R_{sn}, and specificity, R_{sp} which are calculated using the true positives (TP), false positive (FP) and false negatives (FN). TP is the percentage of accurately detected seizure epochs, FP is the percentage of nonseizure epochs detected as seizure and FN is the percentage of seizure epochs missed by the algorithm. The sensitivity and specificity

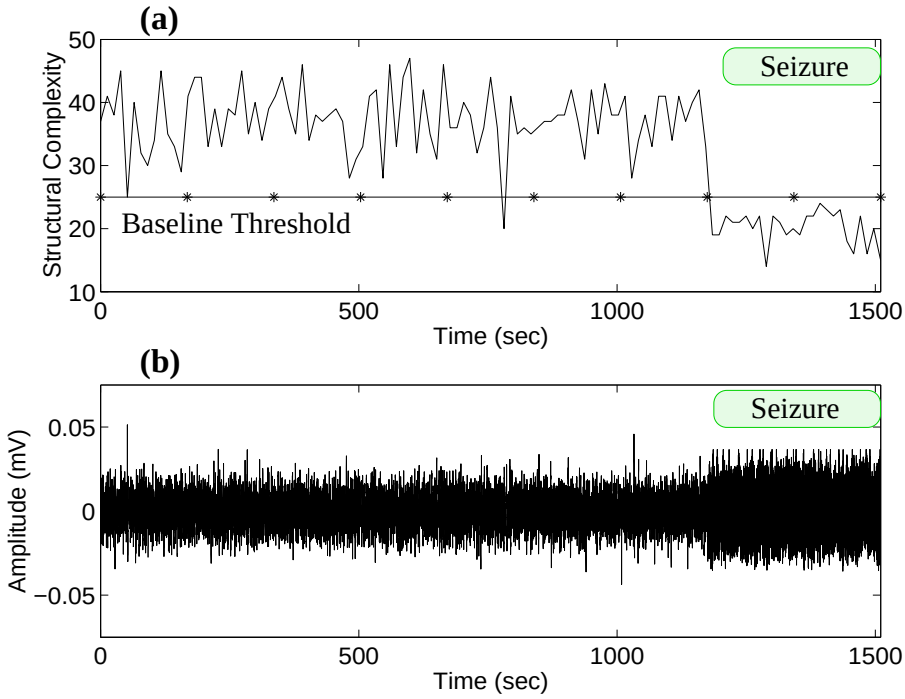

Figure 5.9: (a) The SC measure of the (b) synthetic newborn EEG data containing non–seizure and seizure states.

measures are expressed mathematically as

$$R_{sn} = \frac{TP}{TP + FN} \qquad R_{sp} = 1 - \frac{FP}{TP + FP} \tag{5.4}$$

Table 5.2, shows the optimal results of our SC method for automatic seizure detection applied to the synthetic newborn EEG data. Figure 5.10 shows the corresponding receiver operating characteristics curve associated with a changing threshold value.

Parameter	Rate
TP	100.0%
FP	2.78%
FN	0.00%
R_{sp}	100.0%
R_{sn}	97.3%

Table 5.2: Results of the SC based seizure detection algorithm applied to synthetic newborn EEG seizure

The results of our detection method for the synthetic data are extremely good. This is due to a number of factors. Firstly, the proposed dictionary is highly correlated

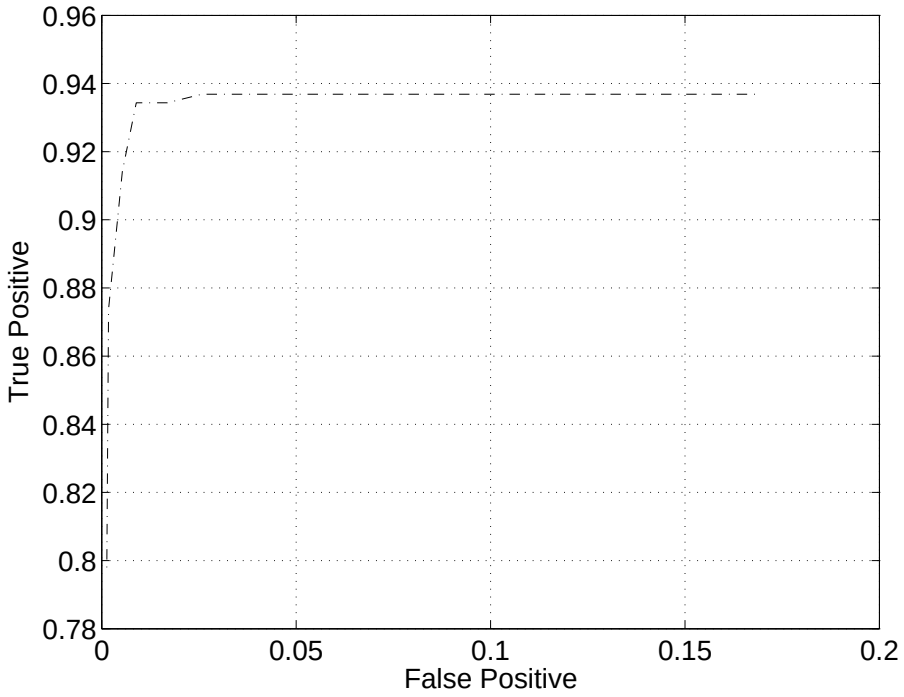

Figure 5.10: Receiver operating characteristics curve for the SC–based seizure detection algorithm.

with the structures in the synthetic newborn EEG seizure and less coherent with the synthetic newborn EEG background. Secondly, both the synthetic background and seizure signals are free from large amplitude artefacts.

Generally, it has been observed using real EEG data that the SC is drops significantly for the epochs covering large amplitude artefacts, as these high energy signal components often correlate well with Gabor atoms. This results in a relatively low number of significant atoms being needed to approximate the epoch. Drops in SC as a result of artefacts can therefore increase the number of FP, deteriorating the performance of the detection algorithm. This, however, can be overcome by incorporating a redundancy criterion such as the first atom being an LFM, as mention previously, or considering a minimum duration below the threshold value for a seizure event to be detected.

Finally, we have not incorporated the gradual onset of seizure into the synthetic signals which is often observed [22]. However, the reason for this is that it is difficult to determine exactly where the seizure starts. Therefore, it would make the evaluation of the automatic seizure detection much more difficult, inaccurate and possibly biased by our own interpretation of where the synthetic seizure starts.

5.4.4 EEG Seizure Detection using SC: Real EEG Data

To validate the excellent results attained in the previous section, we have also analyzed real newborn EEG data using the SC measure with our proposed TF dictionary. The EEG data analyzed in this section was recorded at the Royal Womens Hospital, Brisbane, Australia[5]. The EEG data was digitally bandpass filtered, with cutoff frequencies at 0.5Hz and 10Hz, before resampling the EEG data at 20Hz.

In the previous section, we showed that the development of an automatic seizure detection algorithm, using the SC measure, requires the assessment of baseline data to determine a threshold value. However, in our database of newborn EEG data, there are no recordings consisting of long background sections prior to seizure events. Therefore, we have not been able to assess baseline data to set thresholds and statistically evaluate a SC based automatic detection algorithm on real EEG data. Instead, we have analyzed a number of newborn EEG recordings which contain transitions between nonseizure and seizure to demonstrate how the SC decreases when shifting from the background state to the seizure state and increases when shifting from the seizure state to the nonseizure state.

Figures 5.11 and 5.13, show two different channels of an EEG recording and the SC for the channels. The entire period of the recording has been labeled as seizure. However, the EEG seizure patterns are not consistently present in any one channel over the entire recording period, as indicated by a neurologist.

The EEG channel shown in Figure 5.11(b) is obtained from the right side of the brain and the EEG channel in Figure 5.13(b) is recorded from the left side. The SC measure indicates that the seizure event has begun in the right side of the brain. This is illustrated by the relatively low SC measure at the beginning of the recording period, shown in Figure 5.11(a). An example of the TF pattern associated with and epoch from the beginning of the right side channel is shown in Figure 5.12(a). It can be observed that a dominant LFM component, characteristic of newborn EEG seizure, exists. This resulted in a relatively low SC measure as the signal structures were highly coherent with the proposed decomposition dictionary. However, from approximately 50 seconds to 215 seconds, the SC measure is relatively high, indicating that no seizure patterns are present. This is verified by the TFR shown in Figure 5.12(b), which is an epoch from 100 to 110 seconds. It can be seen that the TFR has no clear TF patterns, which is a characteristic of nonseizure newborn EEG.

In the SC analysis of the EEG channel from the left side of the brain, illustrated in Figure 5.13, we can see that the SC value is relatively high at the beginning of the

[5]A detailed description of the EEG data acquisition is given in Appendix A.

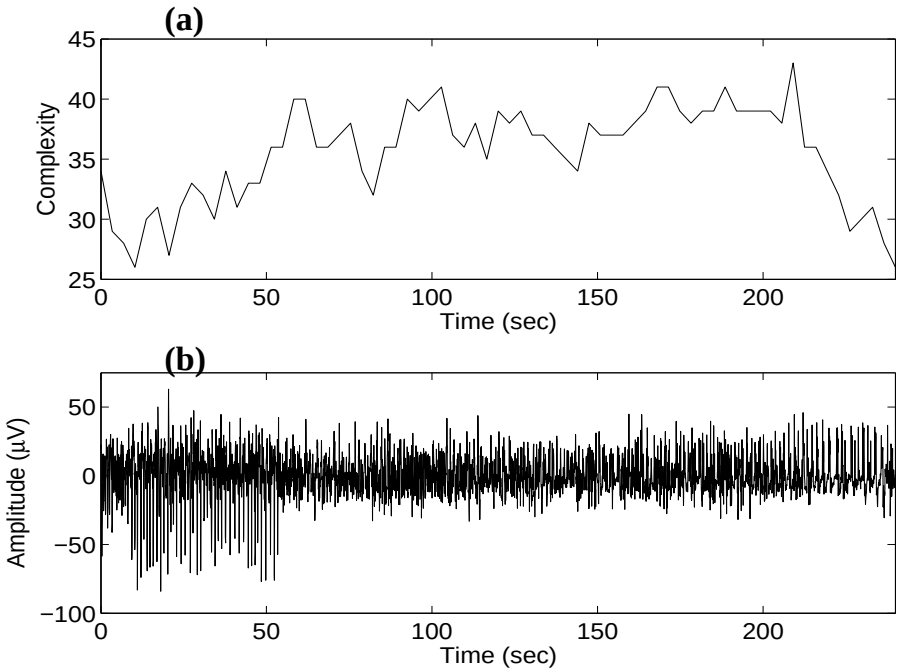

Figure 5.11: (a) The SC measure for the (b) newborn EEG channel, containing seizure, recorded from the right side of the brain.

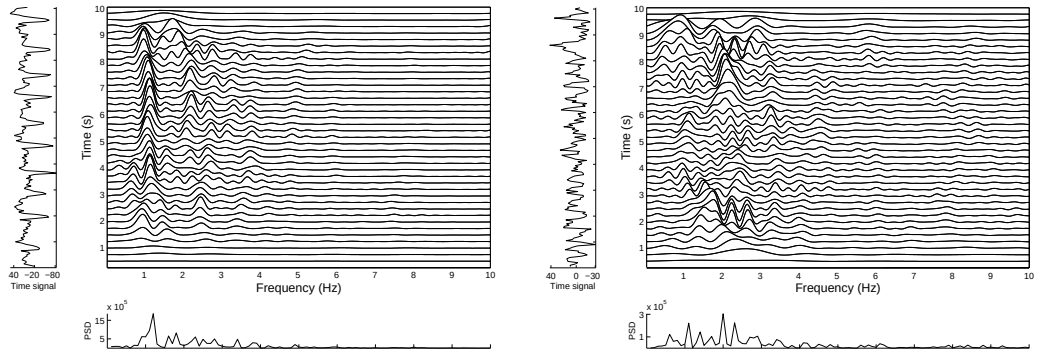

(a) LFM seizure patterns (b) Nonseizure patterns

Figure 5.12: TFR of epochs from the signal in Figure 5.11(b) at (a) the beginning where clear seizure patterns are present and (b) the middle where nonseizure patterns are exhibited.

recording. The high SC indicates that EEG recorded in this channel was not in the seizure state at the beginning of the recording. Figure 5.14(a) shows the TFR of an epoch at the beginning of the recording. It can be seen that no clear TF patterns are present, verifying the SC result which indicates a nonseizure state. However, from

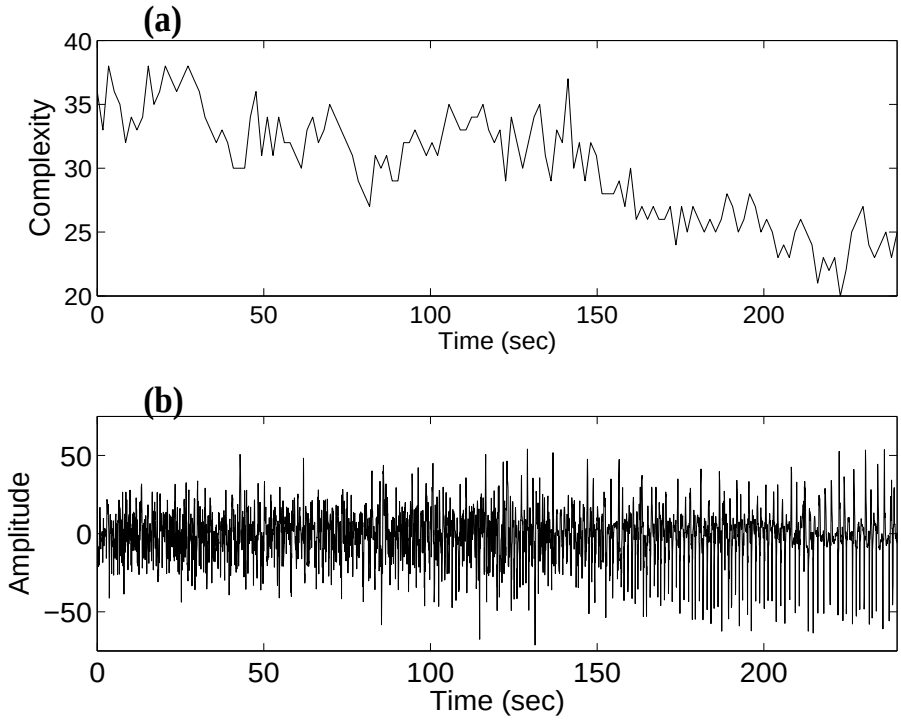

Figure 5.13: (a) The SC measure for the (b) newborn EEG channel, containing seizure, recorded from the left side of the brain.

approximately 50 seconds onward, it can be seen in Figure 5.13(a) that the SC is gradually decreasing. The gradual decline in the SC represents the gradual onset of EEG seizure in this channel. This corresponds well with the observations in [22], that the onset of seizure in newborns is quite often piecemeal. The TFR of an epoch at the end of the recording, where the SC is low, is shown in Figure 5.14(b). It can be seen that the epoch contains a dominant LFM component, therefore providing a low SC value.

From the SC analysis of these two channels, we can see that the seizure begins in the right side of the brain. This was indicated by the neurologist. The SC results then demonstrate that the seizure migrates from the right side to the left side of the brain. This was also suggested by the neurologist, who indicated that clear seizure patterns appeared in the left side channel at approximately 130 seconds. This was also where the SC begins to drop significantly for this channel, as illustrated in Figure 5.13(a).

Figure 5.15(b) shows another example of a real newborn EEG signal that contains a transition from the nonseizure state to seizure state. The structural SC measure again has a gradual decline. The seizure onset has been marked by the neurologist at approximately the 15 seconds, which is also demonstrated by the SC measure in Figure

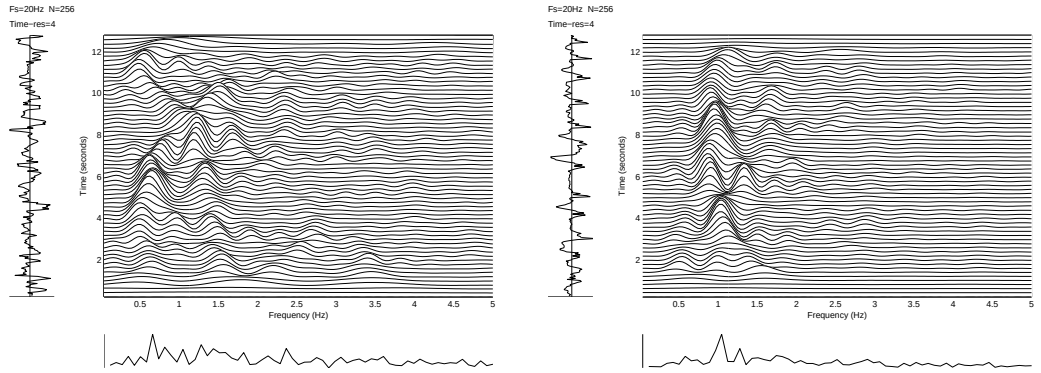

(a) Nonseizure patterns

(b) LFM seizure patterns

Figure 5.14: TFR of epochs from the signal in Figure 5.13(b) at (a) the beginning where nonseizure patterns are present and (b) the end where clear seizure patterns are exhibited.

5.15. A TFR of an epoch at the beginning of this recording is displayed in Figure 5.16(a). It can be seen from the TFR that there are no dominant clear TF patterns, validating the SC measure for this section of the recording. Figure 5.16 shows the TFR for an the epoch from approximately 26 to 39 seconds. This plot shows that two clear LFM components exist, which are characteristic of the newborn EEG seizure. These structures were highly coherent with the proposed decomposition dictionary, resulting in low SC as illustrated in Figure 5.15(a).

The results from these examples are typical of the SC measure when analyzing real newborn EEG data that is in transition from the nonseizure state to the seizure state. This analysis of real newborn EEG data using the SC measure has demonstrated its appropriateness as a potential method for the automatic detection of newborn EEG seizure.

5.5 Summary

This chapter presents a new signal complexity measure called *structural complexity*, which can be used to detect changes in signal structures (i.e. a change in signal state). This measure is extended from the idea of coherent structures which has previously been used for signal denoising by atomic decomposition techniques. The SC measure is obtained from MP decomposition and is a function of the decomposition dictionary and the desired level of signal approximation.

Before developing the SC measure, we have compared the sparsity of the signal

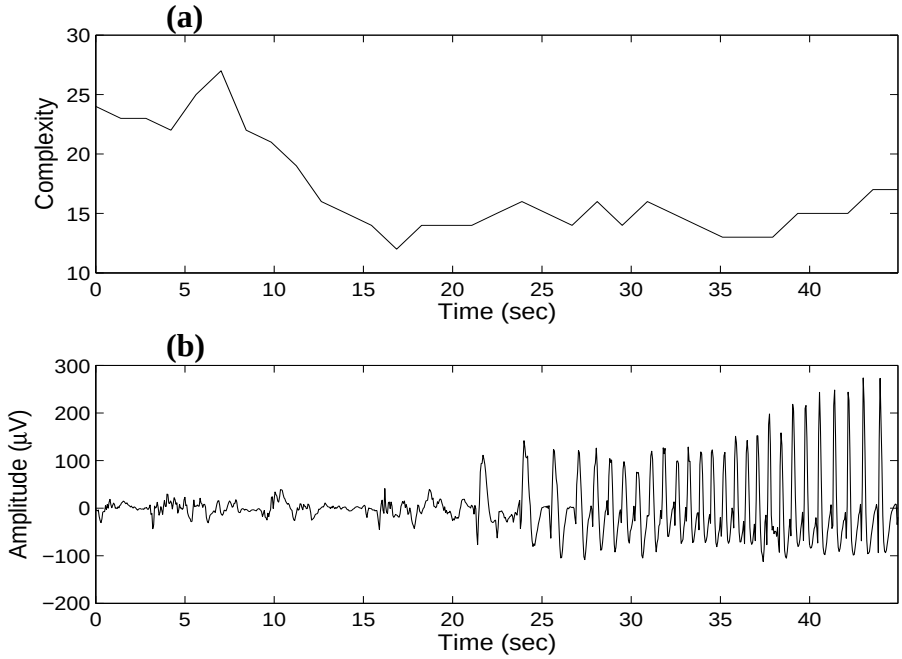

Figure 5.15: (a) The SC measure for the (b) newborn EEG signal, containing a seizure period.

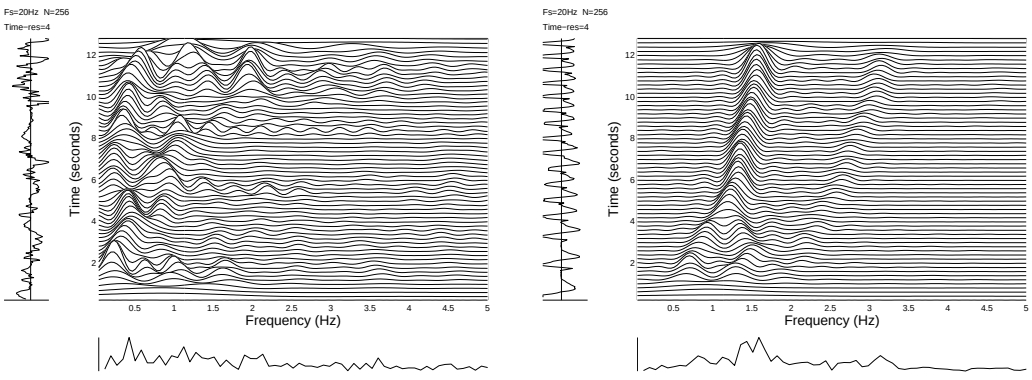

(a) Nonseizure patterns

(b) LFM seizure patterns

Figure 5.16: TFR of epochs from the signal in Figure 5.15(b) at (a) the beginning where nonseizure patterns are present and (b) the end where clear seizure patterns are exhibited.

approximations of BP and MP. One of the major goals in the development of BP was to provide the sparsest possible signal *representation* [88]. However, we have shown that BP does not always provide the sparsest *approximation*. Through our computational examples, we have shown that MP generally provides a sparser approximation than BP.

Our proposed SC measure was shown through a number of experiments to be an indicator of the coherency between the structures in a signal and the decomposition dictionary. Through another synthetic experiment, it was shown how the SC measure could be used to detect changes in signal state.

A real life application of the SC measure was then provided. It was shown that the SC methodology could be applied to the automatic detection of newborn EEG seizure.

The demonstration was done firstly using synthetic EEG data. An automatic detection algorithm, based on the SC measure and the newly proposed TF dictionary, coherent with the newborn EEG seizure state, was developed and tested on the synthetic EEG data. Excellent results for the automatic detection algorithm were obtained with a specificity of 100% and sensitivity of 97.3%. Analysis of real newborn EEG data using the SC measure and the proposed TF dictionary demonstrated its ability in detecting signal transitions in the newborn EEG. Therefore, the analysis of the real EEG data validated the synthetic EEG results and further indicated the appropriateness of the SC measure to be incorporated into an automatic seizure detection algorithm.

Chapter 6

Newborn EEG Seizure Spike and Event Detection using Adaptive TFSP

6.1 Introduction

Paroxysmal events, such as spikes in the newborn EEG, are key indicators of CNS functioning. The detection of spikes in the EEG is generally done by a trained EEG expert, for whom the ability to identify spikes has come through experience in reviewing EEG. This situation is due to the fact that a concise and specific definition of a spike pattern in the EEG is not available. That is, there is no precise, mathematical definition of an EEG spike [104]. The current definitions of an EEG spike have been mostly qualitative.

The difficulty in detecting spikes has previously been described in [105], in which it was shown that the disagreement of spike detections by the same reader (i.e. EEG expert) at different sittings may be as poor as 53%. This is again due to the lack of precise definition of the EEG spike [106]. Therefore, a method for automatically detecting EEG spikes accurately[1] is required.

Isolated spike events, which almost always characterize EEG abnormality in the adult, can often be normal ontogenetic events in the newborn (see chapter 2). However, repetitive rhythmical spiking in the newborn is a major sign of EEG abnormality and is a significant characteristic of newborn EEG seizure. Therefore, EEG seizure detection in the newborn can be based on the ability to automatically detect repetitive rhythmical spiking in the newborn EEG.

[1] In this context, accurately refers to a majority of expert readers referring to the pattern as a spike.

In this chapter we propose a method of automatically detecting EEG seizure in the neonate using adaptive TFSP techniques. Previous methods of automatic spike detection are reviewed in section 6.2, and their limitations explained. In section 6.3, we compare MP and the adaptive spectrogram (ASPEC) for detecting isolated signal spikes using synthetic and real signals. We also show that the optimal window scale (OWS) function of ASPEC can be used directly for spike detection. In section 6.4, we assess the ability of MP and OWS function for detecting repetitive spikes which are harmonically related. In section 6.5, we propose a method of newborn EEG seizure detection based on OWS. The performance of the algorithm is then compared with those of four other well documented seizure detection algorithms.

6.2 Previous Methods for Automatic Spike Detection

A number of methods for detecting and sorting spikes from the adult EEG have previously been proposed[2]. These techniques can be classified into *parametric, stationary nonlinear,* and *nonstationary.* Parametric methods such as [104, 107], define a mathematical model that includes parameters such as duration and relative amplitude of the spike pattern, in an heuristic attempt to mimic the review process of an expert reader. However, the performance of these techniques is restricted significantly due to the highly varying morphology of spike patterns, particularly in the newborn EEG [9].

A stationary nonlinear technique for the detection of spikes was proposed in [108]. In this method a nonlinear energy operator (NEO), proposed in [109], was used to emphasize the spiking activity in the signal. The NEO, applied to a discrete signal, $x(n)$, is expressed as

$$O[x(n)] = x^2(n) - x(n+1)x(n-1) \tag{6.1}$$

This technique is highly sensitive to noise, which degrades its performance in detecting signal spikes. To reduce the effect of noise, a smoothed nonlinear energy operator (SNEO), which involves convolving the NEO output with a Bartlett window, was proposed in [108]. This technique was also shown to be significantly effected by noise [110]. Another problem with using NEO and SNEO is that they assume that the spike events occur in a stationary background signal. This assumption is not valid for the nonstationary EEG background signal of the newborn, therefore, limiting the ability of these techniques to detect spike occurrences.

The detection of nonstationary signal patterns, such as transients or spikes, is one

[2] Although most work done on the automatic detection of EEG spikes has involved the adult EEG, the same broad definition of spike and sharp waves exist for the newborn EEG.

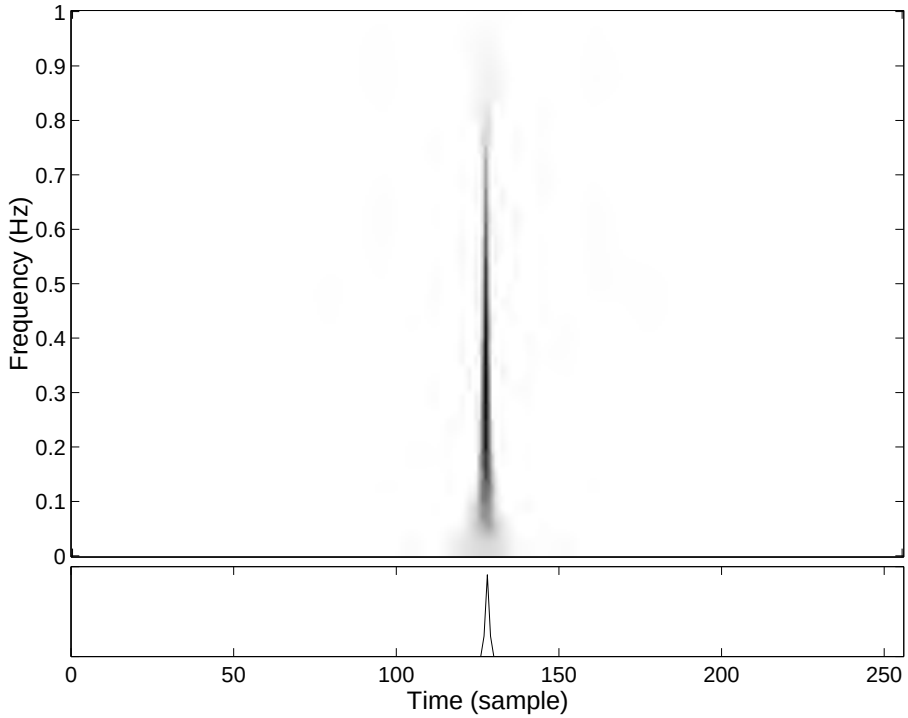

Figure 6.1: The TFR of spike event

application suited to nonstationary techniques such as TFSP and time–scale signal processing. The WT and QTFDs have both been proposed for the detection and extraction of spikes in the EEG [30, 111, 112]. The techniques based on the WT have been shown to perform well on artificial data. However, the WT is not optimal in separating spikes that are close in time. This is because for large wavelet scale values, the time resolution of the wavelets are wider than the width of the spikes. This means that when closely spaced spike events are recorded, the WT fails to separate them [113].

In [112], TF analysis using a smoothed pseudo WVD (SPWVD) of adult EEG which contained spikes was presented. It was shown that isolated spike events were represented in the TF domain by ridges along the time instant at which the spike occurred. However, no method of detecting the spikes was presented.

In [30, 31, 114], a TF approach for the detection of spikes was presented. It was also shown in this method that a spike event was represented in the TF domain as a high energy ridge that extended from low frequency to high frequency along the time instant at which the spike occurred (see Figure 6.1 for illustration). The spike detection method presented in [30, 31, 114] used the Choi-Williams distribution (CWD) to obtain a TFR, so as to minimize cross terms. This detection technique involves taking two arbitrary frequency slices in the high frequency region. These slices were assumed to show high

values around the time instants where the spike occurred and low values at all other times. Also, to enhance these signatures, the SNEO was applied to the frequency slices. A threshold value, related to the median value of the frequency slice, was determined and local maxima above the threshold values were used to indicate spikes and their locations.

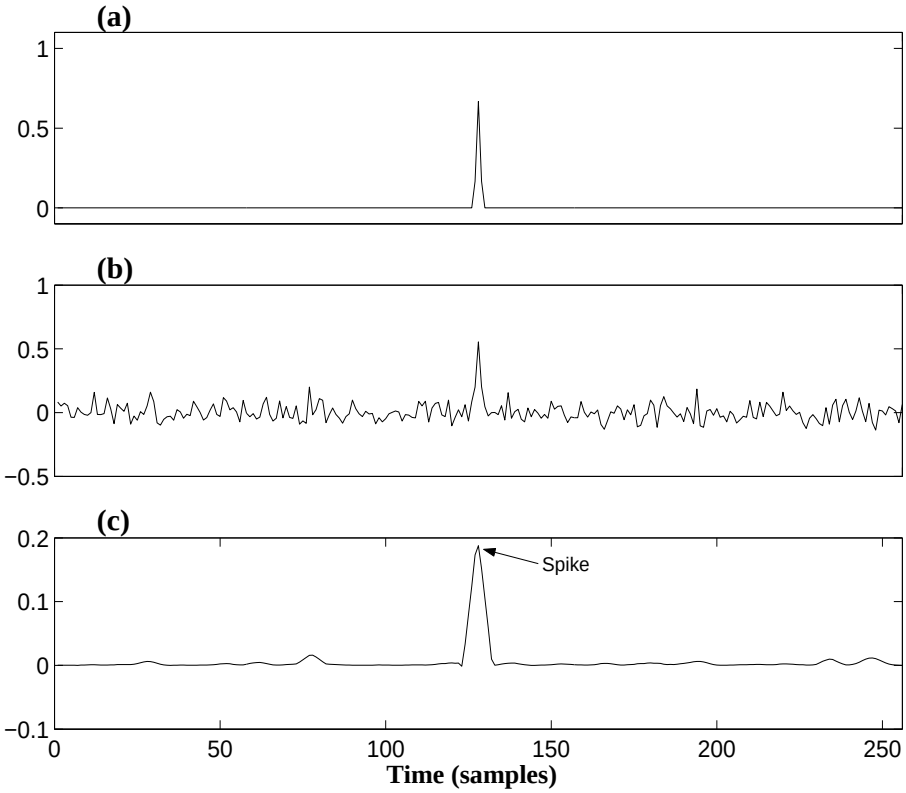

Figure 6.2: (a) A spike signal that is (b) embedded in noise. (c) Is the SNEO output of an arbitrary high frequency slice of the CWD of (b).

This TF method provides good results on synthetic and real signals which have isolated or randomly placed spikes in the signal. An example of this is shown in Figure 6.2, where Figure 6.2(a) shows the spike event, Figure 6.2(b) is the spike event embedded in noise and Figure 6.2(c) is the SNEO of an arbitrary high frequency slice of the CWD. For this example, the spike was assumed to be the signal and it was embedded in -3dB noise for this example.

However, the method performs poorly for a signal with spike events that are harmonically related. An example of this is shown in Figure 6.3. The plots in Figures 6.3(a) and Figures 6.3(b) show a high frequency slice and its SNEO output from the CWD of the spiking signal in Figure 6.3(c). It can be seen in Figure 6.3(b) that the individual

spikes aren't clearly distinguishable from the SNEO output of the high frequency slice.

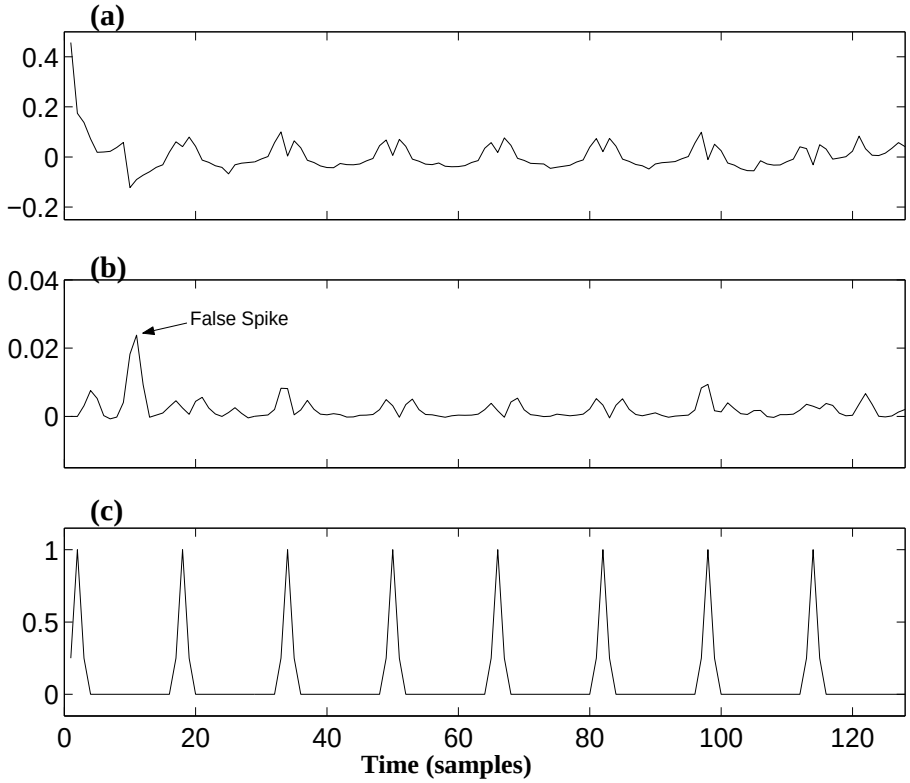

Figure 6.3: (a) An arbitrary high frequency slice and (b) SNEO output of the CWD of the (c) periodically spiking signal.

The ability to detect repetitive spikes which are harmonically related is significant for the application of newborn EEG spike detection. Rhythmical spiking from a particular area of the cerebrum is a classical pattern of newborn EEG seizure [77]. If a spike detection algorithm is to be incorporated into a seizure detection algorithm, it must be able to detect repetitive, harmonically related spikes. Therefore, we investigate the use of adaptive TF methods in detecting spikes.

6.3 Evaluation of Adaptive TFRs for Detection of Isolated Spikes

A method for detecting spikes based on an adaptive TFR technique was presented in [113]. This method incorporated the best orthogonal basis algorithm with a redundant WP dictionary (see chapter 3) in an attempt to improve on the performance of WT methods. However, due to the algorithms criterion of obtaining an orthogonal basis for

signal representation, this method sometimes fails to adequately represent transients [88]. Therefore, a spike detection based on the MP has been recently proposed [42]. In this section, we explain the methodology for detecting spikes using MP and propose a method of detecting spikes using an adaptive QTFD called the ASPEC. We then compare these methods for detecting isolated spikes in real EEG data.

6.3.1 MP Methodology for Detecting Spikes

The MP algorithm provides an adaptive signal representation. It adaptively selects TF atoms from the decomposition dictionary which optimally[3] represents the signal residue at each iteration, as was demonstrated in chapter 3. An advantage of using MP as an adaptive TFSP technique is that it can provide both an adaptive TFR and an adaptive TF parameterization. This is best illustrated with an example.

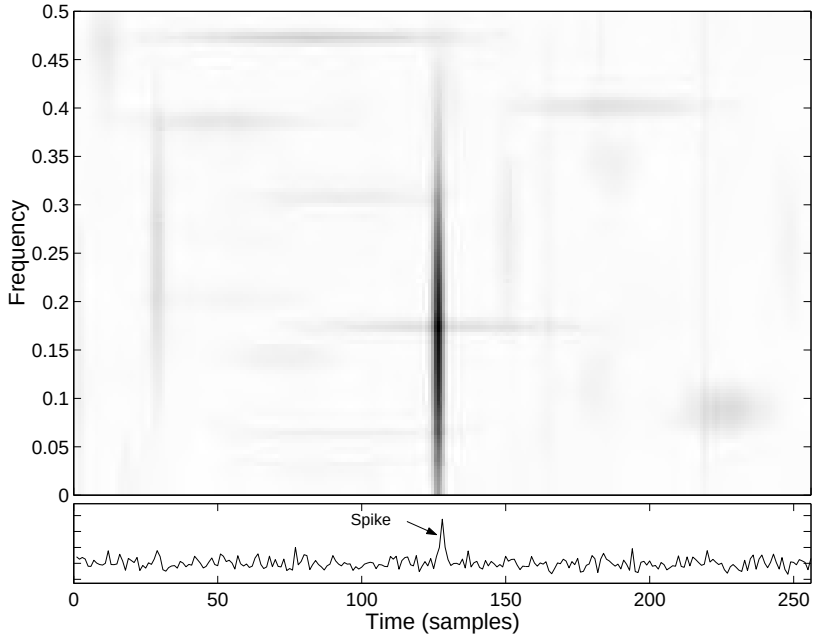

Figure 6.4: TFR of a spike signal embedded in -3dB noise using MP with Gabor TF dictionary.

In Figure 6.4, the lower panel is an example of a spike pattern embedded in -3dB noise. The synthetic spike has a duration of 3 samples and is centered at time, $t = 128$ samples. The upper panel shows the TFR using MP with the redundant Gabor TF dictionary. It can be seen that this TFR provides a high energy ridge, ranging from

[3]The measure of optimality for the MP algorithm is the largest inner product.

low frequency to high frequency along the time instant at which the spike occurred. Therefore, this TFR is quite similar, in its representation of an isolated spike, to other TFRs such as QTFDs.

Coef	Scale	Translation	Modulation	Phase
57.23	**5**	**127**	**0.0781**	**5.511**
24.97	113	85	0.2343	1.102
24.24	3	194	0.4453	1.729
23.47	19	240	0.2928	3.287
22.12	14	130	0.4570	1.838
22.10	34	225	0.4297	2.381
21.73	6	29	0.1211	1.066
20.09	107	128	0.0861	1.917
19.35	77	187	0.1992	4.586
18.67	24	74	0.3010	2.448

Table 6.1: The TF parameterization of a spike signal embedded in -3dB noise using MP with Gabor TF dictionary.

A TF based spike detection method such as that proposed in [30, 31, 114] could be implement using the MP-based TFR. However, in [42], a method of spike detection was developed based on the adaptive TF parametrization obtained from the MP decomposition. Table 6.1, shows the TF parameters of the first 10 atoms selected in the MP decomposition. The parameter list includes the coefficient value for the atom, the scale in samples, the time center (i.e. translation) of the atom in samples, the frequency center (i.e. modulation) in normalized frequency where the sampling frequency $Fs = 1$, and the phase of the real atoms which are in radians.

Since spikes are characterized by high energy and short time duration, they are best represented by atoms with a significantly high coefficient value and small scale parameter. Therefore, by setting adequate thresholds for the coefficient and scale parameters, the signal spikes can be detected directly from the MP adaptive TF parameterization. The temporal information regarding the spike occurrence, can be extracted directly from the translation parameter associated with the spike atom. This is illustrated in Table 6.1, where the first atom has a coefficient significantly larger than all other atoms, and has an extremely small scale parameter, indicating that it is a parameterization of the spike event in the signal. It can be seen that the translation parameter suggests the spike is located at time, $t = 127$ samples which is within 1 sample of the true spike location of $t = 128$ samples. This clearly shows the methodology for spike detection from the MP TF parameterization which was developed in [42].

6.3.2 Adaptive QTFDs Methodology for Detecting Spikes

A number of adaptive QTFDs have been proposed in an attempt to achieve good TF resolution and crossterm suppression for a large class of signals [115]. Adaptive QTFD methods can be separated into two classes: global optimization methods and time–localized methods. Adaptive QTFDs which strive for global optimization, such as that proposed in [116], do so by searching for the QTFD kernel which meets the desired optimization criteria. However, there has been much focus recently on time-localized methods for achieving adaptive QTFDs. Examples of time–optimized methods include the development of optimal short–time ambiguity functions [117], optimal time–varying window lengths to be applied to the IAF [87], and optimal time–varying window lengths for the spectrogram [118, 119, 120].

The adaptive QTFD methods which appear to be the most appealing for spike detection are the time-localized methods with adaptive window lengths. For example, if a spike event occurs within a signal, it should be expected that the optimal window lengths around the time location of the spike would be small and, therefore, fully emphasize the spike event in the TF domain.

For our proposed adaptive QTFD spike detection method, we have incorporated the ASPEC derived in [120]. The optimization criterion for this ASPEC, which determines the OWS at each time instant, is referred to as the *maximum correlation criterion*. This adaption method selects the window scale, p, from the set of windows scales, P, at time instant, t, which maximizes the projection of the signal onto the modulated window. This is shown mathematically as

$$p(t) = \arg\max_{p \in P} \left| \frac{1}{\sqrt{p}} \int_{-\infty}^{\infty} x(\tau) w\left(\frac{\tau - t}{p}\right) e^{-j2\pi f \tau} d\tau \right| \tag{6.2}$$

Using this criterion, the predominant time–frequency–scale structure in the signal, centered at the time instant, t, determines the OWS (i.e. window length) for that time instant. This criterion is similar to the objective function of the MP algorithm.

Figure 6.5 shows the TFR from the ASPEC of a spike signal embedded in -3dB noise. It can be seen that ASPEC also clearly represents the spike in the TF domain with a ridge running from low frequency to high frequency along the time instant at which the spike occurs. This representation is similar to both the CWD and MP TFRs.

Once again a TF based spike detection method such as that proposed in [30, 31, 114] could be implemented using the ASPEC. However, we propose a new method for detecting spikes from the ASPEC output. In our spike detection method, we propose using only the OWS to detect spikes (not the adaptive TFR). In our method, a spike event is detected if the OWS falls in the range associated with the scale or duration of

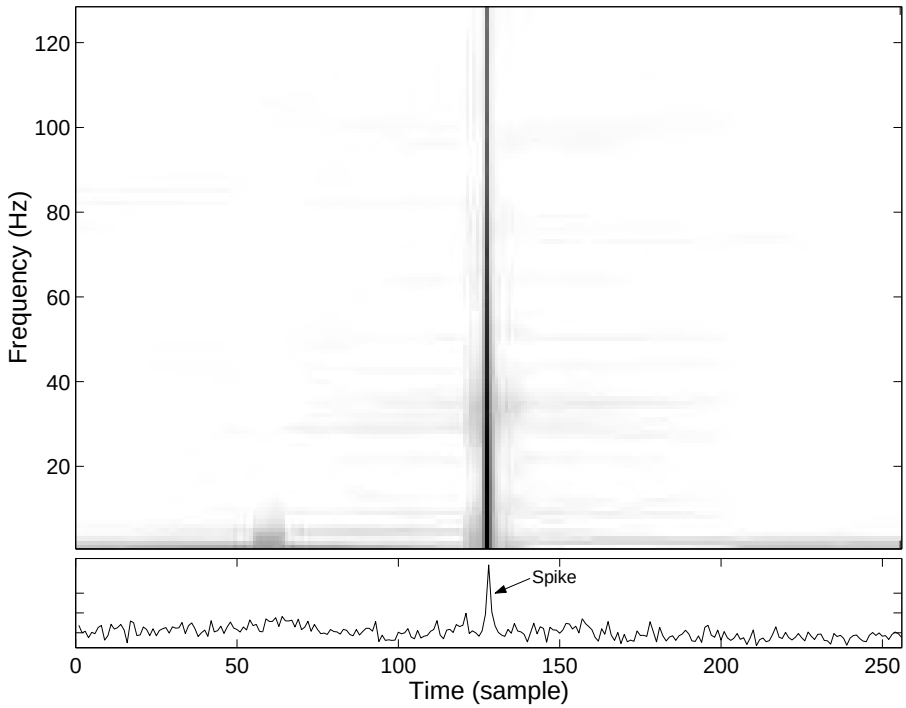

Figure 6.5: TFR of a spike signal embedded in -3dB noise using ASPEC.

a spike event. This is demonstrated in Figure 6.6, where Figure 6.6(a) shows the OWS for the noisy spike signal shown in Figure 6.6(b).

To save on processing time we have used a set of dyadic scales, given by

$$S = [2^d - 1] \tag{6.3}$$

in which $d = [1, 2, \ldots, \log_2(N)]$, and N is the signal length. From Figure 6.6(a) and using (6.3), it can be seen that the optimal window length at time instant $t = 128$ samples is 3 samples. Therefore, the OWS can be used to correctly identify the spike location and its approximate duration.

This methodology can be easily applied to EEG spike detection. The spike pattern in the EEG has been defined as having a duration between 20-70msec and a sharp wave having a duration between 70-200msec. Therefore if the adaptive window length is between 20-200msec at any time instant, we can conclude that a spike/sharp wave has occurred[4].

[4]For the rest of this chapter, we refer to the spike and sharp wave transients in the newborn EEG as spikes only.

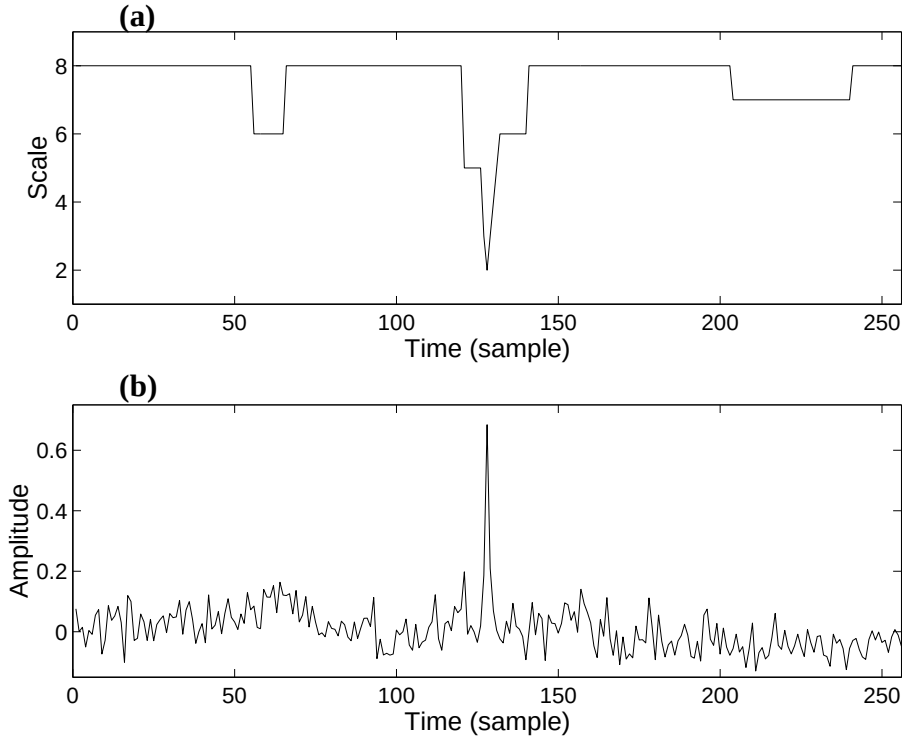

Figure 6.6: (a) The OWS, $s(t)$, for the (b) spike signal embedded in -3dB noise

6.3.3 Comparison of Adaptive TF Spike Detectors on Real EEG Data

It was explained in section 6.3.1, that before MP TF parameterization can be used for spike detection, the parameter values indicating a spike have to be defined. That is, a range of coefficient values (or atom amplitude values) and range of scale values which are representative of a spike have to be defined. These values are generally determined based on *a priori* analysis of the EEG which contains both epochs with spikes and epochs free of spikes.

For the MP spike detection method in [42], the effective scale half widths of the atoms were chosen to be between 30-60msec. The amplitude of the atoms to indicate a spike were chosen to be above 300 a.u. (i.e. arbitrary units). Arbitrary units were used since the conversion ratio of points/μV was unknown for their database. However, if this ratio is known, 300 a.u. can be easily expressed in μV.

The EEG data used in [42] was obtained from http://republika.pl/eegspike, which was created by the authors of [111]. To compare our proposed spike detection method, based on the OWS, with the MP spike detection algorithm in [42], we used the same real EEG data. The data set contained 84 epochs which were divided into three groups [42]:

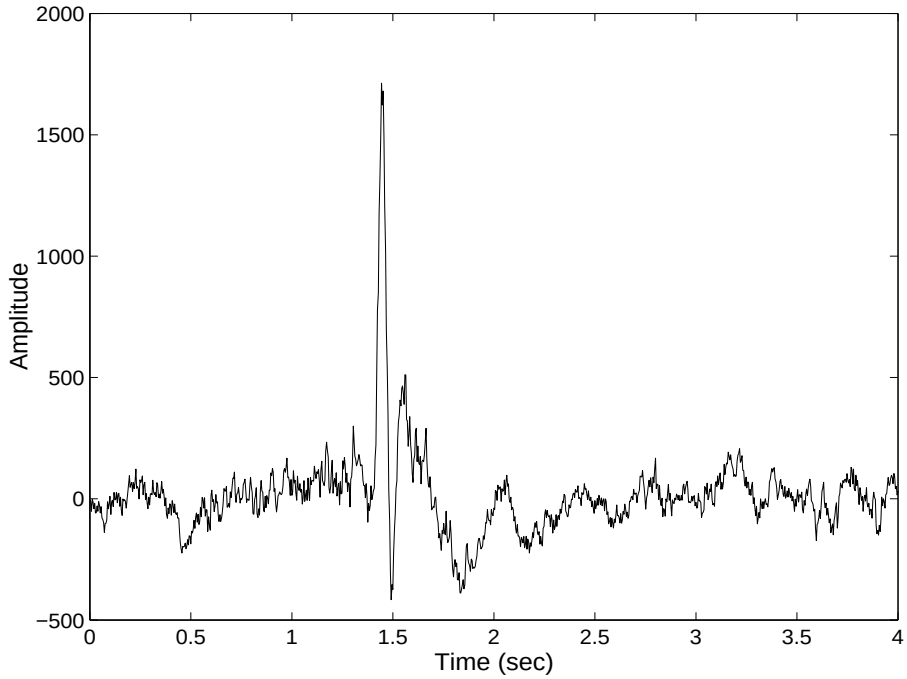

Figure 6.7: Real adult EEG containing an isolated spike event.

1. signals with large, single spikes or sharp waves which are not accompanied by the prominent slow wave – 30 epochs

2. signals with spikes or sharp waves followed by slow waves with comparable amplitudes – 14 epochs

3. signals with artifacts and portions of EEG traces with no spikes or sharp waves – 40 epochs

There were 73 spikes in total from the 44 epochs which contained spikes. An example of an EEG epoch with a spike event from the database is displayed in Figure 6.7. The MP spike detection method proposed in [42] obtain a sensitivity of 92% and a specificity of 84% for this EEG database.

For the OWS method of spike detection we added in a preprocessing step. The signals were initially sampled at $Fs = 256$Hz. We lowpass filtered the signals with a cutoff frequency at $Fs/4$, before downsampling the signal $Fs_{\text{new}} = 128$Hz, which significantly reduced the amount of data to be processed without significantly hindering the shape of the spikes. We processed the signal in epochs of length 512 samples and used a dyadic set of scales. The scale lengths used to detect the spikes were $d = 2, 3, 4$, which equate to time durations between approximately 20-120msec. The OWS method

	Sensitivity	Specificity
MP	92%	84%
OWS	91%	87%

Table 6.2: Results of MP and OWS in detecting isolated spikes from real adult EEG data

of spike detection produced a sensitivity of 91% and a specifity of 87%, which are quite similar to the results for the MP detection method. Table 6.2 shows the results of the two algorithms for easy comparison.

6.4 Evaluation of Adaptive TFRs in Detecting Repetitive Spikes

Rhythmical spiking in the newborn EEG is a classical pattern characterizing a seizure event. Neonatal seizures with rhythmical spiking are often multifocal and the spiking activity may shift from one area to another, with the temporal, occipital and central regions often being involved [77].

The ability to detect repetitive, rhythmical spiking in the newborn EEG may therefore be seen as a method of detecting ictal or EEG seizure events. The detection of individual spikes of a rhythmical, repetitively spiking signal using TF techniques is much more difficult then the detection of isolated spikes. This is caused by the harmonic relationship of quasi-periodic spikes being shown in the TF domain as components with long time duration. In this section, we investigate the ability of MP and OWS in detecting individual spikes of repetitively spiking signals and determine what are the limiting factors of these techniques.

6.4.1 MP Representation of Synthetic Repetitive Spikes

The assessment of the MP algorithm, using a redundant Gabor TF dictionary, for detecting the individual spikes of a repetitively spiking signal begins with the decomposition of synthetic signals. These signals, referred to as ideal periodic spike sequences, are expressed as

$$\mathbf{III}_N^T(n) = \begin{cases} 1 : n = l \cdot T, \;\; l = 0, 1, \ldots, N_t - 1 \\ 0 : \text{else} \end{cases} \tag{6.4}$$

where T is the period between spikes and $N_t = N/T$ is the number of spikes in the signal. We have chosen these signals in our initial investigation because these contain

the most extreme form of a spike and the most extreme form of repetition which is periodicity.

The first ideal periodic sequence to be assessed for spike detection using MP is $\mathbf{III}_{256}^{32}$. Figure 6.8 shows $\mathbf{III}_{256}^{32}$ in the lower panel and its MP TFR in the upper panel. It can be clearly seen from Figure 6.8 that the MP algorithm has accurately represented the individual spikes with spike (i.e. small scaled)[5] atoms, illustrated by the characteristic ridge in the TFR along the time instants of the spike event from low frequency to high frequency. For this ideal periodic signal, the MP spike detection method can accurately detect the spikes.

Figure 6.9 shows the MP TFR of the ideal periodic spike sequence $\mathbf{III}_{256}^{16}$, which has a shorter period between individual spikes than the previous sequence. It can be observed from the TFR in Figure 6.9 that the MP has not represented the individual spikes of the periodic spikes sequence with spike atoms. Instead, the MP algorithm has chosen large scaled atoms to represent the harmonic relationship between the spikes in the periodic spike sequence. Therefore, the MP algorithm would not be able to detect the individual spike events of this ideal periodic spike sequence. However, in Figure 6.10, we have taken an epoch of 128 samples of the ideal periodic sequence $\mathbf{III}_{256}^{16}$, resulting in an ideal periodic spike sequence $\mathbf{III}_{128}^{16}$. It can be seen from the MP TFR that the same individual spikes are now represented with spike atoms, resulting in the characteristic TF patterns of a spike. Therefore, by reducing the epoch length, the MP algorithm has represented the spikes with spike atoms and allowed for individual spike detection of the spike sequence.

The results from the three example signals, $\mathbf{III}_{256}^{32}$, $\mathbf{III}_{256}^{16}$ and $\mathbf{III}_{128}^{16}$ clearly indicate that there is a relationship between the epoch length and spiking period which determines the capability of MP in detecting individual spikes of periodically spiking signal. From our synthetic computational examples, we have observed that if $T > \sqrt{2N}$, MP represents the individual spikes of an ideal periodic spike sequence with spike atoms, therefore allowing for spike detection. However, we found that if $T < \sqrt{2N}$, MP represents the spike sequence with large scale atoms which indicate the harmonic relationship between the spikes.

To further emphasize our results we present another synthetic example in Figure 6.11. The signal in Figure 6.11(a) is of length 512 samples with periodic spiking. The spikes are Gaussian windows with a duration of 3 samples and are separated by a period of 32 samples. This spike sequence also has white Gaussian noise added to it with a

[5]Spikes atoms are characterized by small scale lengths. The specific length of the scale for an atom to be classed as a spike atom is dependent on the application. Therefore, we have generalized "spike atom" as those with small scale and provide a TF pattern which is characteristic of a spike.

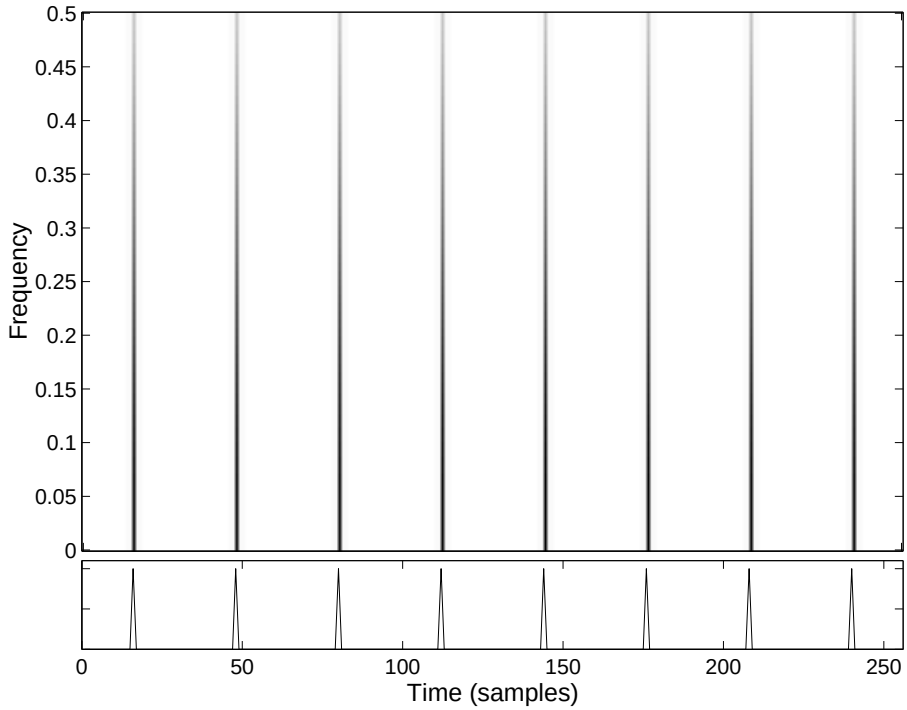

Figure 6.8: MP TFR of the ideal periodic spike sequence $\mathbf{III}_{256}^{32}$.

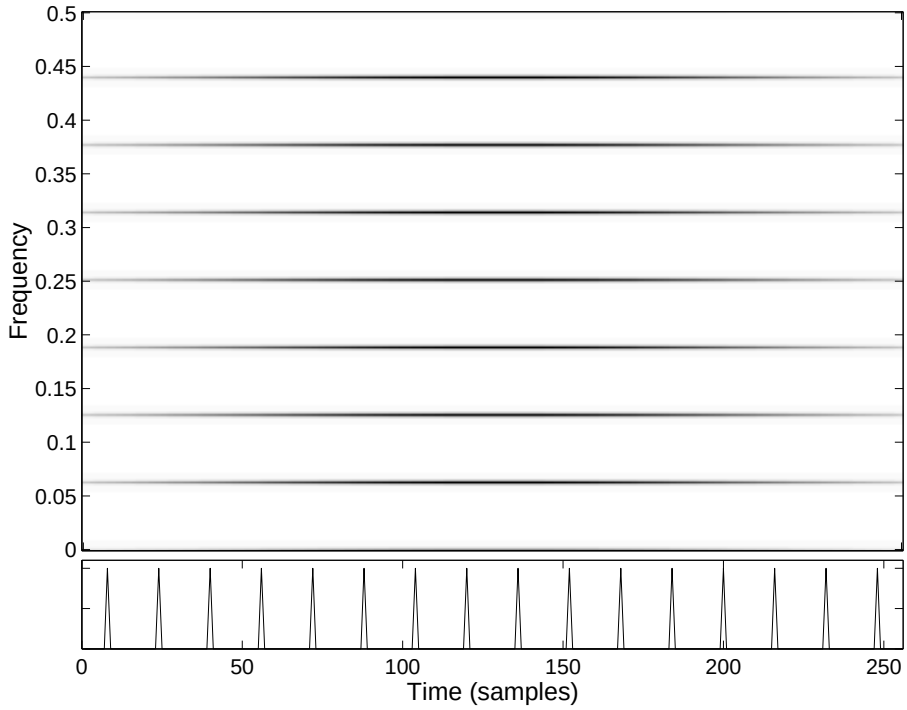

Figure 6.9: MP TFR of the ideal periodic spike sequence $\mathbf{III}_{256}^{16}$.

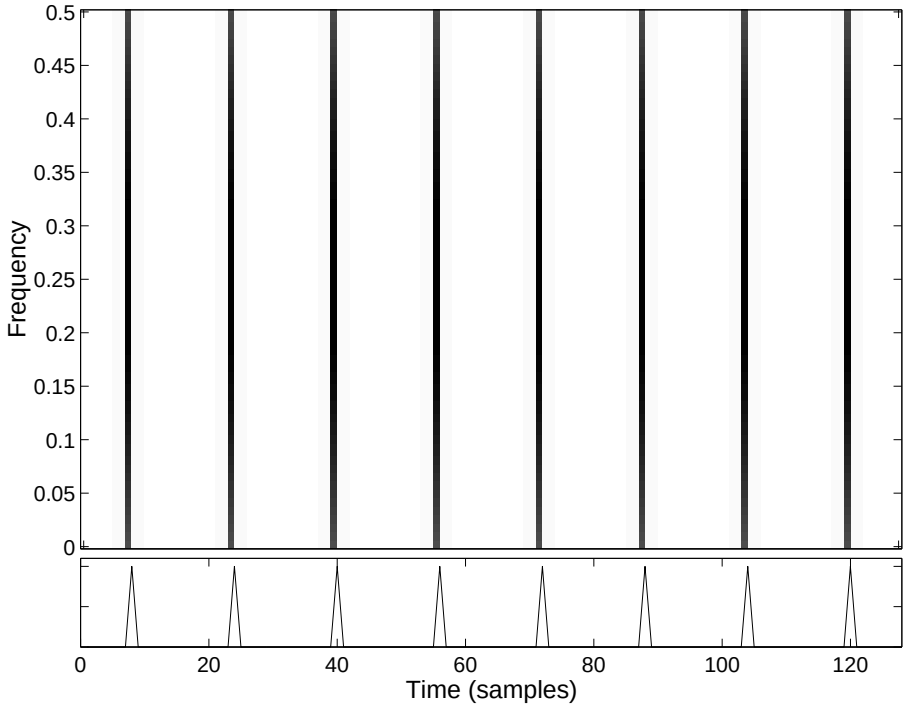

Figure 6.10: MP TFR of the ideal periodic spike sequence $\mathbf{III}_{128}^{16}$.

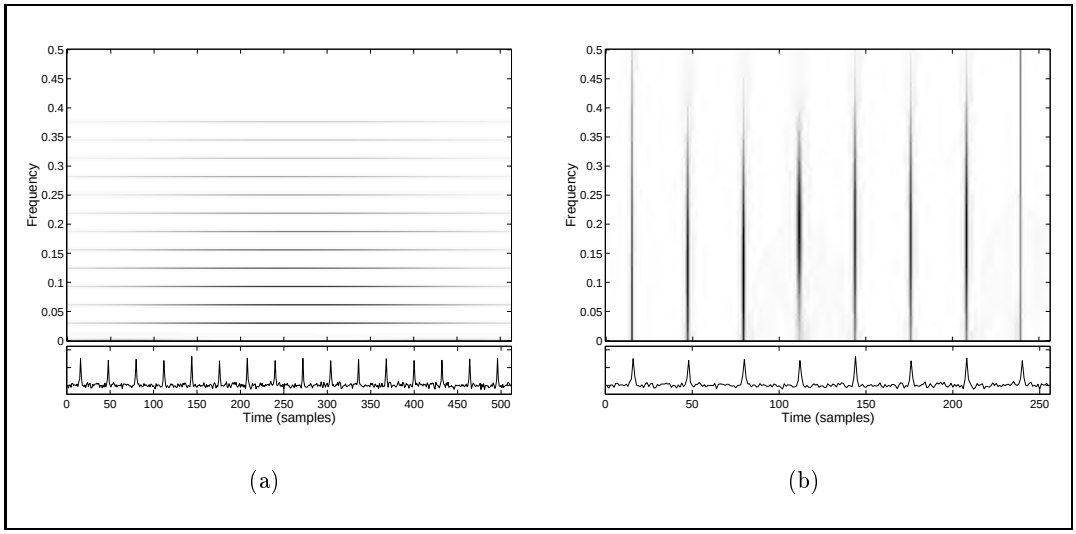

Figure 6.11: The (a) MP TFR of a noisy, repetitively spiking signal only shows the harmonic relationship of the spikes. (b) MP TFR of a shorter epoch of the noisy, repetitively spiking signal is able to indicate the individual spikes.

SNR of 10dB. From the TFR of Figure 6.11(a) it can be seen that MP fails to clearly represent the spikes with spike atoms. Instead, it shows the harmonic relationship between the spikes. However, in Figure 6.11(b), we have taken an epoch of 256 samples at the start of the signal in Figure 6.11(a). It is clear from the TFR in Figure 6.11(b) that MP has represented the individual spikes with spike atoms, therefore allowing for spike detection. This again emphasizes the importance of the relationship between the spike period and epoch length for MP to detect repetitive spikes.

6.4.2 OWS Representation of Synthetic Repetitive Spikes

The first synthetic ideal periodic spike sequence for which MP could not detect the individual spike events was $\mathbf{III}_{256}^{16}$. This was shown in the TFR of Figure 6.9, for which the characteristic ridges of a spike event, occurring at the time instant of the spike and ranging from low frequency to high frequency, were not observed. Figure 6.12 shows the TFR obtained from the ASPEC, which adaptively selects the OWS, for the ideal periodic spike sequence $\mathbf{III}_{256}^{16}$. The TFR in Figure 6.12 shows both the harmonic relationship between the periodic spikes as well as giving the TF characteristics of the individual spikes. Figure 6.13(a) shows the OWS for $\mathbf{III}_{256}^{16}$. It can be seen that the OWS clearly indicates the individual spike occurrences, which is shown by a small scale size being optimal at the time instants when the individual spikes occur. Therefore, OWS has been able to detect the spikes where the MP method failed.

Although the OWS has been shown to be able to detect the individual spikes of $\mathbf{III}_{256}^{16}$, where MP failed, the OWS also has limits in its ability to detect these periodic spikes. In Figure 6.14(a), we show the OWS for the ideal periodic sequence $\mathbf{III}_{256}^{8}$, which has a shorter period that the previous example. It can be seen from Figure 6.14(a), that OWS does not detect any of the individual spike events as in the previous example. The OWS method's ability to detect the individual spikes of an ideal periodic spike sequence is also dependent upon the relationship between the spike period and the signal length. However, OWS is less effected than MP as demonstrated with the periodic spike signal $\mathbf{III}_{256}^{16}$.

To emphasize the superiority of OWS over MP in detecting individual spikes of a repetitively spiking signal we compare OWS and MP using a noisy synthetic signal. The synthetic signal for this example is of length 128 samples. The individual spikes have a duration of 3 samples and are separated by 16 samples. White Gaussian noise is added to the spike sequence resulting in an SNR of 10dB. This signal is shown in Figure 6.15(a). It can be seen from 6.15(b) that the OWS spike detection method can accurately indicate the individual spike events. However, it can be seen from the MP TFR in Figure 6.15(c) that MP does not represent the individual spikes with spike atoms

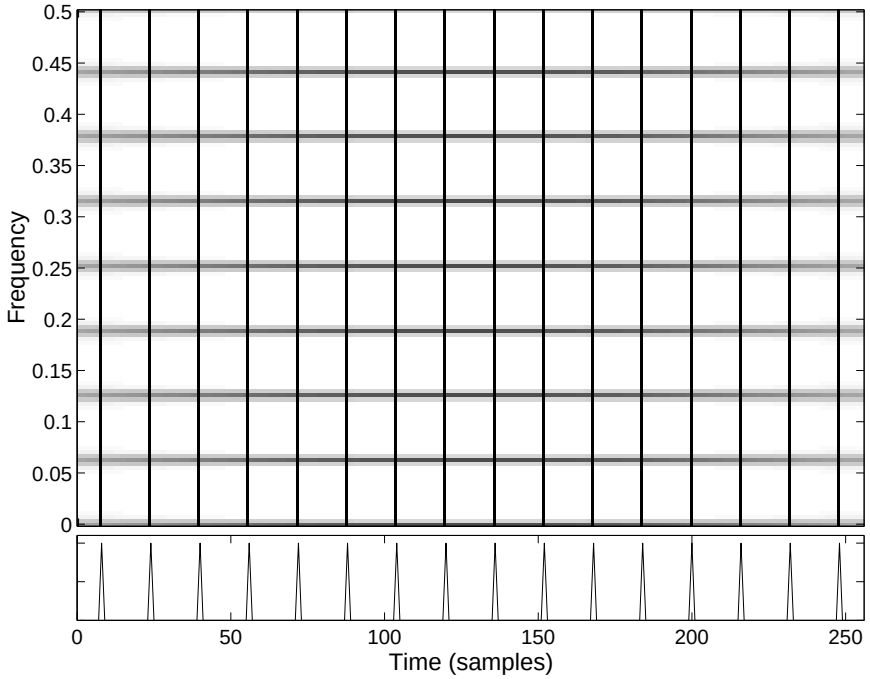

Figure 6.12: ASPEC TFR of the ideal periodic signal $\mathbf{III}_{256}^{16}$.

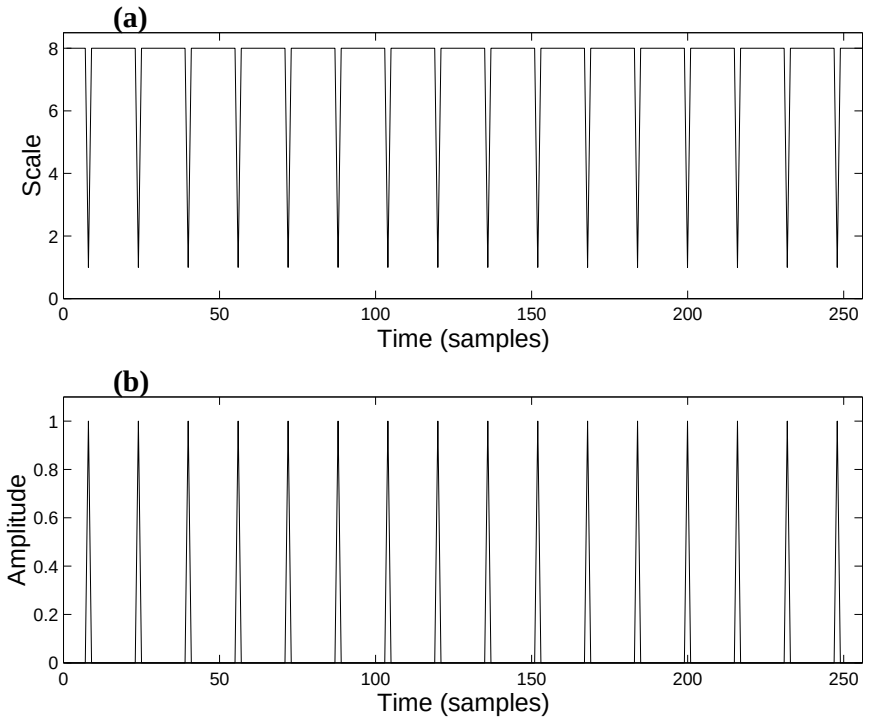

Figure 6.13: (a) The OWS of the (b) ideal periodic signal $\mathbf{III}_{256}^{16}$.

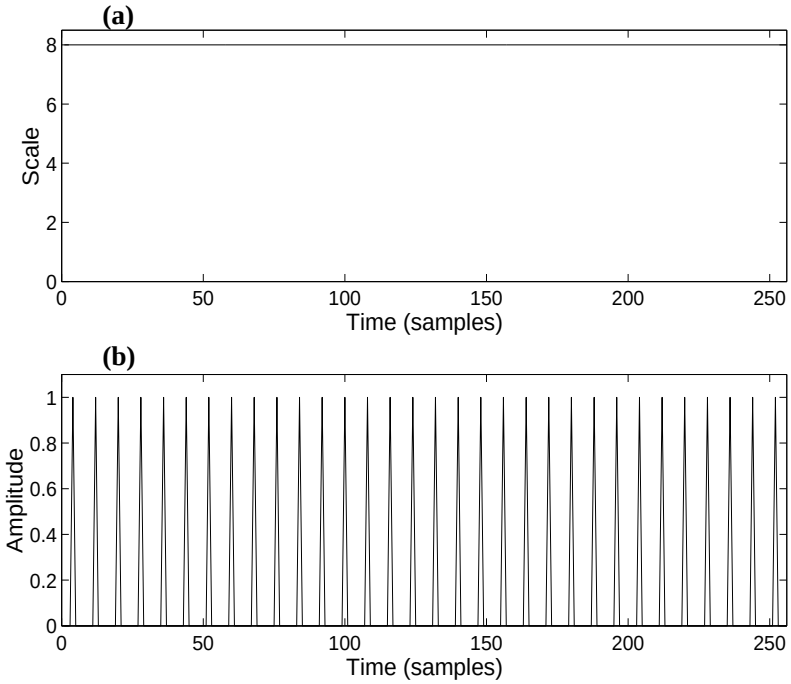

Figure 6.14: (a) The OWS of the (b) ideal periodic signal $\mathbf{III}_{256}^{8}$.

and therefore the MP-based method of spike detection fails to detect these spikes. This results is another case where OWS can detect individual spikes of repetitively spiking signals for which MP fails.

6.4.3 MP and OWS Representation of Real Repetitive EEG Spikes

The previous sections indicated that the OWS method performs better than MP in detecting individual spikes of periodically spiking sequences. To validate these results, we have selected an epoch of real newborn EEG seizure which contains repetitive, rhythmical spikes.

Figure 6.16(a) shows the OWS for the seizure epoch in Figure 6.16(b), which contains repetitive rhythmical spiking. It can be seen from Figure 6.16(a), that the spike events are clearly indicated by the OWS with scale values of 3 and 4. These scale values are associated with time durations of approximately 35-80msec which matches closely with the definition of a spike (i.e. 20-70msec in duration). Also, it can be seen for the first 4 spikes and the last spike that OWS not only detects the spikes but also detects the biphasic[6] nature of the spikes. However, this is unnecessary for our application as we

[6] A biphasic spike has a crest and a trough where as a monophasic spike has only a peak which is generally negative [104].

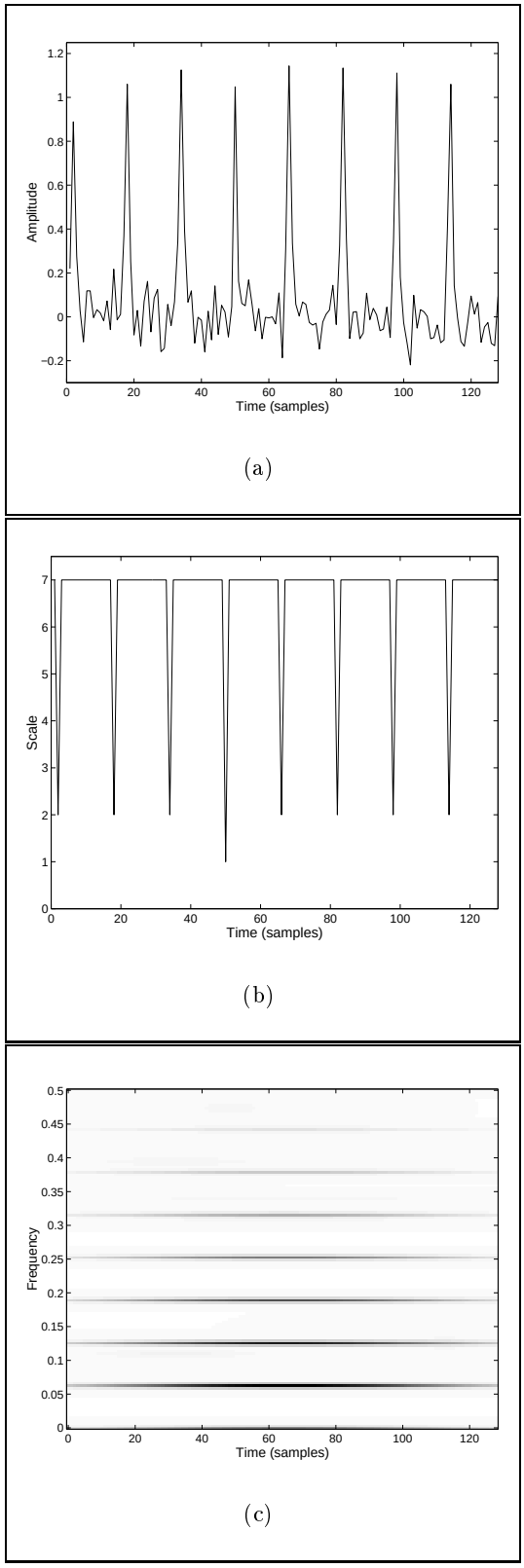

Figure 6.15: The individual spikes of the (a) repetitively spiking signal can be detected by (b) OWS but not (c) MP.

only require the detection of the spike event, whether it is biphasic or monophasic, and not the classification of the spike patterns.

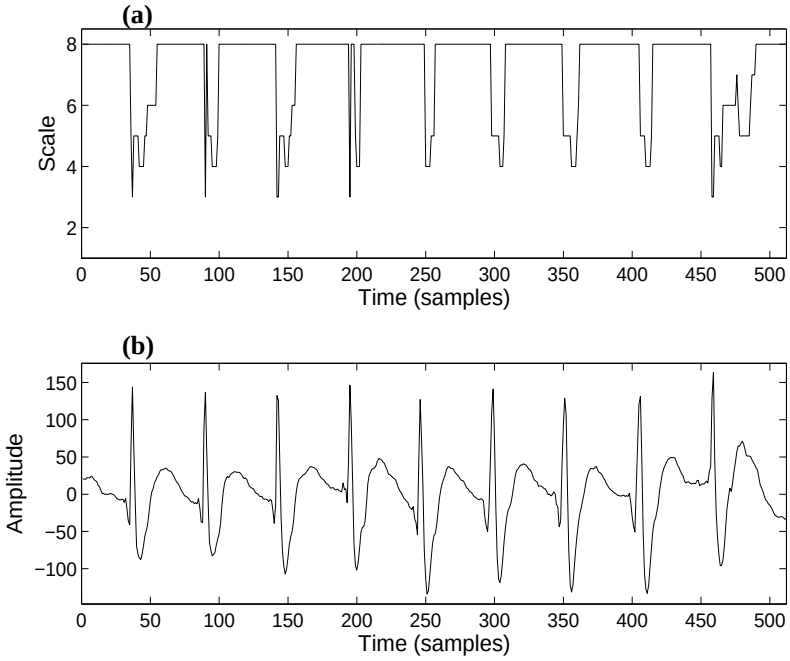

Figure 6.16: (a) OWS indicates the individual spike locations of the (b) real repetitively spiking EEG signal.

In Figure 6.17, we show the MP TFR of the same newborn EEG spiking signal in Figure 6.16(b). The atoms from the MP decomposition which had energy values greater than 2.5% of the total signal energy were defined as the significant atoms. It can be seen from the TFR in Figure 6.17 that only one spike atom, centered at approximately 460 samples, was chosen in the decomposition. Instead, the MP algorithm has selected large scale atoms, which indicate the harmonic relationship between the repetitive spikes, to represent the signal.

This example of real newborn EEG seizure, which contains repetitive spikes, confirms the previous results using synthetic signals which indicate that the OWS method is better at detecting repetitive, harmonically related spikes. Therefore, we will use an OWS-based method for detecting seizure spikes in the newborn EEG.

6.5 OWS-based Newborn EEG Seizure Detection

The automatic detection of seizure in the newborn involves firstly defining a feature, or a set of features, which clearly distinguishes the seizure state of the EEG from all other

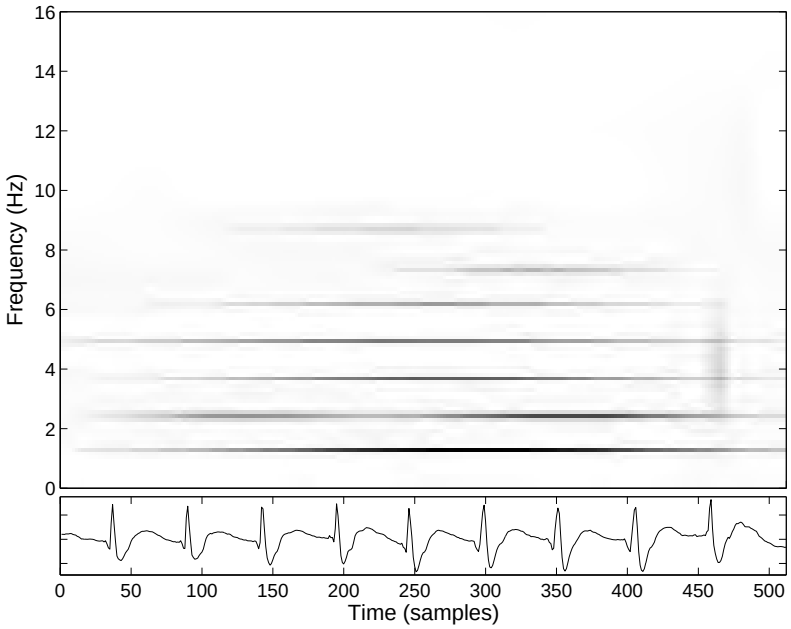

Figure 6.17: (a) MP fails to indicate the individual spike locations of the (b) real repetitively spiking EEG signal.

states. In our proposed automatic seizure detection algorithm, we use the repetitive behaviour of spike/sharp waves in EEG seizure to distinguish the seizure state from all other EEG states.

Although spikes and sharp waves in the EEG can be normal morphological variations of the newborn EEG, it is the continual repetition of spikes or sharp waves for a minimum of approximately 10-20 seconds, which characterize the newborn EEG seizure event [9, 22]. The real newborn EEG data used in the assessment of the proposed automatic seizure detection algorithm was acquired at the Royal Womens Hospital, Brisbane, Australia, using the MEDELEC system[7]. Twenty EEG channels were recorded from fourteen electrodes in a bipolar montage. The raw EEG data was bandpass filtered with cutoff frequencies at 0.5Hz and 70Hz before being digitized at 256Hz. A notch filter at 50Hz was also applied to remove any AC line artefacts.

6.5.1 Automatic Detection Algorithm

The newborn EEG has most of its power in the low frequency range of between 0.4–7.5Hz, with the majority of this in the 0.4–4Hz range [72]. Therefore, the preprocessing step of the automatic EEG seizure detection algorithm consists of digitally low pass

[7] A detail description of the EEG data acquisition is given in Appendix A

filtering the recorded EEG with a cutoff frequency of 15Hz. The filtered signal is then downsampled to 32Hz. By resampling the EEG at this rate, we significantly reduced the amount of EEG data to be processed without affecting spike and sharp wave events too severely.

The repetition of the spiking activity in the newborn EEG seizure is commonly found at rates between 1–3/second [77]. However, for neonates suffering from herpes simplex encephalitis, the seizure spiking rate has been seen as low as 0.5/second [121]. Therefore, we have chosen to segment the EEG signal into non–overlapping epochs of 128 samples (i.e. 4 seconds). This assures that during a seizure event with repetitive spiking, a minimum of two spikes will be contained in the epoch.

Multiple spikes in an EEG epoch is our proposed feature used to detect a newborn EEG seizure event. However, for a seizure event to be detected, at least three out of five successive epochs of any channel had to contain multiple spikes. If three successive epochs contained seizure and no others after that, then the seizure event was marked as the time period for the three epochs only. If the three epochs containing multiple spikes were spread across five successive epochs the seizure event was marked as the time period for the five successive epochs. This is demonstrated in Figure 6.18 with two examples of seizure events characterized by repetitive spiking. This marking system was chosen to account for the highly variable and complex morphology of newborn EEG seizure patterns. It was also used to counteract the effects of large amplitude artefacts which may mask the repetitive spiking characteristic for relatively short periods of time (i.e. less than 4 seconds). The proposed seizure detection algorithm is summarized in Figure 6.19.

6.5.2 Performance Evaluation of Detection Algorithm

At present, there is no unique standard testing procedure for the evaluation of seizure detection algorithms. Two of the most widely used methods of assessing automatic seizure detection algorithms include the *event-detection method* and the *neurologist-correlation method*.

The event-detection method of performance evaluation determines the percentage of seizure events that have been correctly identified during an EEG recording. The false alarm rate for this assessment method is quantified by the number of false detections per hour. Figure 6.20(a) provides an illustration of this assessment method. It can be seen from Figure 6.20(a) that the *example* seizure detection algorithm has correctly identified two out of three seizure events. Therefore, the seizure detection rate is 66.7% for this example. The background period in Figure 6.20(a) is of length 90 minutes. In that period, the *example* seizure detection algorithm has detected two seizure events.

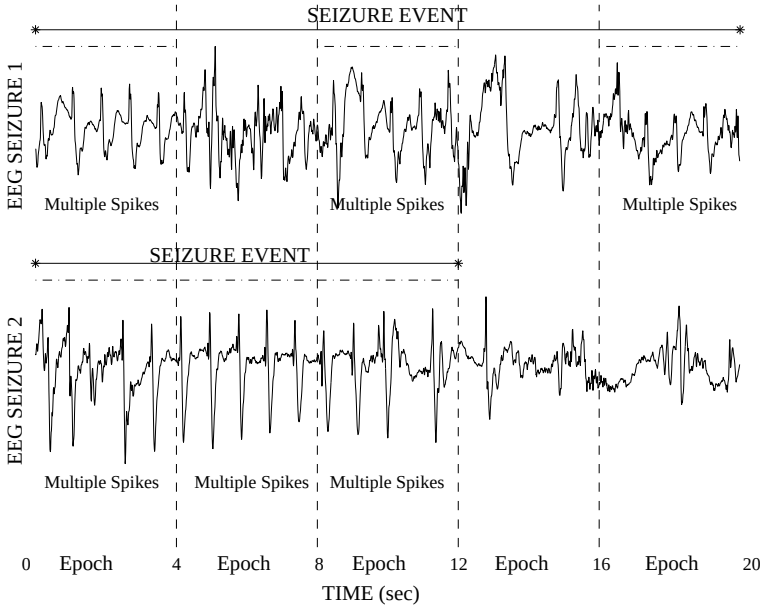

Figure 6.18: Two examples of how the automatic detection algorithm marks seizure events containing repetitive spikes.

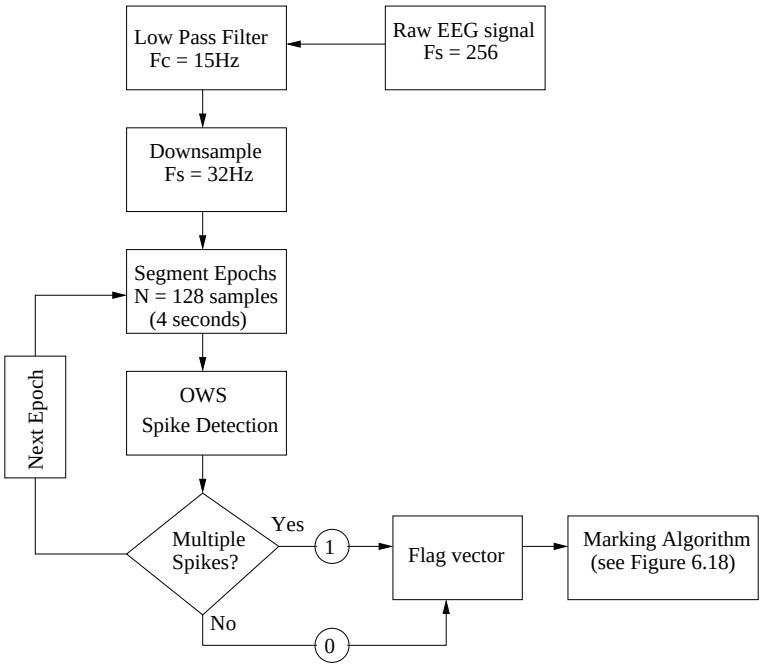

Figure 6.19: Automatic newborn EEG seizure detection algorithm based on OWS repetitive spike detection.

Therefore, the FDR for this algorithm is 1.33 false alarms/hr.

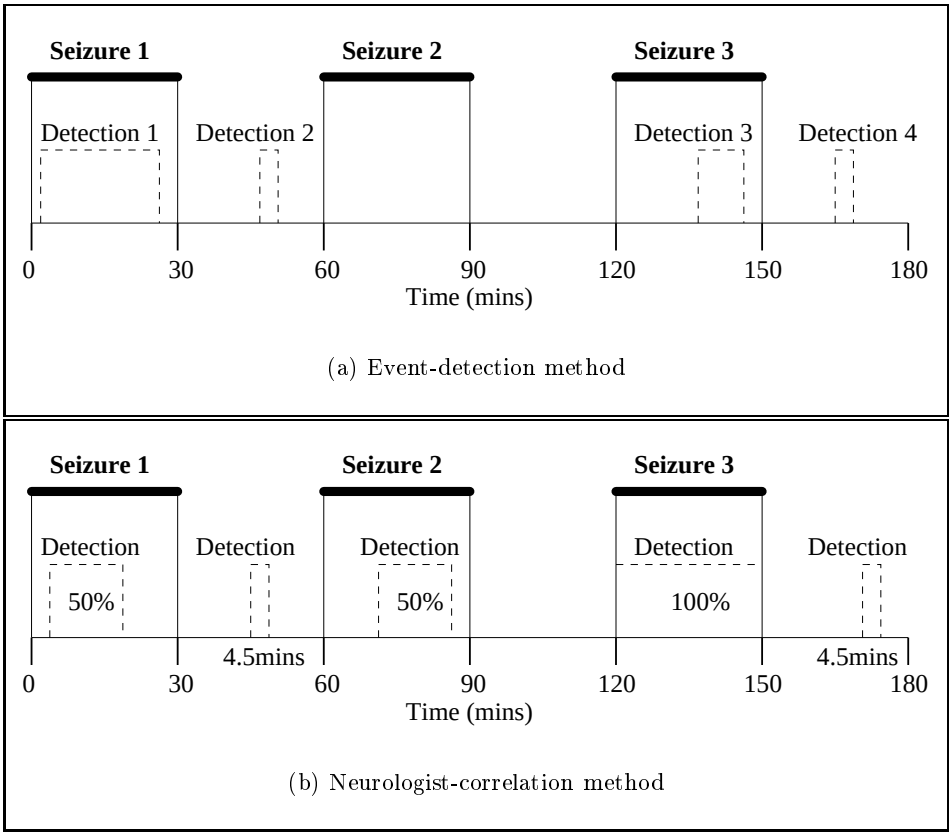

Figure 6.20: Methods for assessing automatic seizure detection algorithms. (a) is the event detection method. It can be seen that 2 out 3 seizure events have been detected correctly during the seizure periods and that 2 false detections have occurred in the nonseizure periods. (b) is the neurologist-correlation method. It can be seen that on average 66.7% of seizure detection correlates with the neurologist with 10% (i.e. 9mins/90mins) false detection.

The neurologist-correlation method is a more ambitious method of assessing seizure detection algorithms. For this assessment criterion, the seizure detection rate is based on the average percentage of seizure event lengths correctly identified by the automatic detection algorithm as seizure. The FDR is determined as the percentage of nonseizure data incorrectly identified as seizure by the automatic detection algorithm. Figure 6.20(b) illustrates the neurologist-correlation method of algorithm assessment. It can be seen from Figure 6.20(b) that the *example* seizure detection algorithm, on average, correctly identifies 66.7% of the seizure events. Figure 6.20(b) also shows that the *example* seizure detection algorithm falsely identifies 10% of nonseizure sections.

Performance assessment using the event-detection method requires a very large database of EEG signals obtained from *long term EEG monitoring* in order to give statistically valid seizure event detection and false alarm rates. However, long term EEG monitoring of the neonate is not practical at this stage.

The neurologist-correlation method does not require a large database to evaluate an algorithm's performance and is more informative than the event-detection method. Therefore, we have adopted the neurologist-correlation method for evaluating our automatic newborn EEG seizure detection algorithm.

To assess the performance of our automatic newborn EEG seizure detection algorithm, we have used the real EEG recordings from 8 newborns. The database contains nine seizure events from six neonatal patients. The seizure events had durations ranging from 12 seconds to 412 seconds (*as marked by an expert in neonatal EEG*). The other two newborn used in this evaluation did not experience any seizure event and were only used to evaluate the FDR.

Tables 6.3(a) and (b) show the results of the our proposed seizure detection algorithm. It can be seen from the results in Table 6.3 that the algorithm correlated well with neurologists markings. The average GDR and average FDR for our algorithm are:

Average GDR :	95.8%
Average FDR :	2.38%

In developing a seizure detection algorithm, a decision on the minimum duration of seizure positive activity for a seizure event to be detected must be decided upon. However, as the minimum duration is decreased (e.g. from 20 seconds to 10 seconds), the FDR generally increases. This tradeoff occurs because the newborn EEG background can sometimes mimic the behaviours of newborn EEG seizure over short periods. Therefore, a promising result from this algorithm is the fact that the shortest duration seizure event (i.e. 12 seconds) was correctly identified by the algorithm while simultaneously providing an extremely low false detection rate.

6.5.3 Comparison of Automatic Newborn EEG Seizure Detectors

To further evaluate our proposed automatic newborn EEG seizure detection algorithm, we compared it with four published and well-documented newborn EEG seizure detection algorithms. These algorithms include LIU [19], GOTMAN [22], CELKA [25] and HASSANPOUR [31]. These algorithms have previously been mentioned in Chapter 1.

Table 6.3: Performance of OWS-based detection algorithm using neurologist-correlation method. (a) Tables the results assessing the GDR and (b) shows the results for FDR assessment.

(a)

CHILD	EVENT	GDR
BABY 1	Seizure 1	100%
BABY 2	Seizure 2	88.4%
BABY 3	Seizure 3	100%
	Seizure 4	100%
BABY 4	Seizure 5	92.9%
	Seizure 6	100%
BABY 5	Seizure 7	100%
BABY 6	Seizure 8	100%
	Seizure 9	96.3%

(b)

CHILD	EVENT	FDR
BABY 7	Nonseizure	2.97%
BABY 8	Nonseizure	0.00%

The methods originally used in assessing the performance of each the published algorithms (i.e. LIU, GOTMAN, CELKA and HASSANPOUR) differ significantly. At this point, we note that the method used for assessing the performance of an automatic detection algorithm often drives the empirical threshold values for the algorithms. Therefore, it may be unfair to compare algorithms using a method of assessment which is different to the original method. However, recently, a method of performance assessment was proposed in [122] which allowed for the comparison of the LIU, GOTMAN and CELKA algorithms.

In the performance assessment method of [122], all EEG data was segmented into 60 second blocks which either contain seizure or nonseizure EEG, as labeled by a neurologist. If an algorithm detected seizure during any period of a seizure segment, a good detection was recorded. If an algorithm detected seizure during any period of a

nonseizure segment, a false detection was recorded. Therefore, the performance results were obtained as:

$$\text{GDR} = \frac{\text{Number of Good Detections}}{\text{Number of Seizure Segments}} \qquad \text{FDR} = \frac{\text{Number of False Detections}}{\text{Number of Nonseizure Segments}}$$

From our experience, the longer the seizure segment is, the better chance a detection algorithm has of detecting some part of the segment as seizure and therefore providing a good seizure detection. However, as the seizure segment length decreases it is more difficult for a detection algorithm to make a good detection. The minimum duration of a seizure event in the newborn is a much debated topic between neonatologists and neurologists, with most agreeing on a period of between 10-20 seconds of ictal characteristics to define a seizure event. Therefore, we believe that segmentation of the EEG into 60 seconds blocks is too long of a period.

To compare our algorithm with the LIU, GOTMAN, CELKA, and HASSANPOUR algorithms, we have adopted the assessment method of [122], describe above. However, we decided upon segmenting the EEG data into 30 second epochs. The LIU algorithm requires the longest epoch length out of the four algorithms, which is 30 seconds. Therefore, it was the discriminating factor in our choice of segmentation length. We then tested the different algorithms on 52 seizure segments and 44 nonseizure segments.

In the comparison of LIU, GOTMAN and CELKA presented in [122], it was found that all three algorithms performed poorly on their data set[8]. Subsequently, slight modifications were made to these algorithms to improve performance.

In our initial testing of the LIU, GOTMAN, CELKA and HASSANPOUR algorithms on our data set, we also found that the algorithms performed poorly. Therefore, we also made slight modifications to these algorithms. In the following section we briefly describe the original algorithms and then explain our modifications.

LIU Algorithm with Modifications

The LIU algorithm segments the EEG data into 30 seconds epochs. Autocorrelation is then performed on 5 windows of the 30 second epoch of which four are of length of 6.4 seconds and one is of length 4.4 seconds. For nonperiodic signals, the peaks and troughs in the autocorrelation are irregularly spaced. The time interval between peaks of the autocorrelation become constant for periodic signals. Since the newborn EEG seizure is characterized by rhythmic, repetitive patterns, the LIU algorithm assumes that seizure

[8]The data set of [122] contained 43 seizure segments and 34 nonseizure segments.

EEG should have peaks in the autocorrelation that are evenly spaced, whereas the nonseizure EEG will have irregular spacing.

To classify the EEG data, the *moment center* of the peaks of the autocorrelation are determined and the ratio between centers are calculated. The closer the ratios are to whole numbers the higher the score that window obtains. The scoring values for the ratio differences are presented in [19].

For the LIU algorithm, either of the following three criterion's must be met for a channel to be considered *seizure positive:*

(a) 2 consecutive window scores within a channel are ≥ 2, with the sum of the two window scores ≥ 10.

(b) 3 consecutive window scores within a channel are ≥ 2, with the sum of the three window scores ≥ 14.

(c) A score from a single window is ≥ 12.

If 2 or more channels in the epoch were *seizure positive,* the epoch was considered to contain EEG seizure.

The results of the original LIU algorithm for our dataset showed excellent GDR but extremely poor FDR. Therefore, to improve the performance of LIU we modified the criterion for a channel to be considered *seizure positive*. The modified criterion are explained as follows.

(a) 2 consecutive window scores within a channel are ≥ 2, with the sum of the two window scores ≥ 14.

(b) 3 consecutive window scores within a channel are ≥ 2, with the sum of the three window scores ≥ 16.

(c) A score from a single window is ≥ 13.

If 2 or more channels in the epoch were *seizure positive,* the epoch was considered as seizure.

GOTMAN Algorithm with Modifications

The GOTMAN algorithm takes a sliding window of 10.24 seconds with an overlap of 75%. The power spectrum of the EEG window is then obatined through the Fast Fourier Transform (FFT). The power spectrum of nonseizure newborn EEG is assumed to exhibit a peak frequency between 0.5-0.8Hz with an exponential decay. However,

	Dominant frequency	Width of dominant peak	Power ratio
First combination	0.5-1.5Hz	≤ 0.6	3-4
Second combination	1.5-10Hz	≤ 0.6	2-4
Third combination	1.5-10Hz	≤ 1	4-80

Table 6.4: Boundary values for features of GOTMAN algorithm.

the rhythmic characteristic of the newborn EEG seizure is often represented in the spectrum with significantly large peaks at the main seizure frequency. Therefore, the GOTMAN algorithm incorporates features which try to emphasize this distinguishing characteristic.

In the GOTMAN algorithm, the spectrum of the window under investigation is compared with the spectra of two windows occurring 60 seconds prior. These previous windows are referred to as the background windows. The features of the GOTMAN algorithm include: dominant frequency, width of dominant spectral peak and power ratio between the dominant spectral band of the current window and background window. Table 6.4 shows the boundary values of the features which distinguish seizure from non-seizure. A seizure detection is made if a current windows meets any of the criteria in Table 6.4.

The results of the original GOTMAN algorithm gave a poor FDR. To improve the FDR of the GOTMAN algorithm we required that 5 successive sliding windows in a channel be seizure positive before a seizure event was detected. The alteration of the algorithm meant that 20 seconds of ictal discharge was required for a seizure to be detected instead of the original 10 seconds. This tradeoff between FDR and minimum seizure duration was previously addressed in section 6.5.2

CELKA Algorithm with Modifications

The CELKA algorithm begins with the determination of an autoregressive moving average (ARMA) model of nonseizure EEG using pre-recorded nonseizure EEG signals. A preprocessing step of filtering the EEG signal using the inverse of the ARMA model is undertaken in an attempt to whiten the background portion of the newborn EEG. The Rissanen MDL [28] of the SVD of the EEG trajectory matrix is then used to determine whether the filtered EEG signal is pure white noise or contains a nonstochastic component.

The details of the CELKA algorithm are as follows. For the filtered EEG signal in state space of dimension n_s, the MDL determines from the SVD, the dimension, $n_o \leq n_s$, which is the minimal size embedding space. In the case of pure white noise,

$n_o = 1$. Otherwise, if $n_o > 1$, the signal contains a nonstochastic component. Therefore, a seizure detection is made if $n_o > 1$.

In [122] it was found that the filter coefficients of the ARMA model varied significantly from one sample section to another. Therefore, using the mean of the filter coefficients for the whitening preprocessing step lead to highly inaccurate results. However, it was found that the frequency response of the filters was consistent from one section to another and therefore an average frequency response was used to obtain the preprocessing filter. We have also taken this approach for the whitening preprocessing step.

HASSANPOUR Algorithm with Modifications

The HASSANPOUR algorithm is composed of three stages: (1) spike detection, (2) training: class forming and (3) seizure detection: classification into one of the predefined classes. The spike detection stage involves segmenting the data into nonoverlapping epochs of 4 seconds. The epoch is then transformed to the TF domain using the CWD. Two frequency slices at approximately 60Hz and 65Hz are then taken from the TFD and fed through SNEO to emphasize the spike events. Two separate threshold values, empirically chosen, were set for each of the frequency slices. The center of the local maximums, which were above the threshold value, were chosen as possible spike locations. If the marked spike locations were observed in both frequency slices, a positive spike detection was made.

The HASSANPOUR algorithm suggests that the distribution of intervals between spikes differs between seizure and nonseizure. Therefore, a histogram of successive spike intervals (HSSI) was used as a feature for the classification stage. Six seizure classes were unsupervisely constructed using the k-nearest neighbour algorithm [31].

In the seizure detection stage, the EEG database was again segmented into epochs of 4 seconds, transformed to the TF domain, SVD-based enhancement of the TFR was applied, and the HSSI obtained. The epoch HSSI was then compared to these classes using the Jensen function and if the output was less than 0.1 (i.e. an epoch was close enough to any of the classes according to this threshold) a seizure detection was declared for that epoch. Otherwise, the EEG data was classed as nonseizure.

We believe that since the minimum duration of ictal patterns in the EEG is 10 seconds for a seizure event to be decided upon, a seizure detection based on 4 seconds of EEG is too short. Therefore, we added in the constraint that at least two successive epochs in any channel be seizure positive before a seizure event detection is declared.

Comparison	Algorithm	Liu	Gotman	Celka	Hassanpour	OWS
Thesis	GDR (%)	69	62	60	29	94
	FDR (%)	43	16	50	36	2.3
Faul et al.	GDR (%)	43	63	66		
	FDR (%)	10	34	46		

Table 6.5: Results of newborn EEG seizure detection algorithms on a common database.

Results and Discussion

The results of LIU, GOTMAN, CELKA, HASSANPOUR and OWS newborn EEG seizure detection algorithms on our EEG database are shown in Table 6.5. It can be seen from the results in Table 6.5 that our OWS-based seizure algorithm performs significantly better than the other algorithms. These results can be attributed to a number of factors for which we will discuss. Table 6.5 also includes the results from the comparison of Faul et al. [122]. The table shows similar results between our results and the results of [122]. The largest variation between comparison occurs for the LIU algorithm. However the GDR-FDR (i.e. difference) is similar. This suggests that the modifications of the LIU algorithm in [122] were driven by the desire to minimize the FDR.

LIU Performance

The most interesting performance measure for the LIU algorithm is its significantly large FDR. From our investigation of this algorithm, with respect to our EEG database, we found two major factors causing this result. Firstly, the data acquisition system used in Liu et al. [19], only recorded 12 channels in a bipolar montage. The LIU algorithm required that two channels or more exhibit seizure activity. This was most likely decided upon because each recording electrode placed on the scalp is used in the acquisition of two or more channels. Therefore, if significant seizure electrical activity was occurring under one electrode, it should be seen in at least two channels.

Our data acquisition system records twenty EEG channels, also in a bipolar montage. This is a significant increase in the number of recording channels for newborn EEG patients whose scalp size is already small. Therefore, the chance that two or more channels may record artefacts mimicking seizure activity is much greater, leading to increased false detections.

The second factor causing an excessively large FDR for the LIU algorithm is the appearance of slow wave activity in the background which has significantly large am-

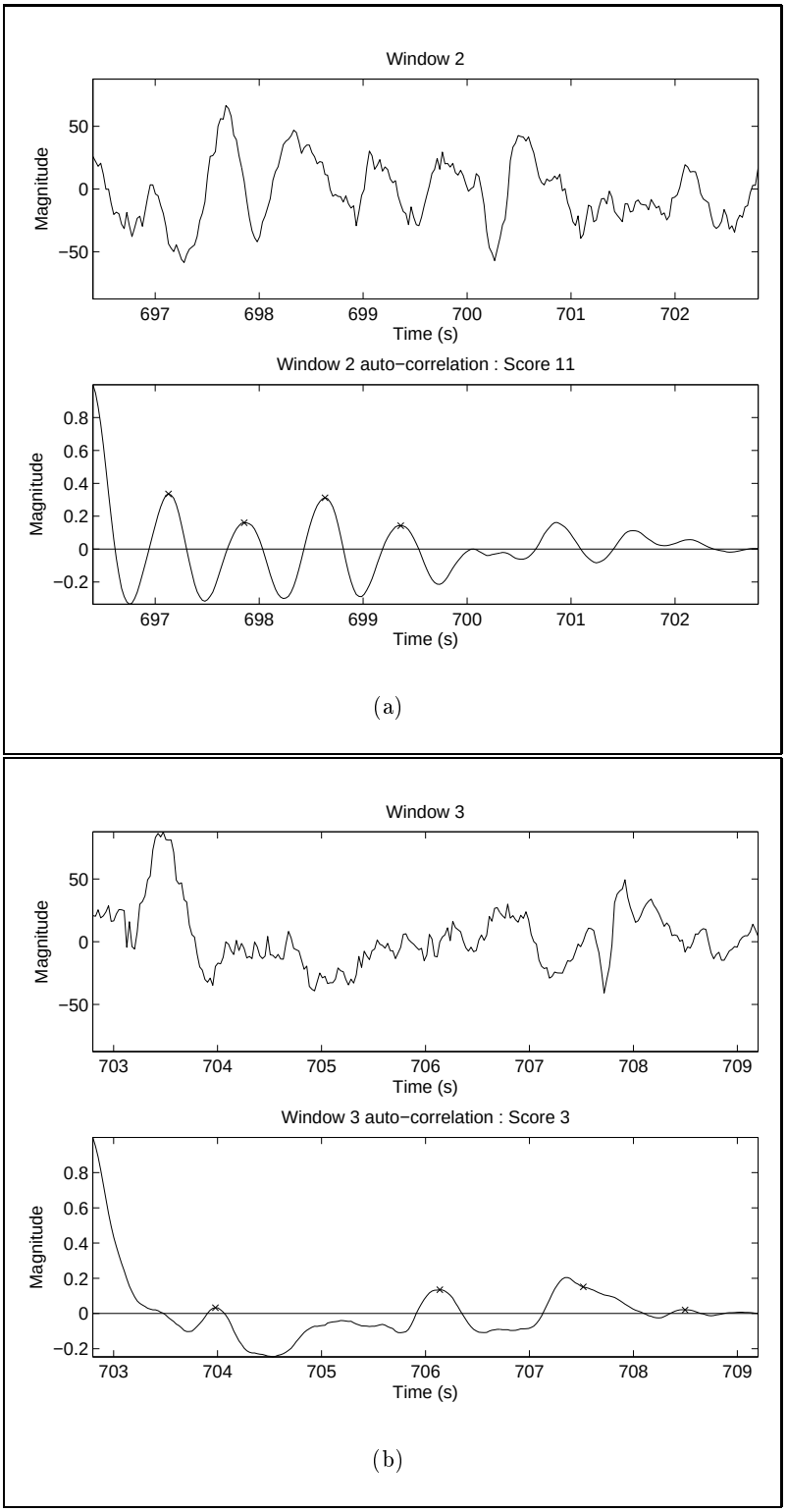

Figure 6.21: Two consecutive windows of nonseizure EEG data which result in a false seizure detection by the LIU algorithm.

plitude. These slow waves result in a repetition in the autocorrelation function, similar to that which is seen for seizure windows. This can be seen in Figure 6.21(a), in which an epoch of real newborn EEG background with a slow wave causes a large score value from the autocorrelation function. The following window in Figure 6.21(b) does not have the slow wave characteristic seen for the previous window. However, the scoring from the autocorrelation function is large enough such that when combined with the previous window, a false detection is made by the algorithm.

GOTMAN Performance

The GOTMAN algorithm compares the spectrum of the current EEG epoch with that of two EEG epochs approximately 60 seconds prior to the current epoch. In our assessment methodology, we have created a database containing 30 second segments of seizure and nonseizure EEG. Therefore, we used 60 seconds worth of marked EEG background data to calibrate the GOTMAN algorithm. This calibration was also employed in the newborn EEG seizure detection algorithm comparison presented in [122]. However, we found that the both the GDR and FDR were extremely high. Therefore, the modifications made to the GOTMAN algorithm were aimed at reducing the FDR while maintaining a relatively high GDR.

It can be seen that the GOTMAN algorithm has significantly lower FDR than LIU or CELKA whilst retaining a comparable GDR. It was noted in [122] that the separation of nonseizure and seizure in the defined 3 dimensional feature space of the GOTMAN algorithm was not always distinct. We also found that the there was significant overlap between some seizure and nonseizure data in the feature space, as shown in Figure 6.22. This is a major factor causing the inefficient performance of the GOTMAN algorithm.

CELKA Performance

This algorithm is referred to as a seizure detection algorithm, however, it is essentially a newborn EEG background detector. The whitening pre-processing step of the CELKA algorithm attempts to whiten the background portion of the EEG signal. This means that the whitening process should only be successful if the newborn EEG data is background. In this case the MDL should give a minimal embedding dimension value of $n_o = 1$. Otherwise, if $n_o > 1$ the EEG data is classed as seizure. Therefore, the algorithm only detects the background data and classes everything else as seizure.

The CELKA algorithm performs poorly, as can be seen from Table 6.5. In particular, it gives a particularly high FDR. This is due to the whitening preprocessing step. The static whitening filter cannot always whiten the nonstationary newborn EEG

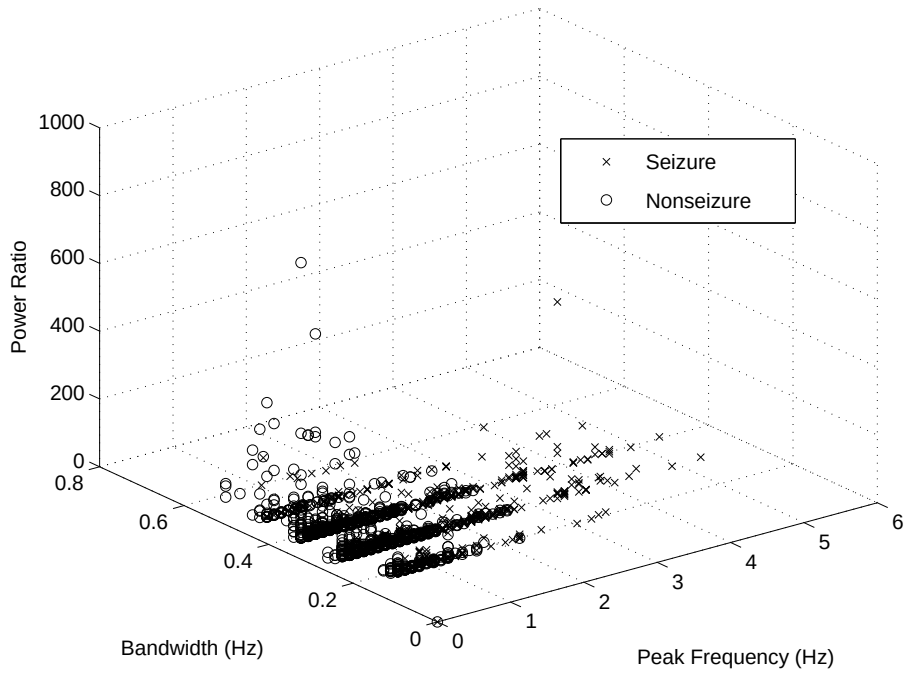

Figure 6.22: Three dimensional feature space of the GOTMAN algorithm showing seizure and nonseizure data points.

background. The result of the background not being whitened properly is that a false seizure detection is made.

The GDR of the CELKA algorithm also suffers from the whitening process. The nonstationary EEG seizure has a time-varying magnitude spectrum. The average of this time–varying magnitude spectrum may be similar to the average of the time–varying magnitude spectrum of the background EEG. Therefore, because the discriminating temporal information is discarded, this may lead to whitening of the EEG seizure data and result in a missed seizure detection. From these results, it is obvious that a time-invariant whitening filter cannot achieve the desired results for nonstationary signals such as the newborn EEG background. Similar observations to ours were also described in [122].

HASSANPOUR Performance

In the assessment of the HASSANPOUR algorithm, we used the set of histograms covering the seizure classes that were defined in [31, 123], as well as the original algorithm. However, it can be seen in Table 6.5 that the HASSANPOUR algorithm has the poorest overall performance. This poor result is due to a number of reasons.

Firstly, it seems that the spike detection stage of the seizure detection algorithm

is extremely sensitive to fast variations in the signal, leading to many false EEG spike detections. In Figure 6.23, we show a four second epoch of EEG data which has a single epileptiform spike, as marked by a neurologist. At the bottom of Figure 6.23, we have shown the HASSANPOUR spike detection locations using pins. It can be seen that the spike detection algorithm detects the true EEG spike correctly, however, it also detects many other spike events which have not been marked by a neurologist as EEG spike events. Therefore, the algorithm is not truly detecting the time interval between EEG spikes which may result in poor detection results.

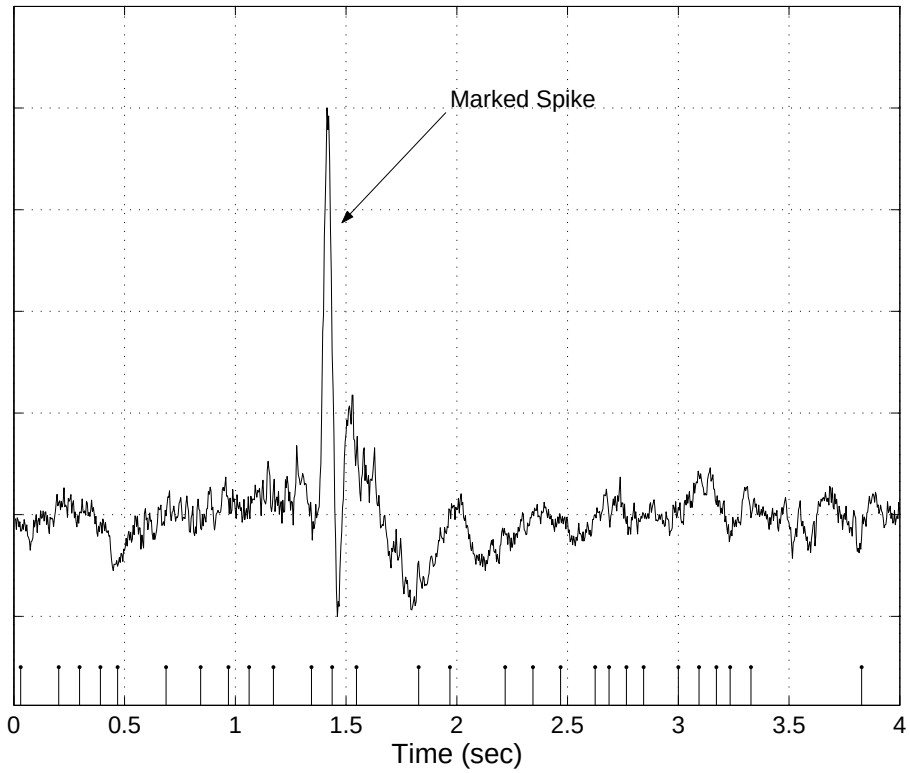

Figure 6.23: Spike detection of a four second EEG epoch using the HASSANPOUR spike detector.

Secondly, the HASSANPOUR algorithm classified newborn EEG seizure into 6 classes using 5000 epochs of seizure from 11 newborns [123]. It then determined that EEG data not falling into any of these classes are nonseizure. However, it seems that the classification process should have been applied to nonseizure EEG data as well. This way, it could be verified that the nonseizure EEG data does not fall into the any of the seizure classes. This may be one reason for the high FDR of the HASSANPOUR algorithm.

Thirdly, the testing of the HASSANPOUR algorithm was previously done using 5

newborns and it achieved good detection rates. However, it was not stated whether these newborn EEG recordings were also used in the classification process, which would be the reason for the good performance of the algorithm in that assessment. Also, it seems that the number of classes of newborn EEG seizure is too small as an extremely large number of EEG seizure epochs were missed by the algorithm. Another way to combat this is to reduce the threshold value of the Jensen function. However this may lead to an increase in the FDR.

Finally, there are a large number of thresholds which can be set in this algorithm. However, because of the long processing times, optimization of these thresholds is extremely difficult and time consuming. Therefore, we only ran the HASSANPOUR algorithm with the original threshold values. By changing these threshold values, it may be possible to improve the performance of the HASSANPOUR algorithm.

OWS Performance

Table 6.5 clearly demonstrates the superiority of our proposed newborn EEG seizure detection algorithm. The excellent results of this algorithm can be attributed to a number of factors. Firstly, the algorithm uses an adaptive TFSP technique (i.e. OWS) to accurately detect repetitive newborn EEG seizure spikes/sharp waves. This method has been shown to provide the best performance in the detection of repetitive spikes when compared with QTFDs such as the CWD, used in HASSANPOUR, and MP, which is another adaptive TFSP technique.

The nonstationarity of the newborn EEG is a major factor which restricts the performance of techniques such as LIU, GOTMAN and CELKA. The time-varying characteristics which may discriminate between the nonstationary seizure data from the nonstationary background data cannot be included in any of the LIU, GOTMAN, or CELKA algorithms. These restrictions are overcome using the adaptive TFSP technique of the OWS.

The major drawback of the OWS-based seizure detection algorithm is its processing time. The LIU, GOTMAN and CELKA algorithms are all computationally efficient and can all be used for real–time newborn EEG seizure detection. Neither the OWS–based nor HASSANPOUR algorithms can be run in real–time. However, the OWS–based algorithm is approximately twice as fast as the HASSANPOUR algorithm. This due to the fact that OWS-based spike detection method does not need to compute the TFR.

Another limitation of the OWS-based seizure detection algorithm is that although a majority of seizures exhibit repetitive spiking, some seizures are characterized by slow waveforms. Therefore, these types of seizures will be missed by the OWS-based seizure detection method.

6.6 Summary

This chapter presents a new method for the automatic detection of seizure in newborns. The proposed seizure detection algorithm is based on the ability to automatically detect the individual spikes of repetitively spiking signals.

It has previously been shown that QTFD-based methods perform better in detecting spikes than time domain based techniques, [114]. However, in this chapter, we gave an example which showed that QTFD-based spike detectors, such as the one proposed in [114], can fail to detect the individual spikes of a repetitively spiking signal. Therefore, a new method of detecting signal transients or spikes based on adaptive TFSP was developed.

The proposed method of spike detection used in this chapter was the OWS method, which was originally developed to optimize the window size of the Spectrogram and other QTFDs. It was shown that if a spike occurred in the signal, the OWS would be small around the time location of the spike and can therefore be used as a basis for spike detection.

The performance of the new method for spike detection was compared with another adaptive TFSP spike detection method based on the MP. It was shown that both methods performed well on the detection of isolated spike in real EEG signals, with both methods having similar specificity and sensitivity rates. However, it was shown that the OWS method of spike detection performed better than MP in detecting repetitively spiking signals. This was illustrated using synthetic and real signals.

A seizure detection algorithm based on the detection of repetitive spikes using the OWS was presented. Firstly, we assessed the proposed algorithm using the neurologist-correlation method of performance evaluation. It was shown that the algorithm correlated extremely well with the neurologist markings, with an average GDR of 95.8% and an average FDR of 2.38%.

Due to the various methods for assessing the performance of seizure detection algorithms, a generic method of performance assessment was required. We chose to use a method proposed in [122], to compare our OWS-based algorithm with the LIU, GOTMAN, CELKA, and HASSANPOUR algorithms. It was observed from this comparison that the OWS-based seizure detection algorithm was superior to the other newborn EEG seizure detection algorithms with 94% of seizure epochs being detected correctly and only 2.3% of nonseizure epochs being falsely detected as seizure. Possible reasons for the poorer performance of each of the other algorithms were provided to validate the comparison results.

Chapter 7

Conclusions and Future Research Intentions

7.1 Thesis Summary

This thesis is focused on the accurate, automatic detection of newborn EEG seizure. A variety of time-frequency signal processing techniques were investigated in this thesis and many sophisticated variations and applications of these techniques were proposed. This led to the development of an automatic newborn EEG seizure detection method which was shown to outperform other well-documented methods.

The first objective of this thesis was to analyze the newborn EEG using nonlinear and nonstationary techniques for the development of a realistic newborn EEG simulator. It was found that a prominent feature associated with the background newborn EEG signal was its self-similarity. This thesis assessed the background EEG of the newborn using the most appropriate method of fractal dimension estimation (i.e. Higuchi method). Using the results of this analysis and the relationship between fractal dimension and power spectrum law, a method of simulating newborn EEG background was developed. This method was shown to exhibit similar characteristics to real newborn EEG in the time, frequency and time-frequency domains, as well having similar nonlinear characteristics.

Nonstationarity is a significant characteristic of newborn EEG seizure, which has also been shown to consist of multiple TF components. To allow for the TF characteristics, a newborn EEG seizure simulator was proposed using TFSS. In this method, a TF template image was constructed based on TF analysis and characterization of newborn EEG seizure. The time domain signal associated with the designed template was then synthesized using the MSTFT magnitude method. This simulator has a number of ben-

efits over previous methods including its simplicity, ability to handle spectral distortion and the discontinuities of the piecewise instantaneous frequency law.

Atomic decomposition techniques were investigated in this thesis for their ability in analyzing and processing newborn EEG. A major goal of atomic decomposition techniques incorporating redundant dictionaries is the ability to provide sparse representations. However, in most engineering applications, only sufficient signal approximations are needed. We investigated two recent atomic decompositions techniques, MP and BP, for their ability to provide sparse approximations. It was shown that although BP provides the sparsest *representation*, it did not always provide the sparsest *approximation*[1]. Instead, it was shown that MP generally provided sparser signal approximations. This was demonstrated using a variety of signals and desired approximation levels. For this reason, MP was chosen as our preferred method of signal decomposition in this thesis.

It was shown that the number of significant atoms (i.e. the minimum number of atoms needed to approximate the signal to a desired level) from MP decomposition, increased as the signal structures became less coherent with the decomposition dictionary. This indicated that the number of significant atoms needed in an approximation quantified the coherency between the signal structures and the decomposition dictionary. The number of significant atoms was termed *"structural complexity"* (SC) as the observed complexity (i.e. number of significant atoms) is totally dependent on the structures in the signal and the decomposition dictionary.

A method of detecting changes in signal structure was then derived based on the change in SC. It was established that if a dictionary, which was highly coherent with a particular signal state, was developed, then changes from this signal state could be detected through a change in the SC. This generic method of detecting signal transitions was demonstrated using synthetic signals, which clearly showed its applicability.

The SC-based method of detecting signal transitions was applied to the newborn EEG for detecting the transition of the EEG signal into and out of the EEG seizure state. A TF dictionary, coherent with the newborn EEG seizure state, was developed based on the TF characterization of the newborn EEG seizure and background states. The SC-based detection method was first demonstrated with, and applied to, a large database of synthetic newborn EEG signals, created using the simulation methods of Chapter 4. The algorithm achieved a sensitivity and specificity of 100% and 97.3% respectively. The SC measure applied to real newborn EEG was used to validate the synthetic results, in which it was shown that a significant change in SC occurred during signal transitions.

[1]Signal representation infers that all signal energy is represented, whereas signal approximation means that some residual signal energy is not accounted for.

Spike events are paroxysmal events which often occur in the EEG of abnormal newborns. The MP algorithm was previously used for adult EEG epileptic spike detection [42], and showed promising results. However, the results were based on isolated spike events in the EEG signal.

The newborn EEG seizure is characterized by repetitive, rhythmical spiking. Therefore, we assessed the MP algorithm for detecting repetitive spikes. It was demonstrated, using synthetic and real signals, that the ability of MP in detecting individual spikes of a repetitively spiking signal was dependent on the relationship between signal length and period between successive spikes.

The adaptive spectrogram using a window adaption method referred to as the maximum correlation criterion [120], was shown to be another valid method of detecting spikes. In particular, it was demonstrated that the method could be used to detect repetitive spikes as well as provide information about the harmonic relationship between successive spikes. It was illustrated that this representation of *dual* information was not attainable using MP.

It was then shown that spike detection could be determined directly from the adaptive window optimization algorithm used for the adaptive spectrogram. That is, the optimal window scale (OWS), provided by the adaption algorithm, was small at the time instants where spike events occurred, therefore, allowing for spike detection. This OWS-based method of spike detection was shown to detect isolated spikes in the EEG with the same accuracy as MP. It was also shown to detect repetitive spikes much better than the MP method.

A seizure detection algorithm was proposed based on the OWS method of spike detection. The algorithm was evaluated using the neurologist-correlation method of assessment and achieved an average GDR of 95.8% and an average FDR of 2.38%. The algorithm was then compared with four well documented seizure detection algorithms [19, 22, 25, 31], and was shown to outperform these algorithms.

7.2 Conclusions

In accordance with the results obtained in this thesis, a number of conclusions have been made. These conclusions are detailed in the following:

- **EEG simulation methods should address all significant nonlinear and nonstationary characteristics of the real EEG.**

  The newborn EEG has both significant nonlinear and nonstationary characteristics which must be addressed in the development of a newborn EEG simulator.

Previous simulation techniques have not addressed the nonstationarity associated with the newborn EEG background or the multicomponent nature of the newborn EEG seizure, which have both been accounted for in our proposed simulation methods. *This has led to more realistic simulation of the newborn EEG which can be used confidently in the development and assessment of newborn EEG seizure detection algorithms.*

◇ **Atomic decomposition techniques which provide sparse signal representations do not necessarily provide sparse signal approximations.**

Previously, much work has been done in the development of atomic decomposition techniques which provide highly sparse signal representations. This thesis has demonstrated that decomposition techniques which provide sparse signal *representations* do not necessarily provide sparse signal *approximations. Therefore, a decision on which atomic decomposition technique to use should incorporate the a priori knowledge of whether a signal approximation or signal representation is desired for a particular application.*

◇ **Sparse approximations can also be achieved through the use of carefully designed coherent TF dictionaries.**

This thesis also shows that sparse signal approximations can be achieved through careful dictionary design. It was shown, using the real life signal example of newborn EEG seizure, that sparse signal approximations could be achieved through the design of a coherent time-frequency dictionary. The coherent dictionary was developed based on the observed time-frequency characteristics of the newborn EEG seizure state. By developing a time-frequency dictionary that is coherent with a specific state in a signal, we demonstrated that transitions into and out of this state could be detected using the number of significant atoms needed in an approximation (i.e. using the structural complexity measure). *This has introduced to the area of atomic decomposition the idea of using application specific dictionaries to achieve sparse signal approximations and detect particular signal states.*

◇ **Difficulties arise when trying to detect repetitive rhythmical spikes using TF techniques. Therefore, adaptive TF techniques should be used for detection of repetitive spikes.**

Time-frequency signal processing techniques have been shown to be suitable tools for the detection of signal transients. However, difficulties in detecting repetitive rhythmical transients using time-frequency signal processing techniques have been

identified in this thesis. It was shown in this thesis that adaptive quadratic TFDs can provide more information about the TF characteristics of repetitive rhythmically spiking signals than QTFDs. *Therefore, adaptive QTFDs should be used in place of QTFDs for detecting repetitive rhythmical spikes, which occur in real life signals such as the newborn EEG.*

◇ **Detection of repetitive rhythmical spikes can be achieved using the window optimization algorithm used by adaptive QTFDs.**

The optimal window scale which gives the adaptive window length used by adaptive QTFDs can be used for the detection of transients without having to compute the TFR. Spikes are indicated by small window scales/lengths at the time locations of the spike events. This technique of spike detection was developed in this thesis and also shown to be better than QTFDs and matching pursuit for the detecting repetitive rhythmical spiking. *This is significant as the optimal window scale method of spike detection reduces processing time in the application of spike detection. It also signifies the use of the optimal window scale in solving signal processing problems.*

◇ **Seizure detection can be achieved by the detection of repetitive rhythmical spiking in the EEG signal.**

A significant characteristic of the newborn EEG that is synonymous with the EEG seizure state is repetitive rhythmical spiking. It was demonstrated in this thesis that techniques capable of indicating the occurrence of repetitive rhythmical spiking, such as the optimal window scale method, could be used for newborn EEG seizure detection. In fact, the seizure detection algorithm proposed in this thesis was based on the OWS method of spike detection and was shown to outperform other highly recognized seizure detection algorithms. *Therefore, this presents a suitable algorithm for possible use in the clinical setting for offline automatic seizure detection. Further refinement of the algorithm and increased computer speeds may one day see this algorithm being used for real-time/online automatic seizure detection.*

7.3 Future Research Directions

In achieving the objectives and reaching the goal of the this thesis, outlined in section 1.3, a number of future research directions were identified. Specifically, the following research areas could be addressed:

- **Newborn EEG background simulation.** The simulator proposed in this thesis provides nonstationary newborn EEG background with nonlinear characteristics. However, in the simulation of the EEG, envelope variation, which is common in the newborn over lengthy periods, was not considered. It should therefore be observed how the envelope varies over time for a collection of newborns. Also, it would be beneficial to test for any correlations between envelope (or epoch energy) and fractal dimension estimates. Further analysis on the distribution of the fractal dimension estimate of the newborn EEG using more background recordings should be undertaken.

- **Newborn EEG seizure simulation.** A wide variety of newborn EEG seizure patterns with varying TF characteristics are available. We considered a number of factors including the number of linear frequency modulated (LFM) piecewise parts to the IF law, the slope of the LFM, frequency range and multiple components (i.e. the harmonics of the fundamental component). We have proposed a constant law that governs the amplitude of the harmonic components. However, further investigation into the amplitude laws for various components should be assessed. It is believed that this will lead to a variety of spiking patterns in the time domain signal, which will mimic the complex morphology of repetitive spikes found in real newborn EEG seizure.

  The parameters for the proposed newborn EEG seizure model were estimated through the subjective analysis of a large number of newborn EEG seizure epochs. Future work should include a quantitative extraction of these parameters and justification using some statistical hypothesis testing. Also, investigations into possible validation methods of the model should be undertaken.

- **Coherent dictionary development.** This thesis proposed a TF dictionary that was coherent with the signal structures found in the newborn EEG seizure state. This included LFM atoms, which were representative of the patterns observed in the seizure state. Improvements in this dictionary could be made by defining atoms more coherent with the newborn EEG seizure structures. Suggestions include scaled LFM atoms, piecewise LFM atoms, FM atoms with other IF laws and multicomponent LFM atoms which include harmonics. However, care should be taken so that the new TF atoms are not coherent with the background EEG state.

- **Signal transition detection applications using structural complexity.** The generic method of detecting changes in signal structure proposed in this

thesis has only been applied to newborn EEG to distinguish between seizure and nonseizure. This method of detection may also be used in other applications such as EEG sleep stage detection and machine condition monitoring.

- **Improving spike detection methods.** The seizure detection method proposed in this thesis was based on the ability to detect repetitive spikes. Improving the accuracy of spike detection algorithms will correspond with improved seizure detection algorithms. For the matching pursuit method of spike detection, we suggest a weighting function be applied to the Gabor dictionary that is inversely proportional to the atom scale. We believe that this biasing would improve the MP algorithm in selecting smaller scaled atoms to represent individual spikes of a repetitively spiking signal, rather than selecting large scaled atoms to show the harmonic relationship between spikes. This type of weighting function could also be applied to the maximum correlation criterion for the adaptive window optimization method used by the adaptive spectrogram. For both techniques, the weighting function would need to be optimized based on the trade off between true positives and false positives.

  We have used only one method of adapting the window length of QTFDs. However, there are many other methods of adapting the window length for QTFDs. These window adaption methods may be tested and compared to the maximum correlation criterion for detecting spikes to see which method performs the best.

Appendix A

Appendix 1: EEG Data Acquisition

A.1 Introduction

The recording of EEG in the newborn has proven to be a highly valuable tool. It has been shown to be superior in many ways to clinical examination of neonatal patients, particularly in the detection and prognostication of brain dysfunctions [9].

The EEG is a measure of the electrical activity generated by the physiological processes of the brain. The non–invasive nature of the EEG means it is a relatively simple method for assessing the health of the CNS and brain functioning.

There are currently a number of devices for the simultaneous recording, monitoring and pre-processing of EEG data. **AMLAB** [124], **PHOENIX Clinical Lab EEG** [125] and **MEDELEC** [126] are some commonly used EEG recording systems.

In this thesis, the EEG data has been acquired using MEDELEC's Profile long term monitoring system. Therefore, this appendix is restricted to the description of MEDELEC Profile.

A.2 MEDELEC Profile System

The MEDELEC Profile System is a product of the Taugagering company. It is distributed by Oxford Instruments Medical which is a world leading distributor of cardiology, neurophysiology and obstetric equipment [127].

In routine adult EEG recording using MEDELEC Profile, 20 EEG electrodes are placed over the scalp. The recorded signals are extremely small, (μV). The MEDELEC Profile system amplifies and displays the recorded electrical activity, while simultaneously saving the data for review by an EEG expert. The MEDELEC Profile system also allows for the recording of other biological signals such as EOG, ECG, EMG and

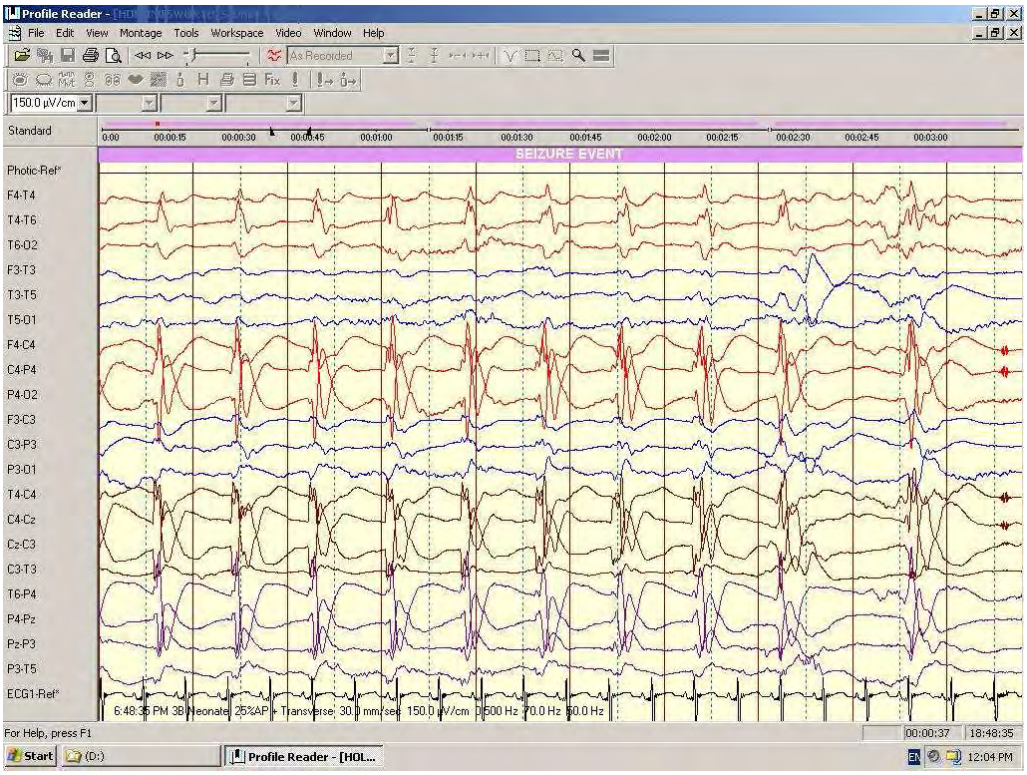

Figure A.1: EEG display on windows operating system using the MEDELEC Profile system.

respiration. An example of the Profile display of 20 newborn EEG channels and 1 ECG channel is shown in Figure A.1. It can be seen from the top of Figure A.1 that this period of EEG data has been labeled as seizure by the neurologist.

Features of the MEDELEC Profile system are discussed briefly as follows [127]:

- **Providing distributed data:** Information of a patient in the database is instantly available over the network using Microsoft access. Fast and intensive search capabilities with integral work flow software provide an appropriate solution for a distributed EEG system.

- **Simple, high quality recording:** To ensure quality recordings, an electrode impedance check is available at the head–box and a remote event marker is built-in. High quality amplifiers and high sampling rates allow for high quality digitization of up to 40 EEG channels.

- **Multimedia EEG:** The Profile system takes advantage of sound and vision PC-technology to display and store EEG, video and audio signals creating true multimedia EEG. Digital videometry means no complicated wiring and no need to

Figure A.2: A frame of the video record using the MEDELEC Profile system.

program VCRs. The video picture can be moved around the screen or can be changed in size. A still frame of the video record is shown in Figure A.2.

- **Mapping:** Further investigation of the recorded data is possible using the animated mapping features of the Profile system. Head map displays can be calculated for power spectrum and coherence analysis across four frequency bands, as well as instantaneous scalp potential and current–density amplitude mapping. The possible mappings are listed below[1].

  - *Amplitude mapping:* provides a picture of the instantaneous EEG amplitude when a referential montage is selected and displays either amplitude or current density.

  - *Band power analysis:* allows for the determination of dominant frequency band and location of frequency content using four head maps for the various frequency bands.

  - *Coherence analysis:* provides an index of the synchrony of the EEG signal between two different cortical regions, reflecting the degree of shared electrical activity between those areas.

[1] To view the raw EEG data we use the MEDELEC Profile Reader software. This software does not include the mapping capabilities.

A.3 Location of EEG Recording

The EEG data used in this thesis was recorded at the neonatal intensive care unit (NICU) at the Royal Womens Hospital[2], Brisbane, Australia. The patients in the NICU are often monitored by members of the Perinatal Research Centre (PRC), located in the RBWH. The PRC is directed by Prof. Paul Colditz who is an expert in neonatal intensive care and qualified in biomedical engineering.

The EEG data used in this thesis were thoroughly reviewed by Dr. Chris Burke and assisted by Jane Richmond, an EEG technologist. Dr. Burke is a neurologist from the Neurosciences department at the Royal Children's Hospital, Brisbane, Australia.

A.4 EEG Recording Specifics

The MEDELEC Profile system allows for a number of filtering and sampling possibilities. All EEG data recorded at the RWH has the same recording protocol. This protocol is explained in the following:

1. Placement of 14 electrodes on the newborn EEG scalp. 20 EEG channels are recorded using bipolar montage.
2. EEG data digitized. Sampling frequency: $F_s = 256$Hz
3. EEG data digitally bandpass filtered. Cutoff frequencies: $F_{Low} = 0.5$Hz and $F_{High} = 70$Hz.
4. EEG data notch filtered. Notch center: $F_n = 50$Hz

[2]The Royal Womens Hospital has now merged with the Royal Brisbane Hospital and is now known as the Royal Brisbane and Womens Hospital (RBWH).

Bibliography

[1] M. Roessgen, A. Zoubir, and B. Boashash, "Seizure detection of newborn EEG using a model–based approach," *IEEE Transactions on Biomedical Engineering*, vol. 45, no. 6, pp. 673–685, 1998.

[2] R. Northrop, *Signals and Systems Analysis in Biomedical Engineering*, R. Northrop, Ed. Boca Raton: CRC Press, 2003.

[3] A. Cohen, *Biomedical Signal Processing*, A. Cohen, Ed. Boca Raton: CRC Press, 1986, vol. 1.

[4] E. Mizrahi and P. Kellaway, *Diagnosis and Management of Neonatal Seizure*. Philadelphia: Lippincott–Raven, 1998.

[5] M. van de Bor, "The recognition and management of neonatal seizures," *Current Paediatrics*, vol. 12, pp. 382–387, 2002.

[6] M. Lanska, D. Lanska, R. Baumann, and R. Kryscio, "A population-based study of neonatal seizures in Fayette County," *Neurology*, vol. 45, no. 4, pp. 724–732, April 1995.

[7] R. Saliba, J. Annegers, D. Waller, J. Tyson, and E. Mizrahi, "Incidence of neonatal seizures in Harris County, 1992-1994," *American Journal of Epidemiology*, vol. 150, no. 7, pp. 763–769, October 1999.

[8] J. Hahn and B. Tharp, "Neonatal and pediatric electroencephalography," in *Electrodiagnosis in Clinical Neurology*, 3rd ed., M. Aminoff, Ed. New York: Churchill Livingstone, 1992, pp. 93–141.

[9] C. Lombroso, "Neonatal EEG polygraphy in normal and abnormal newborns," in *Electroencephalography: Basic Principles, Clinical Applications and Related Fields*, 3rd ed., E. Niedermeyer and F. L. D. Silva, Eds. Baltimore: Williams and Wilkins, 1993, pp. 803–875.

[10] M. Scher, M. Painter, I. Bergman, M. Barmada, and J. Brunberg, "EEG diagnoses of neonatal seizures: Clinical correlations and outcome," *Pediatric Neurology*, vol. 5, pp. 17–24, 1989.

[11] J. Connell, R. Oozeer, L. D. Vries, L. Dubowitz, and V. Dubowitz, "Continuous EEG monitoring of neonatal seizures, diagnostic and prognostic considerations," *Archives of disease in children*, vol. 64, pp. 452–458, 1989.

[12] M. Andre, M. Matisse, P. Vert, and C. Debruille, "Neonatal seizures– recent aspects," *Neuropediatrics*, vol. 19, 1988.

[13] B. Wical, "Neonatal seizures and electrographic analysis: Evaluation and outcomes," *Pediatric Neurology*, vol. 10, pp. 271–275, 1994.

[14] J. Volpe, *Neurology of the Newborn*, 4th ed. Philadelphia: W.B. Saunders, 2001.

[15] M. Toet, L. Hellström-Westas, F. Groenendaal, P. Eken, and L. de Vries, "Amplitude integrated EEG 3 and 6 hours after birth in full term neonates with hypoxic–ischaemic encephalopathy," *Archives of Disease in Childhood*, vol. 81, pp. F19–F23, 1999.

[16] B. Boashash and M. Mesbah, "Time–frequency methodology for newborn electroencephalographic seizure detection," in *Applications in Time–Frequency Signal Processing*, A. Papandreou-Suppappola, Ed. Boca Raton: CRC Press, 2003.

[17] S. Qian and D. Chen, *Joint Time-Frequency Analysis: Methods & Applications.* Upper Saddle River, NJ: Prentice-Hall, 1996.

[18] P. P. Jr., *Probability, Random Variables and Random Signal Principles*, 4th ed. Singapore: McGraw-Hill, 2001.

[19] A. Liu, J. Hahn, G. Heldt, and R. Coen, "Detection of neonatal seizures through computerized EEG analysis," *Electroencephalography and Clinical Neurophysiology*, vol. 82, pp. 30–37, 1992.

[20] B. Boashash and M. Mesbah, "A time-frequency approach for newborn seizure detection," *IEEE Engineering in Medicine and Biology Magazine*, vol. 20, no. 5, pp. 54–64, 2001.

[21] B. Boashash, "Heuristic formulation of TFDs," in *Time–Frequency Signal Analysis and Processing: A Comprehensive Reference*, B. Boashash, Ed. London: Elsevier, 2003, pp. 29–57.

[22] J. Gotman, D. Flanagan, J. Zhang, and B. Rosenblatt, "Automatic seizure detection in the newborn: methods and initial evaluation," *Electroencephalography and Clinical Neurophysiology*, vol. 103, no. 3, pp. 356–362, 1997.

[23] L. Rankine, H. Hassanpour, M. Mesbah, and B. Boashash, "EEG simulation using fractal dimension analysis," in *Proc. Thirteenth Iranian Conference on Electrical Engineering*, vol. 3, Zanjan, Iran, May 2005.

[24] F. L. D. Silva, A. Hoeks, H. Smits, and L. Zetterberg, "Model of brain rhythmic activity: The alpha-rhythm of the thalamus," *Kybernetik*, vol. 15, pp. 27–37, 1974.

[25] P. Celka and P. Colditz, "A computer-aided detection of EEG seizures in infants: A singular-spectrum approach and performance comparison," *IEEE Transactions on Biomedical Engineering*, vol. 49, no. 5, pp. 455–462, May 2002.

[26] M. Mesbah and B. Boashash, "Performance comparison of seizure detection methods using EEG of newborns for implementation of a DSP subsystem," in *Proc. IEEE International Conference on Acoustics, Speech an Signal Processing*, May 2002, pp. 3860–3863.

[27] P. Celka and P. Colditz, "Nonlinear nonstationary weiner model of infant EEG seizures," *IEEE Transactions on Biomedical Engineering*, vol. 49, no. 6, pp. 556–564, June 2002.

[28] J. R. A. Barron and B. Yu, "The minimum description length principle in coding and modeling," *IEEE Transactions on Information Theory*, vol. 44, no. 6, 1998.

[29] B. Boashash, "Theory of quadratic TFDs," in *Time–Frequency Signal Analysis and Processing: A Comprehensive Reference*, B. Boashash, Ed. London: Elsevier, 2003, pp. 59–81.

[30] H. Hassanpour and M. Mesbah, "Neonatal EEG seizure detection using spike signatures in the time–frequency domain," in *Proc. International Symposium on Signal Processing and its Applications*, vol. 2, July 2003, pp. 41–44.

[31] H. Hassanpour, M. Mesbah, and B. Boashash, "Time–frequency based newborn EEG seizure detection using low and high frequency signatures," *Physiological Measurement*, vol. 25, pp. 935–944, 2004.

[32] M. Menendez, J. Pardo, L. Pardo, and M. Pardo, "The Jensen-Shannon divergence," *Journal of the Franklin Institute*, vol. 334, no. 2, pp. 307–318, March 1997.

[33] H. Hassanpour, M. Mesbah, and B. Boashash, "Enhanced time-frequency features for neonatal EEG seizure detection," in *Proc. International Conference on Circuits and Systems*, vol. 5, May 2003, pp. V–29 – V32.

[34] L. Rankine, N. Stevenson, M. Mesbah, and B. Boashash, "A quantitative comparison of non-parametric time-frequency representations," in *EUSIPCO 2005*, Antalya, Turkey, September 2005, CD-Rom.

[35] P. Zarjam, M. Mesbah, and B. Boashash, "Detection of newborn EEG seizure using optimal features based on discrete wavelet transform," in *Proc. International Conference on Circuits and Systems*, vol. 2, May 2003, pp. II–265 – II–26.

[36] A. Al-Ani and M. Deriche, "Feature selecting using a mutual information based measure," in *Proc. IEEE Conference on Pattern Recognition*, vol. 4, Quebec, Canada, 2005, pp. 82–85.

[37] S. Mallat and Z. Zhang, "Matching pursuits with time-frequency dictionaries," *IEEE Trans. on Signal Processing*, vol. 41, no. 12, pp. 3397–3415, December 1993.

[38] P. D. P.J. Franaszczuk, G.K. Bergey and H. Eisenberg, "Time–frequency analysis using matching pursuit algorithm applied to seizure originating from the mesial temporal lobe," *Electroencephalography and Clinical Neurophysiology*, vol. 106, no. 6, pp. 513–521, 1998.

[39] G. Bergey and P. Franaszczuk, "Epileptic seizures are characterised by changing signal complexity," *Clinical Neurophysiology*, vol. 112, no. 2, pp. 241–249, 2001.

[40] K. Blinowska and P. Durka, "Unbiased high resolution method of EEG analysis in time-frequency," *Acta Neurobiolgiae Experimentalis*, vol. 61, pp. 157–174, 2001.

[41] C. Jouny, P. Franaszczuk, and G. Bergey, "Characterization of epileptic seizure dynamics using gabor atom density," *Clinical Neurophysiology*, vol. 114, no. 3, pp. 426–437, 2003.

[42] P. Durka, "Adaptive parameterization of epileptic spikes," *Physical Review E*, vol. 69, no. 051914, 2004.

[43] S. Wilson, M. Scheuer, R. Emerson, and A. Gabor, "Seizure detection: evaluation of the Reveal algorithm," *Clinical Neurophysiology*, vol. 115, no. 10, pp. 2280–2291, 2004.

[44] L. Rankine, H. Hassanpour, M. Mesbah, and B. Boashash, "Newborn eeg simulation from nonlinear analysis," in *Proc. IEEE International Symposium on Signal Processing and its Applications*, Sydney, Australia, Aug. 2005, pp. 191–194.

[45] N. Stevenson, L. Rankine, M. Mesbah, and B. Boashash, "Newborn EEG seizure simulation using time-frequency signal synthesis," in *Proc. Workshop on Digital Image Computing*, Brisbane, Australia, Feb. 2005, pp. 145–150.

[46] L. Rankine and M. Mesbah, "Significant atom determination of basis pursuit decomposition," in *Proc. International Symposium on Signal Processing and its Applications*, Paris, France, July 2003, pp. 573–576.

[47] L. Rankine, M. Mesbah, and B. Boashash, "Atomic decomposition for detecting changes in signal structure: Application to EEG," in *Proc. International Conference on Biomedical Engineering*, Innsbruck, Austria, Feb 2004, pp. 285–288.

[48] ——, "Newborn seizure detection using signal structural complexity," in *Proc. EUSIPCO 2004*, Vienna, Austria, Sept. 2004, pp. 2207–2210.

[49] ——, "Atomic decomposition complexity for seizure detection in neonates," in *Proc. International Federation for Medical and Biological Engineering*, Sydney, Australia, Aug. 2003, pp. CD–Rom.

[50] ——, "A novel algorithm for newborn EEG seizure detection using matching pursuits with a coherent time-frequency dictionary," in *Proc. International Conference on Scientific and Engineering Computation*, Singapore, July 2004, pp. CD–Rom.

[51] H. Hassanpour, L. Rankine, M. Mesbah, and B. Boashash, "Comparative performance of time-frequency based EEG spike detection," in *EUSIPCO 2005*, Antalya, Turkey, September 2005, CD-Rom.

[52] L. Rankine, M. Mesbah, and B. Boashash, "Improving the ability of matching pursuit algorithm in detecting spikes," in *EUSIPCO 2005*, Antalya, Turkey, September 2005, CD-Rom.

[53] ——, "Automatic newborn EEG seizure spike and event detection using adaptive window optimization," in *Proc. ISSPA 2005*, Sydney, Australia, Aug. 2005, pp. 187–190.

[54] E. Niedermeyer, "Historical aspects," in *Electroencephalography: Basic Principles, Clinical Applications and Related Field*, 3rd ed., E. Niedermeyer and F. L. D. Silva, Eds. Baltimore: Williams and Wilkins, 1993, pp. 1–14.

[55] M. Brazier, "The emergence of electrophysiology as an aid to neurology," in *Electrodiagnosis in Clinical Neurology*, 3rd ed., M. Aminoff, Ed. New York: Churchill Livingstone, 1992, pp. 1–16.

[56] J. Cadwell and R. Villarreal, "Electrophysiological equipment and electrical safety," in *Electrodiagnosis in Clinical Neurology*, 3rd ed., M. Aminoff, Ed. New York: Churchill Livingstone, 1992, pp. 17–39.

[57] H. Huppertz, E. Hof, J. Klisch, M. Wagner, C. Lücking, and R. Kristeva-Feige, "Localization of interictal delta and epileptiform EEG activity associated with focal epileptogenic brain lesions," *NeuroImage*, vol. 13, pp. 15–28, 2001.

[58] E. R. John, "The role of quantitative EEG topographic mapping or 'neurometrics' in the diagnosis of psychiatric and neurological disorders: the pros," *Electroencephalography and Clinical Neurophysiology*, vol. 73, pp. 2–4, 1989.

[59] M. Aminoff, "Electroecephalograhy: General principles and clinical applications," in *Electrodiagnosis in Clinical Neurology*, 3rd ed., M. Aminoff, Ed. New York: Churchill Livingstone, 1992, pp. 41–91.

[60] J. Wackermann, P. Pütz, S. Büchi, I. Strauch, and D. Lehmann, "Brain electrical activity and subjective experience during altered states of consciousness: ganzfeld and hypnagogic states," *International Journal of Psychophysiology*, vol. 46, pp. 123–146, 2002.

[61] E. Speckmann and C. Elger, "Introduction to the neurophysiological basis of the EEG and DC potentials," in *Electroencephalography: Basic Principles, Clinical Applications and Related Fields*, 3rd ed., E. Niedermeyer and F. L. D. Silva, Eds. Baltimore: Williams and Wilkins, 1993, pp. 15–26.

[62] R. Cooper, J. Osselton, and J. Shaw, *EEG Technology.* London: Butterworths & Co, 1980.

[63] S. Gilman and S. Newman, *Essentials of Clinical Neuroanatomy and Neurophysiology*, 9th ed. Philadelphia: FA Davis, 1996.

[64] J. Nolte, *The human brain: an introduction to its functional anatomy.* St. Louis: Mosby, 2002.

[65] P. Nunez, *Electrical Fields of the Brain.* New York: Oxford U. Press, 1981.

[66] A. Petrosian, D. Prokhorov, R. Homan, R. Dasheiff, and D. Wunsch, "Recurrent neural network based prediction of epileptic seizures in intra- and extracranial EEG," *Neurocomputing*, vol. 30, pp. 201–218, 2000.

[67] M. Bozek-Kuzmicki, D. Colella, and G. Jacyna, "Feature-based epileptic seizure detection and prediction from ECoG recordings," in *Proc. IEEE-SP Int. Symp. on Time-Frequency and Time-Scale Analysis*, Philadelphia, USA, 1994, pp. 564–567.

[68] E. Reilly, "EEG recording and operation of the apparatus," in *Electroencephalography: Basic Principles, Clinical Applications and Related Fields*, 3rd ed., E. Niedermeyer and F. L. D. Silva, Eds. Baltimore: Williams and Wilkins, 1993, pp. 104–124.

[69] G. Dumermuth and L. Molinari, "Spectral analysis of EEG background activity," in *Methods and Analysis of Brain Electrical and Magnetic Signals*, A. Gevins and A. Rémond, Eds. Amsterdam: Elsevier, 1987, vol. 1, pp. 85–130.

[70] E. Niedermeyer, "The normal EEG of the waking adult," in *Electroencephalography: Basic Principles, Clinical Applications and Related Fields*, 3rd ed., E. Niedermeyer and F. L. D. Silva, Eds. Baltimore: Williams and Wilkins, 1993, pp. 131–152.

[71] D. Schramm, B. Scheidt, A. Hübler, J. Frenzel, K. Holthausen, and O. Breidbach, "Spectral analysis of electroencephalogram during sleep related apneas in pre-term and term born infants in the first weeks of life," *Clinical Neurophysiology*, vol. 111, pp. 1788–1791, 2000.

[72] M. Scher, M. Sun, D. Steppe, R. Guthrie, and R.J.Sclabassi, "Comparison of EEG spectral and correlation measures between healthy term and preterm infants," *Pediatric Neurology*, vol. 10, no. 2, pp. 104–108, 1994.

[73] S. Giaquinto, F. Marciano, N. Monod, and G. Nolfe, "Applications of statistical equivalence to newborn EEG recordings," *Clinical Neurophysiology*, vol. 42, pp. 406–413, 1977.

[74] F. Sharbrough, "Nonspecific abnormal EEG patterns," in *Electroencephalography: Basic Principles, Clinical Applications and Related Fields*, 3rd ed., E. Niedermeyer and F. L. D. Silva, Eds. Baltimore: Williams and Wilkins, 1993, pp. 197–215.

[75] E. Niedermeyer, "Abnormal EEG patterns: Epileptic and paroxysmal," in *Electroencephalography: Basic Principles, Clinical Applications and Related Fields*,

3rd ed., E. Niedermeyer and F. L. D. Silva, Eds. Baltimore: Williams and Wilkins, 1993, pp. 217–240.

[76] P. Prior, "Cerebral anoxia: Clinical aspects," in *Electroencephalography: Basic Principles, Clinical Applications and Related Fields*, 3rd ed., E. Niedermeyer and F. L. D. Silva, Eds. Baltimore: Williams and Wilkins, 1993, pp. 431–444.

[77] E. Niedermeyer, "Epileptic seizure disorders," in *Electroencephalography: Basic Principles, Clinical Applications and Related Fields*, 3rd ed., E. Niedermeyer and F. L. D. Silva, Eds. Baltimore: Williams and Wilkins, 1993, pp. 461–564.

[78] A. Oliveira, M. Nunes, L. Haertel, F. Reis, and J. da Costa, "Duration of rhythmic EEG patterns in neonates: new evidence for clinical prognostic significance of brief rhythmic discharges," *Clinical Neurophysiology*, vol. 111, pp. 1646–1653, 2000.

[79] R. Clancy and A. Legido, "The exact ictal and interictal duration of electroencephalographic neonatal seizure," *Epilepsia*, vol. 28, pp. 537–541, 1987.

[80] B. Boashash, "Time–frequency concepts," in *Time–Frequency Signal Analysis and Processing: A Comprehensive Reference*, B. Boashash, Ed. London: Elsevier, 2003, pp. 4–27.

[81] S. Mallat, *A Wavelet Tour of Signal Processing*. San Diego: Academic Press, 1998.

[82] F. Hlawatsch and G. Boudreaux-Bartels, "Linear and quadratic time-frequency signal representations," *IEEE Signal Processing Magazine*, pp. 21–67, April 1992.

[83] N. T.-M. L. Giulieri and P. Arquès, "Blind sources separation using bilinear and quadratic time-frequency representations," in *Proc. International Conference on Independent Component Analysis and Blind Signal Separation*, Dec. 2001, pp. 486–491.

[84] L. Debnath, *Integral Transforms and Their Applications*. Boca Raton: CRC Press, 1995.

[85] H.-I. Choi and W. Williams, "Improved time–frequency representation of multicomponent signals using exponential kernels," *IEEE Transactions on, Acoustics, Speech, and Signal Processing*, vol. 37, no. 6, pp. 862–871, June 1989.

[86] B. Barkat and B. Boashash, "A high-resolution quadratic time–frequency distribution for multicomponent signal analysis," *IEEE Transactions on signal processing*, vol. 49, no. 10, pp. 2232–2239, Oct. 2001.

[87] Z. Hussain and B. Boashash, "Adaptive instantaneous frequency estimation of multicomponent FM signals using quadratic time–frequency distributions," *IEEE Transactions on Signal Processing*, vol. 50, no. 8, pp. 1866–1876, Aug 2002.

[88] S. Chen, D. Donoho, and M. Saunders, "Atomic decomposition by basis pursuit," *Society for Industrial and Applied Mathematics: Review*, vol. 43, no. 1, pp. 129–159, 2001.

[89] R. Coifman and Y. Meyer, "Entropy-based algorithms for best-basis selection," *IEEE Transactions on Information Theory*, vol. 38, no. 2, pp. 713–718, Mar. 1992.

[90] I. Daubechies, "Time–frequency localization operators: A geometric phase space approach," *IEEE Transactions on Information Theory*, vol. 34, no. 4, pp. 605–612, July 1988.

[91] P. Colditz, C. Burke, and P. Celka, "Digital processing of EEG signals," *IEEE Engineering in Medicine and Biology*, vol. 20, no. 5, pp. 21–22, 2001.

[92] H. Abarbanel, "Tools for the analysis of chaotic data," in *Nonlinear Signal and Image Analysis*, J. Buchler and H. Kandrup, Eds. Annals of the New York Academy of Sciences, 1997.

[93] H. Kantz and T. Shreiber, *Nonlinear Time Series Analysis.* Cambridge: Cambridge University Press, 1997.

[94] T. Higuchi, "Approach to an irregular time series on the basis of the fractal theory," *Physica D*, vol. 31, pp. 277–283, 1988.

[95] G. Wornell and A. Oppenheim, "Estimation of fractal signals from noisy measurements using wavelets," *IEEE Trans. Signal Processing*, vol. 40, no. 3, pp. 611–623, 1992.

[96] R. Esteller, G. Vachtsevanos, J. Echauz, and B. Litt, "A comparison of waveform fractal dimension algorithms," *IEEE Trans. Circuits and Systems-I: Fundamental Theory and Applications*, vol. 48, no. 2, pp. 177–183, 2001.

[97] A. Gelman, J. Carlin, H. Stern, and D. Rubin, *Bayesian Data Analysis*, 2nd ed. CRC Press, 2003.

[98] J. Altenburg, R. Vermeulen, R. Strijers, W. Fetter, and C. Stam, "Seizure detection in the neonatal EEG with synchronization likelihood," *Clinical Neurophysiology*, vol. 114, pp. 50–55, 2003.

[99] B. Boashash, M. Mesbah, and P. Colditz, "Newborn EEG seizure pattern characterisation using time-frequency analysis," in *Proc. IEEE International Conference on Acoustics, Speech ad Signal Processing*, Salt Lake City, USA, May 2001, pp. 1041–1044.

[100] D. Griffin and J. Lim, "Signal estimation from modified short–time Fourier transform," *IEEE Transactions on Acoustics, Speech, and Signal Processing*, vol. 32, no. 2, pp. 236–243, April 1984.

[101] D. Donoho and X. Huo, "Uncertainty principles and ideal atomic decomposition," *IEEE Transactions on Information Theory*, vol. 46, no. 7, pp. 2845–2862, Nov. 2001.

[102] J. Tropp, "Greed is good: Algorithmic results for sparse approximation," *IEEE Transactions on Information Theory*, vol. 50, no. 10, pp. 2231–2242, Oct 2004.

[103] B. Boashash, M. Mesbah, and P. Colditz, "Time-frequency detection of EEG abnormalities," in *Time–Frequency Signal Analysis and Processing: A Comprehensive Reference*, B. Boashash, Ed. London: Elsevier, 2003, pp. 663–670.

[104] P. Ktonas, W. Luoh, M. Kejariwal, E. Reilly, and M. Seward, "Computer-aided quantification of EEG spike and sharp wave characteristics," *Electroencephalography and Clinical Neurophysiology*, vol. 51, pp. 237–243, 1981.

[105] W. Hostetler, H. Doller, and R. Homan, "Assessment of a computer program to detect epileptiform spikes," *Electroencephalography and Clinical Neurophysiology*, vol. 83, no. 1, pp. 1–11, 1992.

[106] S. Wilson, R. Harner, F. Duffy, B. Tharp, M. Nuwer, and M. Sperling, "Spike detection. i. Correlation and reliability of human experts," *Electroencephalography and Clinical Neurophysiology*, vol. 98, no. 3, pp. 186–198, 1996.

[107] J. Gotman and P. Gloor, "Automatic recognition and quantification of interictal epileptic activity in the human scalp eeg," *Electroencephalography and Clinical Neurophysiology*, vol. 41, no. 5, pp. 513–529, 1976.

[108] S. Mukhopadhyay and G. Ray, "A new interpretation of nonlinear energy operator and its efficacy in spike detection," *IEEE Transactions on Biomedical Engineering*, vol. 45, no. 2, pp. 180–187, Feb. 1998.

[109] J. Kaiser, "On a simple algorithm to calculate the energy of a signal," in *Proc. IEEE International Conference on Acoustics, Speech and Signal Processing*, vol. 1, Alburquerque, USA, 1990, pp. 381–384.

[110] G. Calvagno, M. Ermani, R. Rinaldo, and F. Sartoretto, "A multiresolution approach to spike detection in EEG," in *Proc. IEEE International Conference on Acoustics, Speech and Signal Processing*, vol. 6, 2000, pp. 3582–3585.

[111] M. Latka, Z. Waś, A. Kozik, and B. West, "Wavelet analysis of epileptic spikes," *Physical Review E*, vol. 67, no. 5, p. 052902, 2003.

[112] L. Senhadji and F. Wendling, "Epileptic transient detection: wavelets and time–frequency approaches„" *Clinical Neurophysiology*, vol. 32, no. 3, pp. 175–192, June 2002.

[113] E. Hulata, R. Segev, and E. Ben-Jacob, "A method for spike sorting and detection based on wavelet packets and shannon's mutual information," *Journal of Neuroscience Methods*, vol. 117, no. 1, pp. 1–12, May 2002.

[114] H. Hassanpour, M. Mesbah, and B. Boashash, "A time-frequency approach for spike detection," in *Proc. IEEE International Conference on Electronics, Circuits and Systems*, vol. 1, 2003, pp. 56–59.

[115] R. Baraniuk and D. Jones, "Adaptive time-frequency analysis„" in *Time–Frequency Signal Analysis and Processing: A Comprehensive Reference*, B. Boashash, Ed. London: Elsevier, 2003, pp. 178–184.

[116] ——, "A radially Gaussian, signal-dependent time-frequency representation," *Signal Processing*, vol. 32, pp. 263–284, June 1993.

[117] D. Jones and R. Baraniuk, "An adaptive optimal-kernel time-frequency representation," *IEEE Transactions on Signal Processing*, vol. 43, no. 10, pp. 2361–2371, Oct 1995.

[118] ——, "A simple scheme for adapting time-frequency representations," *IEEE Transactions on Signal Processing*, vol. 42, no. 12, pp. 3530–3535, Dec 1994.

[119] I. Djurović and L. Stanković, "Adaptive windowed fourier transform," *Signal Processing*, vol. 83, pp. 91–100, 2003.

[120] H. Kwok and D. Jones, "Improved instantaneous frequency estimation using an adaptive short-time Fourier transform," *IEEE Transactions on Signal Processing*, vol. 48, no. 10, pp. 2964–2972, Oct 2000.

[121] K. Sainio, M. Granström, O. Pettay, and M. Donner, "EEG in neonatal herpes simplex encephalitis," *Electroencephalography and Clinical Neurophysiology*, vol. 56, pp. 556–561, 1983.

[122] S. Faul, G. Boylan, S. Connolly, L. Marnane, and G. Lightbody, "An evaluation of automated neonatal seizure detection methods," *Clinical Neurophysiology*, vol. 116, no. 7, pp. 1533–1541, July 2005.

[123] H. Hassanpour, "Time–frequency based detection of newborn EEG seizure," Ph.D. dissertation, Queensland University of Technology, Brisbane, Australia, 2004.

[124] "www.amlabtech.com.au."

[125] "www.emsbiomed.com/emsint/phoenixshortdescr.htm."

[126] "www.oxford-instruments.com."

[127] P. Zarjam, "EEG data acquisition and automatic seizure detection using wavelet transforms in the newborn," Master's thesis, Queensland University of Technology, Brisbane, Australia, 2003.